

**IOSUD – UNIVERSITATEA „DUNĂREA DE JOS” DIN GALAȚI**

**Școala doctorală de Inginerie mecanică**



# **TEZĂ DE DOCTORAT**

## **ABSTRACT**

**NUMERICAL SIMULATION OF THE SHIP  
HULL HYDRODYNAMIC PERFORMANCE**

**SIMULAREA NUMERICĂ A  
PERFORMANȚELOR HIDRODINAMICE ALE  
CORPULUI NAVEI**

**Doctorand,**

**ing. Adham S. Bekhit**

**Conducător științific,**

**Prof.dr.ing. Florin Popescu**

**Seria I 6 Nr. 60**

**GALAȚI**

**2021**

IOSUD – UNIVERSITATEA „DUNĂREA DE JOS” DIN GALAȚI

Școala doctorală de Inginerie mecanică



# TEZĂ DE DOCTORAT

NUMERICAL SIMULATION OF THE SHIP  
HULL HYDRODYNAMIC PERFORMANCE

SIMULAREA NUMERICĂ A  
PERFORMANȚELOR HIDRODINAMICE ALE  
CORPULUI NAVEI

Doctorand

ing. Adham S. Bekhit

**Președinte**

Academician Prof.dr.ing. Eugen Victor Cristian Rusu

**Conducător științific,**

Prof.dr.ing. Florin Popescu

**Referenți științifici**

Prof univ.dr.ing. Radu Mircea Damian

Conf.dr.ing. Florin Ioan Bode

Prof.dr.ing. Leonard Domnișoru

**Seria I 6 Nr. 60**

**GALAȚI**

**2021**

Seriile tezelor de doctorat susținute public în UDJG începând cu 1 octombrie 2013 sunt:

**Domeniul fundamental ȘTIINȚE INGINEREȘTI**

- Seria I 1: **Biotehnologii**
- Seria I 2: **Calculatoare și tehnologia informației**
- Seria I 3: **Inginerie electrică**
- Seria I 4: **Inginerie industrială**
- Seria I 5: **Ingineria materialelor**
- Seria I 6: **Inginerie mecanică**
- Seria I 7: **Ingineria produselor alimentare**
- Seria I 8: **Ingineria sistemelor**
- Seria I 9: **Inginerie și management în agricultură și dezvoltare rurală**

**Domeniul fundamental ȘTIINȚE SOCIALE**

- Seria E 1: **Economie**
- Seria E 2: **Management**
- Seria SSEF: **Știința sportului și educației fizice**

**Domeniul fundamental ȘTIINȚE UMANISTE ȘI ARTE**

- Seria U 1: **Filologie- Engleză**
- Seria U 2: **Filologie- Română**
- Seria U 3: **Istorie**
- Seria U 4: **Filologie - Franceză**

**Domeniul fundamental MATEMATICĂ ȘI ȘTIINȚE ALE NATURII**

- Seria C: **Chimie**

**Domeniul fundamental ȘTIINȚE BIOLOGICE ȘI BIOMEDICALE**

- Seria M: **Medicină**

## **Acknowledgments**

I would like to express my endless gratitude and thanks for those who helped me and offered their unconditional support to finish this thesis.

## Abstract

The modern ship design process imposes several challenges from geometry, economy and most recently, energy efficiency points of view. In order to understand the ship hydrodynamic performance of a moving ship, whether in calm water or in waves, it is very important to have a flexible, reliable and efficient tool to assess the different hydrodynamic aspects in that condition.

The conventional ship hydrodynamic tools, represented in experimental and theoretical based methods, have their own limitation considering their cost, applicability and flexibility to handle generic, optimization purposes and unconventional ship shapes. Although experimental methods are the most accurate and realistic approaches in all engineering applications and particularly in ship hydrodynamic field, their cost is significant and their applicability in the optimization process is unfeasible. On the other hand, the theoretical based approaches suffer from their limited applications for conventional ships, which make their possibility to cover new designs impossible. The past three decades in ship hydrodynamic applications showed a significant rise in the CFD applications in ship hydrodynamics, regarding the resistance, propulsion, seakeeping, maneuvering and many other applications. Thanks to the latest development in the physical and numerical modeling approaches, encouraged by the enormous development in computational capacities, which recently resulted in high performance and cloud computing facilities, in the recent days, the CFD can be useful to analyze the ship hydrodynamic aspects with a very mature level of accuracy. In addition, the flexibility of the CFD method is unlimited, which made it suitable for analyzing even the most complex scenarios in ship hydrodynamics, such as sinkage, loss of stabilities or complex accidental scenarios, which definitely are not applicable to be studied using an experimental approach.

With all these features possible in the numerical simulation, a new trend in ship hydrodynamics field nowadays launched the term (Numerical Towing Tank, or Virtual Towing Tank). This shows that the numerical simulations recently have their internationally recognized role in predicting ship hydrodynamic performance. Yet, the accuracy of the numerical simulation should always be controlled by serious systematic verification and validation studies, especially for novel concepts, with collaborate integration between the numerical and experimental approaches.

Heading from this perspective, this study proposes a first step for a numerical towing tank that should assess the ship hull hydrodynamic performance from resistance, propulsion and seakeeping points of view. Rigorous and extensive studies are performed, all aimed at investigating the capability of a unique CFD viscous flow solver (ISIS-CFD of the FINE<sup>TM</sup>/Marine) to handle the different aspects of ship hydrodynamics. Extensive systematic verification and validation with the experimental data are conducted to assess the consistency and accuracy of the numerical solutions compared to the available experimental data from similar analysis perspectives.

To ensure the applicability and consistency of the proposed method for various ship aspects, geometries and functions, three ships are used to validate the numerical simulations in this study which are; the Japan Bulk Carrier JBC ship model, the very large crude carrier KVLCC2 ship model, and finally, the DTMB surface combatant ship model. Worth mentioning that the scope of this research, which is directly connected to validation of the proposed method against experimental data, covers only model scale investigation similar to the tank tests results available in the public domain, in order to demonstrate that the numerical approach can replicate the same tests performed in the towing tanks, with much less complexity and cost.

Ship resistance simulations are performed for the three ship models with different sailing and appendage conditions. Besides, an experimental study is carried out for the DTMB ship model at the medium-high speed mode to study the influence on the total resistance and wave reflections at the wall experimentally and numerically.

Ship propulsion simulations are executed for JBC and KVLCC2 ship model for open water propeller condition and for nominal and effective propulsion condition based on the simplified actuator disk method and the 3D modeled propeller using the sliding grid technique.

Ship seakeeping performance is assessed using three sets of simulations performed for the DTMB regarding the ship sailing in regular head waves while fixed with no degrees of freedom, and with two degrees of freedom free to heave and pitch, and finally, the roll decay condition in calm water.

All the three aspects were validated taking into consideration the hydrodynamic forces, motions, free-surface and local flow. All the obtained results are validated against the EFD data showing a promising correspondence, especially for resistance and propulsion applications, with slightly less accuracy for local parameters in seakeeping, such as pitch motion prediction.

Overall, the study concluded the possibility of the CFD method to handle reliably and accurately the ship hydrodynamic performance in several aspects. More aspects and simulation cases are proposed in the future plan of this research in order to concur more aspects in the ship hydrodynamics domain.

## Rezumat

În contextul actual procesul modern de proiectare a navelor impune mai multe provocări din punct de vedere al geometriei, economiei și, mai recent, al eficienței energetice. De aceea este foarte importantă existența unui instrument flexibil, fiabil și eficient pentru a înțelege performanța hidrodinamică a navei aflate în mișcare, fie în apă calmă, fie în valuri, și a evalua diferitele aspecte hidrodinamice în diverse stări ale navei.

Metodele clasice experimentale, statistice sau analitice au propriilor lor limitări având în vedere costul, aplicabilitatea și flexibilitatea lor pentru a gestiona scopuri generice, de optimizare și forme neconvenționale ale navelor. Deși metodele experimentale sunt cele mai exacte și cele mai realiste abordări în toate aplicațiile de inginerie și în special în domeniul hidrodinamic al navelor, costul lor este semnificativ și aplicabilitatea lor în procesul de optimizare este irealizabilă. Pe de altă parte, abordările bazate pe metodele teoretice sunt limitate doar la navele convenționale, ceea ce face imposibilă aplicarea lor la noile modele. Ultimele trei decenii au arătat o creștere semnificativă a aplicațiilor CFD (Computational Fluid Dynamic) în hidrodinamica navelor, în ceea ce privește rezistența, propulsia, performanțele de seakeeping, manevrabilitatea și multe alte aplicații. Ținând cont de dezvoltarea enormă a capacităților de calcul, care a dus recent la performanțe ridicate (High Performance Computing) și facilități de cloud computing, recent CFD poate fi util pentru a analiza aspectele hidrodinamice ale navei cu un nivel de precizie foarte mare. Totodată, flexibilitatea metodei CFD este nelimitată, ceea ce o face potrivită pentru a analiza chiar și cele mai complexe scenarii din hidrodinamica navelor, cum ar fi scufundarea, pierderea stabilităților sau scenarii de accidente complexe, care cu siguranță nu pot fi studiate folosind o abordare experimentală.

Cu toate aceste facilități posibile în simularea numerică, o nouă tendință în domeniul hidrodinamicii navelor a lansat termenul de “bazin de carene numeric” sau “bazin de carene virtual”. Acest fapt confirmă acuratețea simulărilor numerice, recunoscută în rândul specialiștilor, în estimarea performanțelor hidrodinamice ale navelor. Cu toate acestea, acuratețea simulării numerice ar trebui întotdeauna confirmată prin studii sistematice consistente de verificare și validare, în special pentru conceptele noi, cu integrarea abordărilor numerice și experimentale.

Plecând de la această perspectivă, studiul de față propune un prim pas pentru un bazin de carene numeric menit să evalueze performanțele hidrodinamice ale corpului navei din punctul de vedere al rezistenței, propulsiei și al seakeeping-ului. Sunt efectuate studii riguroase și extinse, toate având ca scop investigarea capacității unui solver CFD unic pentru curgere vâscoasă (ISIS-CFD al FINE™/Marine) de a trata diferitele aspecte ale hidrodinamicii navelor. Verificarea și validarea sistematică extensivă cu datele experimentale sunt efectuate pentru a evalua consistența și acuratețea soluțiilor numerice în comparație cu datele experimentale disponibile din perspective analitice similare.

Pentru a asigura aplicabilitatea și coerența metodei propuse pentru diferite aspecte, geometrii și funcții ale navei, se utilizează trei corpuri de nave pentru a valida simulările numerice din acest studiu care sunt: modelul navei Japan Bulk Carrier (JBC), modelul de navă de tip petrolier KVLCC2 și, în cele din urmă, modelul navei de de tip combatant DTMB. Merită menționat faptul că scopul acestei cercetări, care este direct legat de validarea metodei propuse față de datele experimentale, acoperă doar analiza la scară a modelului, similar cu rezultatele testelor experimentale disponibile în literatură de specialitate, pentru a demonstra că abordarea numerică poate reproduce aceleași teste efectuate în bazinul de carene, cu o complexitate și costuri mult mai mici.

Simulările de rezistență ale navei sunt efectuate pentru cele trei modele de nave cu condiții diferite de navigație și apendici. În plus, se efectuează un studiu experimental pentru modelul navei DTMB la regimul de viteză medie-mare pentru a studia, experimental și numeric, influența efectului pereților din bazin asupra rezistenței și suprafeței libere a navei.

Simulările de propulsie a navei sunt executate pentru modelul de navă JBC și KVLCC2 pentru cazul elicei în apă liberă, siaj nominal și efectiv pe baza metodei simplificate a discului actuator (a discului activ) și a elicei modelate în 3D, utilizând tehnica "sliding grid".

Performanța navelor în valuri este evaluată folosind trei seturi de simulări efectuate pentru DTMB în ceea ce privește nava în mișcare în valuri regulate frontale în timp ce este fixată fără grade de libertate și, respectiv, cu două grade de libertate pe direcțiile verticală și longitudinală (mișcarea vertical, respective tangaj) și, în cele din urmă, amortizarea ruliului în apa calmă.

Toate cele trei aspecte au fost validate luând în considerare forțele hidrodinamice, mișcările, suprafața liberă și siajul. Toate rezultatele obținute sunt validate pe baza datelor experimentale care arată o corespondență promițătoare.



## Nomenclatures

$S_L$	Minimum oscillation value in simulation
$S_U$	Maximum oscillation value in simulation
$T_e$	Wave encounter period
$U_P$	General parameter uncertainty
$\delta_P$	General parameter error
$\Delta_y$	Distance of the first point from the solid wall
$CD_{k\omega}$	Cross-diffusion in the $K - \omega$ model.
$g_i$	Gravity vector
$\Omega_{ij}$	Vorticity magnitude
$C_F$	Frictional Resistance coefficient
$C_R$	Residual Resistance coefficient
$CF_\infty$	Value of fitted function in verification process
$C_T$	Total resistance coefficient
$C_i$	Correction factor
$E_{av}$	Average absolute error
$F_S$	Factor of safety
$I_j$	Unity vector whose components vanish, except for the component $j$
$Q^*$	Second invariant $Q$ criterion
$R_F$	Frictional Resistance
$R_R$	Residual Resistance
$R_G$	Grid convergence ratio
$R_T$	Time step convergence ratio
$R_T$	Total resistance
$R_i$	Convergence ratio
$S_C$	Simulation benchmark
$S_{ij}$	Total stress tensor
$U_{S_c^N}$	Corrected uncertainty
$U_{V_c}$	Corrected validation uncertainty
$\vec{U}$	Velocity vector
$U_\infty$	Far field velocity
$U_D$	Data uncertainty
$U_G$	Grid uncertainty
$U_I$	Iteration uncertainty
$U_S$	Simulation uncertainty
$U_{SM}$	Modeling uncertainty
$U_{SN}$	Numerical uncertainty
$U_T$	Time step uncertainty
$U_V$	Validation uncertainty
$U_{reqd}$	Required level of uncertainty
$c_i$	Volume fraction for fluid $i$
$f_e$	Wave encounter frequency
$f_w$	Wave frequency
$\vec{n}$	Unit normal vector directed outward
$p_\infty$	Far field pressure
$p_G$	Grid order of accuracy
$p_T$	Time step order of accuracy
$p_a$	Atmospheric pressure
$p_i$	Simulation order of accuracy
$r_G$	Grid refinement ratio
$r_i$	General verification ratio
$y^+$	Non-dimensional distance from the wall
$\gamma_I$	Wave initial phase angle

$\delta_D$	Data error
$\delta_G$	Grid error
$\delta_I$	Iteration error
$\delta_{RE}^*$	Richardson Extrapolation error
$\delta_S$	Simulation error
$\delta_{SM}$	Modeling error
$\delta_{SN}$	Numerical error
$\delta_{SN}^*$	Estimated value with sign and magnitude of the numerical error
$\delta_T$	Time step error
$\delta_{ij}$	Kronecker (delta) operator
$\varepsilon_{av}$	Average relative error
$\zeta_i$	Incident wave height
$\nu_t$	Turbulent eddy viscosity
$\rho_a$	Mass density of air
$\rho_w$	Mass density of water
$\sigma_a$	Tangential force on the free-surface in water
$\sigma_w$	Tangential force on the free-surface in water
$\tau_{ij}$	Viscous stress tensor
$\bar{\tau}_{ij}$	Mean viscous stress tensor
$\Delta p_\gamma$	Pressure jump at the free-surface interface
$\Delta x$	Cell size in x-direction
$\Delta y$	Cell size in y-direction
$\Delta z$	Cell size in z-direction
$A$	Wave amplitude
$A_0$	Propeller disk area
$A_E$	Expanded blade area
$B$	Beam of the ship
$C_{AW}$	Added resistance in waves coefficient
$C_B$	Block coefficient
$C_H$	Heave force coefficient
$C_M$	Mid-ship section coefficient
$C_M$	Pitch moment coefficient
$C_{TCW}$	Calm water total resistance coefficient
$C_{TW}$	Total resistance coefficient in waves
$D$	Measured value in tank test
$D$	Depth of the ship
$D_h$	Propeller hub diameter
$D_p$	Propeller diameter
$Fr$	Froude number
$He$	Helicity
$H_w$	Wave height
$J$	Propeller advance coefficient
$k$	Wave number
$K_Q$	Propeller torque coefficient
$K_T$	Propeller thrust coefficient
LCB	Longitudinal center of buoyancy
$L_{PP}$	Length between perpendicular
$L_{ref}$	Reference length
$M_i$	General representation for grid density, $i=1:n$ , finest grids $i=1$ , coarsest grid $i=n$
$\emptyset$	Roll angle
$\emptyset_0$	Initial roll angle
$\emptyset_m$	mean decay roll value
$Q$	Propeller torque
RAO	Response Amplitude Operator
$Re$	Reynolds number
$S$	Simulation value computed based on CFD

$S_0$	Wetted surface area of the ship without appendages
$SFC$	Shear Force Correction
$S_R$	Wetted surface area of the rudder
$T$	Draft of the ship
$T$	Simulation time
$T$	Propeller thrust
$T$	Wave period
$t$	Simulation time
$TF$	Response Transfer Function
$U$	Ship Speed, axial flow velocity in x-direction
$V$	Axial flow velocity in y-direction
$W$	Axial flow velocity in x-direction
$x_{CG}$	Longitudinal position of C.O.G
$Z$	Number of propeller blades
$z_{CG}$	Vertical position of C.O.G
$\Delta$	Ship displacement
$\Delta\theta$	Roll angle decrement
$\Delta t$	Simulation time step
$\zeta$	Absolute free-surface elevation
$\lambda$	Wave length
$\omega$	Specific dissipation rate of turbulent frequency
$\omega$	Wave circular frequency
$E$	Absolute error
$K$	Kinetic energy
$P(t)$	Fourier transform parameter
$S$	Control surface in fluid governing equation
$V$	Control volume in fluid governing equation
$c$	Volume fraction coefficient
$n$	Propeller rotation rate
$p$	Pressure field
$u$	Fluid velocity in x-direction
$v$	Fluid velocity in y-direction
$w$	Fluid velocity in z-direction
$\mathcal{D}()$	Divergence operator
$\nabla$	Volume of displacement
$\beta$	Modeling coefficient for $K$ - $\omega$ turbulence model
$\gamma$	Surface tension
$\varepsilon$	Turbulent energy dissipation
$\varepsilon\%$	Relative error
$\mu$	Viscosity
$\rho$	Mass density of fluid
$\sigma$	Sinkage
$\tau$	Trim

## Abbreviations

A.P.	Aft Perpendicular
ABKV	Aft-Body Keel Vortices
AIAA	American Institute of Aeronautics and Astronautics
ALE	Lagrangian-Eulerian
ASM	Algebraic Stress Model
AW	Active Wall
BEM	Boundary Element Method
BKV	Bilge Keel Vortices
BSV	Bottom-Shaft Vortices
CAD	Computer Aided Design
CFD	Computational Fluid Dynamic
CFL	Courant–Friedrichs–Lewy number
CMT	Circular Motion Test
CPU	Central Processing Unit
DARPA	Defense Advanced Research Projects Agency
DDES	Delayed Detached Eddy Simulation
DES	Detached Eddy Simulation
DHRL	Dynamic Hybrid RANS/LES
DNS	Direct Numerical Simulation
DOF	Degrees of Freedom
DTMB	David Taylor Model Basin
DTRC	David Taylor Research Center
DW	Disabled Wall
EASM	Explicit Algebraic Stress Model
EEDI	Energy Efficiency Design Index
EEO	Energy Efficiency Operational Indicator
EFD	Experimental Fluid Dynamic
ESD	Energy Saving Devices
F.P.	Forward Perpendicular
FBKV	Fore-Body Keel Vortices
G2K	Gothenburg 2000 Workshop on Computational Ship Hydrodynamics
GD	General Domain
GHG	Green-House Gases
HMRI	Hyundai Maritime Research Institute
HPC	High Performance Computing
HSVA	Hamburgische Schiffbau-Versuchsanstalt (Hamburg Ship Model Basin)
IDB	International Data Base
IDDES	Improved Delayed Detached Eddy Simulation
IIHR	Iowa Institute of Hydraulic Research
IMO	International Maritime Organization
INSEAN	Istituto Nazionale per Studi Ed Esperienze di Architettura Navale
ITTC	International Towing Tank Conference
JBC	Japan Bulk Carrier
KCS	KRISO Container Ship
KRISO	Korea Research Institute of Ships and Ocean Engineering
KVLCC	KRISO Very Large Crude Carrier
<i>k-<math>\omega</math> SST</i>	<i>k-<math>\omega</math> Shear Stress Transport turbulence model</i>
LBM	Lattice Boltzmann Method
LDV	Laser Doppler Velocimetry
LES	Large Eddy Simulation
LIF	Laser Induced Fluorescence
MAC	Marker-And-Cell
MARIN	Maritime Research Institute of Netherlands
MEPC	Marine Environment Protection Committee

MOERI	Maritime and Ocean Engineering Research Institute
NMRI	National Maritime Research Institute
NSE	Navier-Stokes Equations
NSWC	Naval Surface Warfare Center (Carderock Division)
NTNU	Norwegian University of Science and Technology
ONRT	Office of Naval Research Tumblehome
OU	Osaka University
PISO	Pressure-Implicit with Splitting of Operators
PIV	Particle Image Velocimetry
PMM	Planar Motion Mechanism
POW	Propeller Open Water
PTV	Particle Tracking Velocimetry
RANS	Reynolds-Averaged Navier-Stokes
RANSE	Reynolds-Averaged Navier-Stokes Equations
RAO	Response Amplitude Operator
RE	Richardson Extrapolation
RSM	Reynolds Stress Model
RTV	Rudder Tip Vortices
SDV	Sonar Dome vortices
SIMMAN	Workshop on Verification and Validation of Ship Manoeuvring Simulation Methods
SIMPLE	Semi-Implicit method for Pressure-Linked Equations
SPIV	Stereo Particle Image Velocimetry
SV	Shaft Vortices
TKE	Turbulent Kinetic Energy
URANSE	Unsteady Reynolds-Averaged Navier-Stokes Equations
VLM	Vortex Lattice Method
VOF	Volume Of Fluid

## List of Figures

	Pg.	
Figure 1.1	Classification of methods used in viscous computational hydrodynamics	8
Figure 1.2	The development of CFD in ship hydrodynamics	12
Figure 2.1	General CFD process	35
Figure 3.1	Sources of errors in CFD results	36
Figure 3.2	Geometrically similar grid for a simple cube configuration	46
Figure 3.3	Geometrically similar grids for the JBC ship model	47
Figure 4.1	JBC model geometry highlighting stern, fore, duct, propeller and rudder	49
Figure 4.2	Computational domain, dimensions and boundary conditions	50
Figure 4.3	Computational grid, showing: (a) JBC with ESD, (b) duct and strut, (c) free-surface refinement, (d) fore and (e) stern comparison between fine and coarse grids	52
Figure 4.4	Computed total resistance coefficient $C_T$ with: (a) JBC w/o. ESD, (b) JBC w. ESD and (c) Richardson Extrapolation error	55
Figure 4.5	Computed free-surface at $T=30$ s, showing: (a) free-surface configuration, (b) mass fraction, (c) CFD vs. EFD for the free-surface topology, (d, e and f) CFD vs. EFD for wave profile at the hull, at distances $y/L_{pp}=0.1043$ and $y/L_{pp}=0.19$ , respectively	55
Figure 4.6	PIV measuring sections	57
Figure 4.7	EFD and CFD results for the axial velocity contours computed at $T=30$ s for ship without ESD at section S2 using different turbulence models	57
Figure 4.8	Section S4 EFD and CFD results for the axial velocity contours computed at $T=30$ s for ship without ESD using different turbulence models	58
Figure 4.9	Section S7 EFD and CFD results for the axial velocity contours computed at $T=30$ s for ship without ESD using different turbulence models	58
Figure 4.10	Comparison between the streamwise velocity contours measured and computed at $T=30$ s using EASM turbulence model for ship with ESD for sections S2, S4 and S7	59
Figure 4.11	Workshop data for the second invariant iso-surface $Q^*=25$ colored by helicity and the corresponding CFD results computed at $T=30$ s using EASM model	59
Figure 4.12	KVLCC2 model geometry highlighting propeller and rudder	61
Figure 4.13	Discretization grid for ship with; simplified rudder (left) and actual rudder (right)	63
Figure 4.14	Obtained results for ship without rudder: (a) Computed total resistance coefficient $C_T$ compared to the EFD, (b) estimated error as a function of grid density	63
Figure 4.15	CFD results compared to EFD showing: (a) total resistance coefficient $C_T$ (b) sinkage $\sigma$ and (c) trim $\tau$	64
Figure 4.16	Free-surface topology (left), and wave cuts at $y/L_{pp}=-0.0964$ and $-0.1581$ (right)	65
Figure 4.17	CFD vs. EFD streamwise velocity contours at sections: $x/L_{pp}=0.85$	65

	and 0.9825	
Figure 4.18	Velocity and TKE contours in the wake	66
Figure 4.19	Second invariant iso-surface $Q^*=25$ colored by non-dimensional helicity	66
Figure 4.20	DTMB model geometry viewing: front, profile, bottom and rear	67
Figure 4.21	Computational grids showing: (a) Fine and coarse grids, (b) free-surface refinement and (c) a forward section	69
Figure 4.22	Total resistance results based on the grid density	70
Figure 4.23	Total resistance error computed for $Fr=0.28$ based on the wall treatment approach	71
Figure 4.24	Free-surface profile (left), and wave cuts at $y/L_{pp}=0.082$ and $y/L_{pp}=0.172$ (right)	72
Figure 4.25	CFD vs. EFD streamwise velocity contours at different sections	73
Figure 4.26	Discretization grid highlighting the appendages refinement	74
Figure 4.27	Resistance results for the fully appended ship and hull components individually	75
Figure 4.28	Free-surface profiles for bare and appended hull	76
Figure 4.29	Comparison between bare and appended hull for axial velocity contours (U) and Turbulent Kinetic Energy (TKE)	77
Figure 4.30	Second invariant iso-surface $Q^*=10$ colored by non-dimensional helicity bottom view: (a) Bare hull, (b) appended hull, and (c) appended hull profile	78
Figure 4.31	Ship model and the towing carriage arrangement	80
Figure 4.32	Free-surface topology at ship extremities during the test: bow (left), stern (right)	82
Figure 4.33	Extrapolated data of the UGAL – Model compared to INSEAN – Model	83
Figure 4.34	Wave pattern for active tank walls domain showing wave reflection at the wall	85
Figure 4.35	Wave elevation diagram: (a) general domain, (b) active walls domain	86
Figure 4.36	The numerically predicted against the measured free-surface profile at model extremities	86
Figure 5.1	Simulation domain dimensions and boundary conditions in $x$ - $z$ and $y$ - $z$ view	89
Figure 5.2	Discretization grids for the finest grid illustrating blades grid and refinement zone	90
Figure 5.3	Thrust coefficient $K_T$ , torque coefficient $K_Q$ and propeller open water efficiency $\eta$ curves compared to EFD data	91
Figure 5.4	Pressure distribution on the suction and pressure sides of the propeller at different advance ratios $J$ : a) $J=0.7$ , a) $J=0.5$ , a) $J=0.3$ and a) $J=0.1$	91
Figure 5.5	Axial flow velocity, pressure distribution, Turbulent viscosity and TKE in the propeller wake for $J=0.3$ and $J=0.6$	92
Figure 5.6	Vortical structure of the wake flow computed at $T=5$ sec. for: (a) $J=0.3$ , (b) $J=0.6$	93
Figure 5.7	Longitudinal cut in the vortical structure of the wake flow at $J=0.6$	93
Figure 5.8	Computational domain and boundary conditions for self-propulsion simulation	94
Figure 5.9	Sliding grid arrangement for JBC without ESD (left) and with ESD	95

	(right)	
Figure 5.10	Grid arrangement for: actuator disk(left) and sliding grid (right) approaches	96
Figure 5.11	CFD results for nominal (a and b) and effective (c and d) velocity contours computed for ship with and without ESD using actuator disk method	98
Figure 5.12	Results interpolation to predict the propeller revolution rate	99
Figure 5.13	Comparison between the streamwise velocity contours measured and ship without ESD for sections S4 and S7	100
Figure 5.14	Comparison between the streamwise velocity contours for ship without ESD and the second invariant $Q^*=50$ for ship with and without rudder, computed using DES turbulence model	101
Figure 5.15	Mesh arrangement of the fine grid	103
Figure 5.16	Open water propeller performance curves CFD results against EFD data	104
Figure 5.17	Vorticity at $J=0.2$ : (a) vector form, (b) magnitude, (c) trajectory and (d) vortex cores	104
Figure 5.18	Second invariant computed for $J=0.2$ based on different turbulence models for iso-surface=500	105
Figure 5.19	Flow characteristics computed for $J=0.2$ based on DDES turbulence model	105
Figure 5.20	Second invariant computed for $J=0.4$ based on different turbulence models for iso-surface=250	106
Figure 5.21	Flow characteristics computed for $J=0.4$ based on DDES turbulence model	106
Figure 5.22	Second invariant computed for $J=0.6$ based on different turbulence models for iso-surface=125	107
Figure 5.23	Flow characteristics computed for $J=0.6$ based on DDES turbulence model	107
Figure 5.24	Grid geometry for actuator disk approach (top) and fully discretized propeller (bottom) highlighting the propeller and rudder	109
Figure 5.25	Prediction of the self-propulsion point using interpolation method	110
Figure 5.26	Streamwise velocity contours comparison between CFD and EFD	111
Figure 5.27	Vortices formation in the wake showing the profile and bottom view	111
Figure 6.1	Domain geometry, dimensions and boundary conditions	114
Figure 6.2	Grid configuration showing: stern, bow, longitudinal section free-surface top view	115
Figure 6.3	Resistance $C_T$ , Heave $C_H$ and Pitch $C_M$ coefficients compared to EFD	116
Figure 6.4	Grid resolution effect on the total resistance coefficient	117
Figure 6.5	Comparison between the time history of the total resistance based on wave steepness for $Ak = 0.025, 0.050$ and $0.075$	117
Figure 6.6	Schematic diagram for the quartering wave instants corresponding to the encountering moment with the F.P. of the ship	118
Figure 6.7	Computed free-surface at four wave quarters compared EFD	118
Figure 6.8	Wave visualisation at the bow and stern of the ship for $Ak=0.075$ at different encountering instants	119
Figure 6.9	Wave profile and mass fraction for $Ak=0.075$ when the peak and trough encounter F.P., from left to right, respectively	119
Figure 6.10	Relative velocity contours at $x/L_{PP}=0.935$ and $t/T=0$ compared to	120



	EFD	
Figure 6.11	Streamwise velocity contours for different wave steepness	120
Figure 6.12	Total resistance coefficient $C_{TW}$ computed based on grid convergence study for C1	123
Figure 6.13	Heave response computed based on the grid convergence study for C1	124
Figure 6.14	Pitch response computed based on the grid convergence study for C1	125
Figure 6.15	Added resistance in wave schematic representation	126
Figure 6.16	Unsteady signal of the total resistance time history at $\lambda=1.0 L_{pp}$ and $\lambda=1.25 L_{pp}$	127
Figure 6.17	RAO for: (a) heave and (b) pitch compared to EFD data [87] at cases2~8	127
Figure 6.18	Relative wave elevation computed for free and fixed ship conditions	129
Figure 6.19	Free surface profile and mass fraction computed for case C11 at $Fr=0.41$	129
Figure 6.20	Hull wave interaction at $t/T=0$ and $t/T=0.5$	130
Figure 6.21	Relative velocity contours at $x/L_{pp}=0.935$ and $t/T=0$ compared to EFD	130
Figure 6.22	Axial velocity contours computed at equal distances $\Delta x=0.1L_{pp}$ , and second invariant iso-surface=50 at a random momewnt during simulation	131
Figure 6.23	Vortices formation in wave at $t/T=0$ and 0.5 compared to calm water	132
Figure 6.24	Simulation domain and boundary conditions	133
Figure 6.25	Finest grid discretization, spotting: (a) 3D hull; (b): longitudinal section; (c,d): lateral section depicting the refinement boxes around the hull and bilge keels; (e): the free-surface refinement section top view	134
Figure 6.26	Time history for roll simulation at altered initial roll angles	136
Figure 6.27	Fitted decay curves for computed results compared to EFD data	137
Figure 6.28	Time history for roll decay based on: (a) grid & (b) time step convergence tests	138
Figure 6.29	Free-surface topology recorded in the second roll period at the four quarters in case of initial roll angle $\varnothing_0=10$ and $Fr=0.28$	139
Figure 6.30	Time history for roll decay curves corresponding to various ship speeds	140
Figure 6.31	Computed free-surface at the 6 <sup>th</sup> roll for various ship speeds	140
Figure 6.32	Computed and measured velocity contours at $x/L_{pp}=0.675$ for the second roll period instances: (a) $t/T=0.5$ ; (b): $t/T=0.75$	141
Figure 6.33	Vortices formations during the roll period quarters showing: (a) ship bottom, (b, c) starboard port sides, respectively for $t/T=0$	142
Figure 6.34	(a): U contours, (b): TKE contours and (c): $Q^*=25$ second invariant visualized at section $x/L_{pp}=0.675$ at 8 segments of the roll period	144
Figure A.1	Main components of the ship hydrodynamics computational methods	166
Figure A.2	Hierarchy of turbulence models based on physical modeling and computational cost	168
Figure A.3	Most popular turbulence models used in CFD applications	173
Figure A.4	Height function for a 2D open interface	176
Figure A.5	Interface representation using MAC method	177

## List of Tables

	Pg.	
Table 3.1	Geometrically similar grids parameters for a cube	46
Table 4.1	Principal particulars of ship and duct	49
Table 4.2	Boundary conditions for open boundaries and solid walls	51
Table 4.3	Computational grids	52
Table 4.4	$C_T$ results computed at $T=30s$ Compared to EFD data	53
Table 4.5	Sinkage and trim results computed at $T=30s$ Compared to EFD data	53
Table 4.6	Grid convergence parameters for total ship resistance Coefficient $C_T$	54
Table 4.7	Validation data for total ship resistance Coefficient $C_T$	54
Table 4.8	Principal particulars of ship and rudder	61
Table 4.9	Computational cases and corresponding ship speed parameters	62
Table 4.10	Computational grids for ship with and without rudder	63
Table 4.11	Grid convergence parameters for total ship resistance Coefficient $C_T$	64
Table 4.12	DTMB ship models and full scale characteristics	68
Table 4.13	Computational cases and corresponding ship speed parameters	68
Table 4.14	Computational grids for ship based on the wall treatment modeling	69
Table 4.15	Verification and validation parameters for total ship resistance in the wall modeled case	70
Table 4.16	Sinkage and trim results	71
Table 4.17	Computational grids for ship based on the wall treatment modeling	74
Table 4.18	Total resistance computed for the appended hull and appendages drag force	74
Table 4.19	Total resistance coefficient $C_T$ computed for the bare hull component compared to EFD data	75
Table 4.20	Sinkage and trim values computed for the fully appended hull compared to the measured value	76
Table 4.21	Test cases and corresponding ship speed parameters	79
Table 4.22	Measured total resistance and corresponding resistance coefficients	80
Table 4.23	Extrapolated data from the UGAL model to the INSEAN model scale	82
Table 4.24	Total resistance comparison between CFD and EFD results	84
Table 5.1	Principal characteristics and parameters of the JBC propeller	88
Table 5.2	POW simulation cases and flow parameters	89
Table 5.3	Computational grids	90
Table 5.4	Number of grid cells based on simulation conditions and grid density	95
Table 5.5	Self-propulsion results for ship with and without ESD based on actuator disk method	97
Table 5.6	Self-propulsion coefficient for ship with and without ESD using sliding grid method	99
Table 5.7	Self-propulsion results for ship with and without rudder	100
Table 5.8	Principal particulars of KVLCC2 E698 propeller model	102
Table 5.9	Computational grids for the self-propulsion simulation	108
Table 5.10	Thrust and torque coefficients computed using the actuator disk method compared to the EFD data extracted	109
Table 5.11	Interpolation of the propeller rotation based on resistance and thrust results	110
Table 6.1	Simulation conditions and corresponding wave parameters	114
Table 6.2	Computed versus measured $C_T$ , $C_H$ , $C_M$ coefficients	116
Table 6.3	Simulation cases parameters and corresponding grid density	121
Table 6.4	Grid convergence parameter for the total resistance coefficient in wave $C_{TW-G}$	123
Table 6.5	Time step convergence parameter for the total resistance coefficient in wave $C_{TW-T}$	123
Table 6.6	Grid convergence parameter for the heave response	124
Table 6.7	Time step convergence parameter for the heave response	124

Table 6.8	Grid convergence parameter for the pitch response	125
Table 6.9	Time step convergence parameter for the pitch response	125
Table 6.10	Validation parameter for resistance in wave, heave and pitch in C1	126
Table 6.11	Added resistance in waves for cases C2~C8	127
Table 6.12	Heave and pitch responses in at different $Ak$ from C9	128
Table 6.13	Grid arrangement for the grid convergence study	135
Table 6.14	Computed results for roll amplitudes compared to EFD data and corresponding average and mean values for decay fitting curves	137
Table 6.15	Grid convergence study parameters	138
Table 6.16	Time step convergence study parameters	138
Table 6.17	Results for validation test	138
Table 7.1	Ship performance contribution in the present study	150

# Table of Contents

	Pg.
<b>Acknowledgements</b>	i
<b>Abstract</b>	ii
<b>Rezumat</b>	iv
<b>Nomenclatures</b>	vi
<b>Abbreviations</b>	ix
<b>List of Figures</b>	xi
<b>List of Tables</b>	xv
<b>Table of Contents</b>	xvii
<b>Cuprins</b>	xx
<b>Chapter I      Introduction</b>	1
1.1            Motivation	1
1.2            Background	2
1.3            Literature Review	4
1.3.1         Resistance	5
1.3.2         Propulsion	12
1.3.3         Seakeeping	16
1.3.4         Maneuvering	18
1.4            Scope and Objectives	20
1.5            Structure of the Thesis	21
<b>Chapter II      Mathematical Model</b>	24
2.1            Governing Equations	25
2.2            Turbulent Closure Equations	26
2.2.1         Menter Two-Equation Model $k - \omega$ SST	27
2.2.2         Explicit Algebraic Stress Model (EASM)	28
2.3            Boundary Conditions	30
2.4            CFD Process	33
<b>Chapter III     Verification and Validation</b>	36
3.1            Verification and Validation Concept	37
3.2            Verification Methodology	39
3.2.1         Generalized Richardson Extrapolation (RE)	42
3.2.2         Estimating Errors and Uncertainties with Correction Factor	43
3.2.3         Estimating Uncertainties with Factor of Safety	44
3.3            Validation Methodology	44
3.4            Unstructured Grid Generation for Verification and Validation Studies	45
<b>Chapter IV      Ship Resistance</b>	48
4.1            Japan Bulk Carrier (JBC)	49
4.1.1         Analysis Conditions	50
4.1.2         Domain & Boundary Conditions	50
4.1.3         Computational Grids	51
4.1.4         Simulation Strategy	52
4.1.5         Resistance and Motion Results	52
4.1.6         Free-Surface Results	54
4.1.7         Local Flow Results	56
4.2            KRISO Very Large Crude Carrier (KVLCC2)	61
4.2.1         Analysis Conditions	62
4.2.2         Domain & Boundary Conditions	62
4.2.3         Computational Grids	62
4.2.4         Resistance and Motion Results	63
4.2.5         Free-Surface Results	65
4.2.6         Local Flow Results	65
4.3            David Taylor Model Basin (DTMB) Surface Combatant	67

4.3.1	Bare Hull Ship Model	68
4.3.1.1	Analysis Conditions	68
4.3.1.2	Domain & Boundary Conditions	68
4.3.1.3	Computational Grids	69
4.3.1.4	Resistance and Motion Results	69
4.3.1.5	Free-Surface Results	72
4.3.1.6	Local Flow Results	72
4.3.2	Appended Hull Ship Model	73
4.3.2.1	Analysis Conditions	73
4.3.2.2	Domain & Boundary Conditions	73
4.3.2.3	Computational Grids	73
4.3.2.4	Resistance and Motion Results	74
4.3.2.5	Free-surface Results	76
4.3.2.6	Local Flow Results	76
4.3.3	Experimental Test	79
4.3.3.1	Experiment Setup	79
4.3.3.2	Resistance Measurements	80
4.3.3.3	Free-Surface Measurements	81
4.3.3.4	Measurements Validation	82
4.3.3.5	CFD Approach	83
<b>Chapter V</b>	<b>Ship Propulsion</b>	<b>87</b>
5.1	Propulsion Performance of the JBC	88
5.1.1	Propulsion Performance in Open Water	88
5.1.1.1	Analysis Conditions	88
5.1.1.2	Domain & Boundary Conditions	89
5.1.1.3	Computational Grids	89
5.1.1.4	Simulation Strategy	90
5.1.1.5	Thrust and Torque Results	90
5.1.1.6	Wake Flow Analysis	92
5.1.2	Self-Propulsion Simulation	94
5.1.2.1	Analysis Conditions	94
5.1.2.2	Domain & Boundary Conditions	94
5.1.2.3	Computational Grids	95
5.1.2.4	Simulation Strategy	95
5.1.2.5	Self-Propulsion Results	96
5.2	Propulsion Performance of the KVLCC2	102
5.2.1	Propulsion Performance in Open Water	102
5.2.1.1	Analysis Conditions	102
5.2.1.2	Domain & Boundary Conditions	102
5.2.1.3	Computational Grids	103
5.2.1.4	Simulation Strategy	103
5.2.1.5	Thrust and Torque Results	103
5.2.1.6	Local Flow results	104
5.2.2	Self-Propulsion Performance	108
5.2.2.1	Analysis Conditions	108
5.2.2.2	Domain & Boundary Conditions	108
5.2.2.3	Computational Grids	108
5.2.2.4	Simulation Strategy	108
5.2.2.5	Thrust and Torque Results	109
5.2.2.6	Local Flow Results	110
<b>Chapter VI</b>	<b>Ship Seakeeping</b>	<b>112</b>
6.1	Seakeeping Performance in Regular Head Waves	113
6.1.1	Seakeeping in Wave Diffraction Condition	113
6.1.1.1	Analysis Conditions	113
6.1.1.2	Domain & Boundary Conditions	114
6.1.1.3	Computational Grids	115

6.1.1.4	Simulation Strategy	116
6.1.1.5	Resistance, Forces and Moments Results	116
6.1.1.6	Free-surface Results	117
6.1.1.7	Local Flow Prediction	120
6.1.2	Seakeeping in Wave Radiation Condition	121
6.1.2.1	Analysis Conditions	121
6.1.2.2	Domain & Boundary Conditions	122
6.1.2.3	Computational Grid	122
6.1.2.4	Simulation Strategy	122
6.1.2.5	Results	122
6.2	Roll Decay Performance in Calm water	133
6.2.1	Simulation Conditions	133
6.2.2	Domain & Boundary Conditions	133
6.2.3	Computational Grids	134
6.2.4	Simulation Strategy	135
6.2.5	Roll Motion Results	135
6.2.6	Free-surface Analysis	138
6.2.7	Local Flow Analysis during Roll Damping	141
<b>Chapter VII</b>	<b>Conclusions, Contributions and Recommendations</b>	<b>145</b>
7.1	Concluding Remarks	146
7.2	Personal Contributions	149
7.3	Recommendations and Future Perspectives	154
<b>References</b>		<b>155</b>
<b>Appendix A</b>	<b>Numerical Methods used in Ship Hydrodynamics Applications</b>	<b>166</b>
A.1	Physical Modeling	167
A.1.1	Flow Modeling	167
A.1.2	Turbulence Modeling	167
A.1.2.1	Direct Numerical Simulation (DNS)	168
A.1.2.2	Large Eddy Simulation (LES)	168
A.1.2.3	Hybrid RANS/LES (HRL)	169
A.1.2.4	Reynolds-Averaged Navier Stokes (RANS)	170
A.2	Numerical Modeling	173
A.2.1	Reference Frames	173
A.2.2	Spatial Discretization	173
A.2.3	Temporal Discretization	174
A.2.4	Grid Generation	175
A.2.5	Interface Modeling	175
A.2.6	Velocity-Pressure Coupling	178
<b>List of Publications</b>		<b>179</b>
<b>Curriculum Vitae</b>		<b>181</b>

# Cuprins

	Pag.
<b>Mulțumiri</b>	i
<b>Abstract</b>	ii
<b>Rezumat</b>	iv
<b>Nomenclator</b>	vi
<b>Abrevieri</b>	ix
<b>Listă de figuri</b>	xi
<b>Listă de tabele</b>	xv
<b>Table of Contents</b>	xvii
<b>Cuprins</b>	xx
<b>Capitolul I    Introducere</b>	1
1.1           Motivație	1
1.2           Background	2
1.3           Stadiul actual al cunoașterii	4
1.3.1       Rezistență la înaintare	5
1.3.2       Propulsie	12
1.3.3       Seakeeping	16
1.3.4       Manevrabilitate	18
1.4           Scop și obiective	20
1.5           Structura tezei	21
<b>Capitolul II   Modelul matematic</b>	24
2.1           Ecuatiile principale	25
2.2           Ecuatiile de turbulență	26
2.2.1       Ecuatiile lui Menter în modelul $k - \omega$ SST	27
2.2.2       Ecuatiile medelului "Explicit Algebraic Stress Model (EASM)"	28
2.3           Condițiile la limite	30
2.4           Procedura CFD	33
<b>Capitolul III   Verificare și validare</b>	36
3.1           Conceptul verificării și validării	37
3.2           Metodologia pentru verificare	39
3.2.1       Metoda generală a extrapolării lui Richardson	42
3.2.2       Estimarea erorilor și incertitudinilor cu factorul de corecție	43
3.2.3       Estimarea incertitudinilor cu factor de siguranță	44
3.3           Metodologia validării	44
3.4           Generarea de grile nestructurate pentru studii de verificare și validare	45
<b>Capitolul IV   Rezistență la înaintare</b>	48
4.1           Modelul navei Japan Bulk Carrier (JBC)	49
4.1.1       Condiții de analiză	50
4.1.2       Domeniul de calcul și condițiile limită	50
4.1.3       Discretizare	51
4.1.4       Strategia de simulare	52
4.1.5       Rezultate privind rezistența și mișcarea	52
4.1.6       Rezultate privind suprafața liberă	54
4.1.7       Rezultate privind curgerea în jurul navei	56
4.2           Modelul navei tip petrolier (KVLCC2)	61
4.2.1       Condiții de analiză	62
4.2.2       Domeniul de calcul și condițiile limită	62
4.2.3       Discretizare	62
4.2.4       Rezultate privind rezistența și mișcarea	63
4.2.5       Rezultate privind suprafața liberă	65
4.2.6       Rezultate privind curgerea în jurul navei	65
4.3           Modelul navei tip combatant David Taylor Model Basin (DTMB)	67
4.3.1       Modelul navei de carenă nudă	68

4.3.1.1	Condiții de analiză	68
4.3.1.2	Domeniul de calcul și condițiile limită	68
4.3.1.3	Discretizare	69
4.3.1.4	Rezultate privind rezistența și mișcarea	69
4.3.1.5	Rezultate privind suprafața liberă	72
4.3.1.6	Rezultate privind curgerea în jurul navei	72
4.3.2	Modelul navei de carenă cu apendice	73
4.3.2.1	Condiții de analiză	73
4.3.2.2	Domeniul de calcul și condițiile limită	73
4.3.2.3	Discretizare	73
4.3.2.4	Rezultate privind rezistența și mișcarea	74
4.3.2.5	Rezultate privind suprafața liberă	76
4.3.2.6	Rezultate privind curgerea în jurul navei	76
4.3.3	Testul de bazin	79
4.3.3.1	Configurarea experimentului	79
4.3.3.2	Măsurători de rezistență	80
4.3.3.3	Măsurători de suprafață liberă	81
4.3.3.4	Validarea măsurătorilor	82
4.3.3.5	Abordarea CFD	83
<b>Capitolul VI</b>	<b>Propulsia navei</b>	<b>87</b>
5.1	Performanța de propulsie a navei JBC	88
5.1.1	Performanța de propulsie în apă liberă	88
5.1.1.1	Condiții de analiză	88
5.1.1.2	Domeniul de calcul și condițiile limită	89
5.1.1.3	Discretizare	89
5.1.1.4	Strategia de simulare	90
5.1.1.5	Rezultate privind împingerea și cuplul elicei	90
5.1.1.6	Analiza siajului	92
5.1.2	Simulare de autopropulsie	94
5.1.2.1	Condiții de analiză	94
5.1.2.2	Domeniul de calcul și condițiile limită	94
5.1.2.3	Discretizare	95
5.1.2.4	Strategia de simulare	95
5.1.2.5	Rezultate privind autopropulsia elicei	96
5.2	Performanța de propulsie a navei KVLCC2	102
5.2.1	Performanța de propulsie în apă liberă	102
5.2.1.1	Condiții de analiză	102
5.2.1.2	Domeniul de calcul și condițiile limită	102
5.2.1.3	Discretizare	103
5.2.1.4	Strategia de simulare	103
5.2.1.5	Rezultate privind împingerea și cuplul elicei	103
5.2.1.6	Analiza siajului	104
5.2.2	Performanța de autopropulsie	108
5.2.2.1	Condiții de analiză	108
5.2.2.2	Domeniul de calcul și condițiile limită	108
5.2.2.3	Discretizare	108
5.2.2.4	Strategia de simulare	108
5.2.2.5	Rezultate privind împingerea și cuplul elicei	109
5.2.2.6	Rezultate privind curgerea în jurul navei KVLCC2	110
<b>Capitolul VI</b>	<b>Seakeeping</b>	<b>112</b>
6.1	Performanța Seakeeping în valuri regulate frontale	113
6.1.1	Seakeeping în condiția de difracție a valurilor	113
6.1.1.1	Condiții de analiză	113
6.1.1.2	Domeniul de calcul și condițiile limită	114
6.1.1.3	Discretizare	115
6.1.1.4	Strategia de simulare	116



6.1.1.5	Rezultate privind rezistența, forțele și momentele	116
6.1.1.6	Rezultate privind suprafața liberă	117
6.1.1.7	Predicția curgerii în jurul navei	120
6.1.2	Seakeeping în condiția de radiație a valurilor	121
6.1.2.1	Condiții de analiză	121
6.1.2.2	Domeniul de calcul și condițiile limită	122
6.1.2.3	Discretizare	122
6.1.2.4	Strategia de simulare	122
6.1.2.5	Rezultate	122
6.2	Performanța privind amortizarea ruliului în apă calmă	133
6.2.1	Condiții de analiză	133
6.2.2	Domeniul de calcul și condițiile limită	133
6.2.3	Discretizare	134
6.2.4	Strategia de simulare	135
6.2.5	Rezultate privind ruliului	135
6.2.6	Analiza suprafeței libere	138
6.2.7	Analiza curgerii în jurul navei în timpul amortizării	141
<b>Capitolul VII</b>	<b>Concluzii, contribuții și recomandări</b>	<b>145</b>
7.1	Concluzii finale	146
7.2	Contribuții personale	149
7.3	Recomandări și perspective de viitor	154
<b>Bibliografie</b>		<b>155</b>
<b>Anexa A</b>	<b>Metode numerice utilizate în aplicațiile de hidrodinamică a navală</b>	<b>166</b>
A.1	Modelarea fizică	167
A.1.1	Modelarea curgerii	167
A.1.2	Modelarea turbulenței	167
A.1.2.1	Metodă a simulării directe (DNS)	168
A.1.2.2	Metoda simulării vârtejurilor mari (LES)	168
A.1.2.3	Metode hibride RANS/LES (HRL)	169
A.1.2.4	Ecuțiile Reynolds-Averaged Navier Stokes (RANS)	170
A.2	Modelarea numerică	173
A.2.1	Cadre de referință	173
A.2.2	Discretizarea spațială	173
A.2.3	Discretizarea temporală	174
A.2.4	Generarea grilei	175
A.2.5	Modelarea suprafeței libere	175
A.2.6	Cuplaj viteza-presiune	178
<b>Listă de publicații</b>		<b>179</b>
<b>Curriculum Vitae</b>		<b>181</b>

# Chapter I

## Introduction

### 1.1 Motivation

Prediction of the ship hydrodynamic performance is of a major importance in modern ship design. Understanding all related problems of a moving ship, whether in calm water or in waves, is essential to enhance and optimize ship performance to meet the design challenges of the 21<sup>st</sup> century, especially from safety, economy and energy efficiency point of view. The continuous development in the maritime industry increases the demand for more complex geometries and rather intricate design requirements. A need of a robust, flexible and reliable tool to achieve a proper balance between design requirements and design constraints is significantly important.

The past three decades showed a considerable growth of interest in Computational Fluid Dynamic (CFD) as an alternative tool for experimental and empirical based approaches; not just on an academic base, but also for industrial purposes. This progress has reached the milestones of providing the first concept of simulation-based design with extensive capabilities for all ship hydrodynamics problems in both model and full-scale simulations. The broad availability of commercial software, as well as the recent techniques developed for CFD applications gave a proper definition of the physical phenomena, which resulted in higher level of accuracy and more realistic solutions. The currently used methods such as the free-surface modeling (capturing/tracking), turbulence modeling, sliding and overset grid techniques, six Degrees of Freedom (DOF) motions simulations, High Performance Computing (HPC) and automated optimization methods made it possible to cover, not just the main fields of ship hydrodynamics represented by the resistance, propulsion, seakeeping and maneuvering, but also more complicated scenarios such as the stability, capsizing, flooding and interaction between ships. Nevertheless, to increase the fidelity of the numerical results, a continuous improvement of the numerical methods, besides a systematic verification and validation procedures are absolutely necessary.

Following this remarkable success in CFD, especially in model scale simulations, the so-called Numerical Towing Tank (or Virtual Towing Tank) term has begun to impose alongside with classic experimental towing tanks. This technique is widely recognized nowadays, at the level of the most famous maritime organizations, such as the International Maritime Organization (IMO) and the International Towing Tank Conference (ITTC). The latter started recently to provide recommended practice and standardization procedures for CFD codes as it used to do for the Experimental Fluid Dynamic (EFD) since the day of its establishment. The results achieved in CFD are recently used by the IMO to provide new regulations for the assessment of minimum propulsion power to maintain maneuverability under adverse conditions [1]. Still, due to some complications regarding the numerical modeling of the nonlinear flow around the ship, which in some applications cannot avoid the use of approximations or simplified assumptions, and sometimes ignores less important phenomena, these simplifications may generate less accurate results or discrepancies between the CFD solutions and the EFD data or sea trials. Nevertheless, the continuous development in CFD codes associated with the huge development of the computational power is expected to cover more areas of the hydrodynamics and provide more capabilities with fewer approximations.

Taking advantage of the aforementioned opportunities and merits of CFD, and taking into account the present level of accuracy of the numerical solutions, in this study extensive numerical simulations are performed on different types of ships, all aimed at investigating the possibilities of a unique CFD code to solve different ship hydrodynamic problems. The accuracy of the obtained solutions is rigorously investigated through a systematic verification and validation techniques. The global target of these numerical simulations is to predict, where applicable, the forces acting on the hull of the ship under investigation and the flow configurations around that hull, to provide a proper understanding of the physical phenomena and help finding engineering solutions for improving and optimizing the ship hydrodynamic performance in general.

## 1.2 Background

Ship hydrodynamics is by definition concerned with the flow around a given hull and the associated loads induced by the flow itself. Mainly, the attempt to solve a ship hydrodynamic problem is usually focused on calculating the global pressure and the three dimensional velocity components, not only on the submerged part of the ship, but also in the immediate vicinity of it. The further step is to integrate the pressure to compute the forces and moments acting on the hull. Predicting ship hydrodynamic performance can conventionally be divided into four major areas of scientific interest: resistance, propulsion and powering, seakeeping and maneuvering. As mentioned above, any review of the state-of-the-art in the field reveals two different techniques employed to predict the hydrodynamic performance: experimental and theoretical based methods. The former uses experimental modeling of the physical problem, such as in towing tank and cavitation tunnel tests or full scale trials, while the latter uses the theoretical-based approaches to either analyze the data from tank tests, resulting in an analytical technique, or for using the numerical modeling, such as in the case of CFD.

The experimental based methods are the oldest and most accurate method, since it gives a realistic representation of the physical problem. The continuous development in this category continued all over the years and it reached a very reliable level of accuracy and capabilities to capture mostly all the flow details and measure all the corresponding ship hydrodynamic aspects. Unfortunately, its application is very complicated, time consuming and the total cost is very significant.

The statistical- and empirical-based methods were based on two different concepts: the use of systematic hull and propeller series and on the use of statistical data. The systematic series were developed based on a witnessing hull form called “parent” ship. The hull parameters are varied systematically to provide a similar ship from the hydrodynamic performance point of view. On the other hand, empirical-based methods were developed from the same concept and provided empirical formulas for predicting ship resistance and powering for the ship category included in the regression process. Holtrop – Mennen is a famous method in this category. In spite of its apparent attractiveness, it is considered as obsolete [14] mainly because it does not allow much flexibility in taking decisions for a new concept design. Besides, it is only concerned with the forces and moments acting on the hull, while the flow configurations and free-surface are completely disregarded.

The numerical-based methods started to take place in the late 1950s and were basically restricted with the computational power. However, after the advent of computers, the CFD method was implemented in marine hydrodynamics in the mid-1970s following its remarkable success in the aerodynamics field at that time. The largest majority of CFD solvers were initially based on potential flow due either to the limited computation capacity

that was available in that era or to the insufficient development of appropriate numerical methods. The largest majority of CFD solvers nowadays implement the Reynolds-Averaged Navier-Stokes Equations (RANSE hereafter) with a wide range of turbulence models that can help the accurate prediction of the flow characteristics around the hull as well as the free-surface topology and wake flow structure. Recent researches are based on Large Eddy Simulation (LES hereafter) or a hybrid RANSE and LES as a solution to reduce the needed number of cells in the far field which is known as Detached Eddy Simulation (DES hereafter). Most recently, the Direct Numerical Simulation (DNS hereafter), which includes the direct solution of Navier-Stokes Equations (NSE hereafter) without further assumptions for turbulence, is being used for relatively limited applications in ship hydrodynamics because it proved to be prohibitory expensive; yet, it is expected to gain more popularity in the coming decades.

## 1.3 Literature Review

In the followings, the most spectacular CFD achievements in the field of ship hydrodynamics will be reviewed separately for the four main areas previously mentioned, i.e. resistance, propulsion, seakeeping, and maneuvering, respectively. To make the review more specific to the scope of the present thesis, a special focus on the viscous flow solution of the NSE will be provided, aimed at covering as much as possible the specificity of the ship hydrodynamic solvers since they represent the basic tool used in the work performed in the following chapters of the present thesis. The alternative techniques such as experimental, empirical, theoretical or potential based methods are also reviewed but without entering into too many details, just to highlight their strengths and drawbacks.

### 1.3.1 Resistance

The early stage of assessing the associated ship hydrodynamic problems was basically standing for ship resistance and powering due to the need of an accurate estimation of the required power to reach the target design speed. Since the establishment of Froude's principle, the tank testing took the lead in predicting the ship resistance for many decades after that. However, even though the method was shown as being sufficiently accurate for predicting the overall resistance, the wave making component was not clearly defined. A remarkable effort was paid parallel to the development of new towing tank testing techniques and equipment, in advancing complementary analytical approaches meant to derive alternate tools to determine the otherwise unknown components. Early studies delivered by the end of the 19<sup>th</sup> century and the beginning of the 20<sup>th</sup> century [15–19] may sustain the statement before. Most of these approaches were mainly based on the regressive data obtained at the towing tank tests.

With the computers advent, the analytical approaches loosed in popularity and begun to be used less and less. Due to the limitations of the computational power, the potential flow theory-based methods, in which the flow is considered incompressible, inviscid and irrotational, were seen as a workable alternative for a certain period of time. Most of the researches were suited to solve the problem in 2D. The first approach that succeeded to solve the problem for arbitrary 3-D bodies was the method developed by Hess and Smith [22]. The method was simple and fast to solve; nonetheless, it could not be used to solve free-surface flows, and the principle of hull mirroring caused other contradictions that led in some cases to zero resistance.

To solve the free-surface problems, the linearization technique was proposed to simplify the problem; unfortunately, the linearization of the free-surface flow problem have

proven in most of the cases a satisfactory accuracy not only for the ship resistance, but also for the free-surface prediction, at low CPU costs, which is essentially important for common industry needs. Yet, the wave separation and radiation were neglected. That led to the appearance of nonlinear methods to solve wave resistance problems. A well-recognized effort in this scope was made in [25] and [26]. The nonlinear methods for wave resistance simulations have better advantages than the linearized simulation. For example, in the linearized simulation, the domain is bounded by an undisturbed free-surface; this leads to low accuracy for large bow flares or bulbous bow and flat stern. Moreover, the linearization does not account for sinkage and trim, which might be essential for nonlinear contributions. On the other hand, one of the problems associated with the nonlinear simulations is often associated to the convergence. As said before, until the beginnings of 1990's it was common to avoid divergent solutions of the nonlinear simulations by employing the linearization [27].

A step ahead taken by the naval architecture community was represented by the use of the boundary layer theory in predicting the intrinsic features of the flow around the ship hull. Although restrictive to a very limited domain around the solid surface, the approach allowed a deeper insight into the frictional resistance estimation. The most frequently used technique to predict the boundary layer flow in the late 1970s and early 1980s was the momentum integral method, as mentioned in [30]. The method was successful for the 2D flows, but it was very difficult to extend it for the 3-D flows due to the complexity of modeling the cross-flow velocity profile [31].

A tremendous effort had to be paid in the early days of the numerical hydrodynamics to reduce the computation costs required to solve a given problem. Fig. 1.1 shows the classification of methods used in viscous computational hydrodynamics. Unlike the potential flow method, which implies only the discretization of the hull and water surface, in the viscous flow approach the full domain has to be discretized, therefore this led to a series of restrictions due to the existing computational resources limitations at that time.

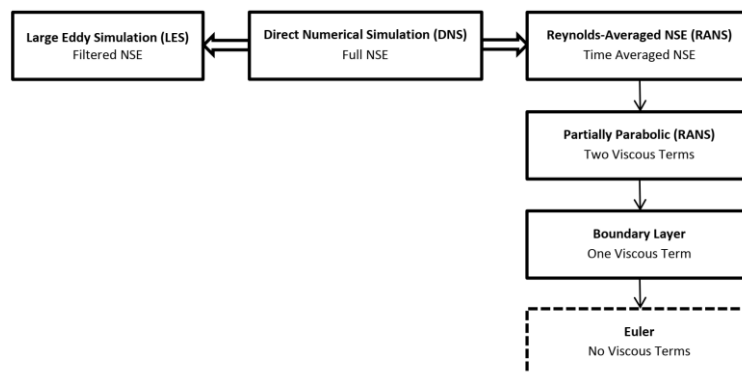


**Figure 1.1** Classification of methods used in viscous computational hydrodynamics [27]

Historically, the first step taken in computing a RANS solution was based on the double-body approach, which simply neglected the free-surface existence and used the symmetry condition along the water surface. The method in itself has been derived from the Hess and Smith work [22] which was devised for aerodynamics applications. Although the approach, in its initial formulation, could not predict the wave resistance, it proved to be enough suitable in determining not only the frictional resistance component, but also the flow structure in the wake.

The focus on using RANS solvers was obvious in the 2<sup>nd</sup> Workshop on Ship Viscous Flow, Gothenburg 1990, where 19 research groups from 12 countries submitted their numerical solutions computed around the HSVA and “Mystery” tankers. 17 solutions were

computed with RANS solvers while only one was based on boundary layer theory and one on the LES [37]. The advantage of the solutions reported in this workshop compared to the previous one was that most of them could predict the intrinsic features of the flow near the propeller plane; however, results inside the propeller disk were less satisfactory due to the inaccurate prediction of the bilge vortex and to the failure in capturing the characteristic “hook” shaped streamwise velocity distribution in the boundary layer, as revealed years later by Wilson in its monograph review [38].

The third Workshop on Computational Ship Hydrodynamics that was held in Tokyo 1994 included viscous flow solution with the free-surface for a series 60 and HSVA tanker ships. Most of the RANS solutions predicted accurately the free-surface for the series 60 ship; however, a damping effect was observed away from the ship hull due to the insufficient grid resolution to predict the transverse and divergent wave systems [41].

In the Gothenburg 2000 Workshop on Computational Ship Hydrodynamics (G2K) the declared scope was to assess not only the state-of-the-art in the numerical ship hydrodynamics, but also to mark the latest progress in the field. Moreover, the organizers provided standards and guidelines for further developments. For that purpose new modern designs were proposed for three different hulls: the KVLCC, the KCS and the US surface combatant DTMB [43, 44]. A special attention was given for predicting the stern flow of the KVLCC ship to capture the hook shape vortices, while a different interest in predicting the stern flow was for the DTMB hull due to the presence of the transom stern. For the first time in the workshop history, a self-propulsion case was considered and validation data from extensive tank tests were provided, so an assessment of the numerical simulation solutions was requested by the organizers to provide detailed validation studies.

Five years later, the workshop was held in Tokyo in 2005. The participants were subjected to submit their solutions computed for the same three hulls as in the previous edition of the workshop, but new tasks such as the self-propulsion at propulsion point for the KCS ship, the static drift for the KVLCC and the unsteady flow for forward speed diffraction seakeeping for the DTMB were imposed by the organizers. A total of 20 groups of researchers participated with solutions computed by using both in-house and commercial codes based mainly on RANS, as described in [45]. A comparative analysis of the submitted solutions revealed slight differences compared to the previous workshop. For the KVLCC model, the reported solutions for ship resistance computations unveiled a higher scatter for the computed force compared to the results obtained in the G2K Workshop, while the flow prediction in the stern revealed a better agreement in predicting the hook-shaped wake profile, especially for the Reynolds stress turbulent models. For the KCS model, the solution of the computed ship resistance was in a better agreement with the EFD data compared to the G2K Workshop, while for the local flow, a similar accuracy with a minor improvement for the boundary layer thinning nearby the center plane was reported. For the free-surface, a well predicted Kelvin wave pattern was observed with less dissipation in the far field in contrast with the previous workshop. The DTMB simulations were reported by 11 research groups and an encouraging overall accuracy in predicting the resistance was concluded. Aside of that, a better prediction of the free-surface topology seemingly due to the increment of grid resolution was reported in comparison with G2K. The streamwise wake flow structure inside the stern region was computed by 10 groups out of the 11 participants with a variable level of accuracy, showing a good prediction for the boundary layer thinning.

In 2010, the workshop was held in Gothenburg, Sweden. The same ship models of the KVLCC, KCS and DTMB hulls were proposed, but imposing new particular simulation conditions, i.e. resistance, propulsion and seakeeping. A total number of 89 competitors were

registered in the prediction of the computed resistance for different speeds, fixed and free sinkage and trim conditions, for a hull with and without a rudder.

The following workshop in Tokyo 2015 and the last one so far maintained the same principle of the previous workshops to assess the state-of-the-art in numerical ship hydrodynamics and to provide guidelines for further developments in the field. Two new hulls were introduced, i.e. the capesize Japan Bulk Carrier (JBC hereafter), which has been designed with an energy saving device at the aft region and the modern surface combatant ONRT, which has a wave piercing hull design with 10° inclined tumblehome sides and a transom stern. The model is appended with two bilge keel stabilizers, a pair of rudders, shafts, and propellers and four propeller shaft brackets [48]. The KCS hull was introduced again in the workshop with two proposed geometrical modifications in the forward part which include an extension of the bulwark on the forecastle to prevent the green water embarking during the seakeeping simulation. 88 research groups reported their solutions for the ship resistance computed for the JBC hull with and without the energy saving device.

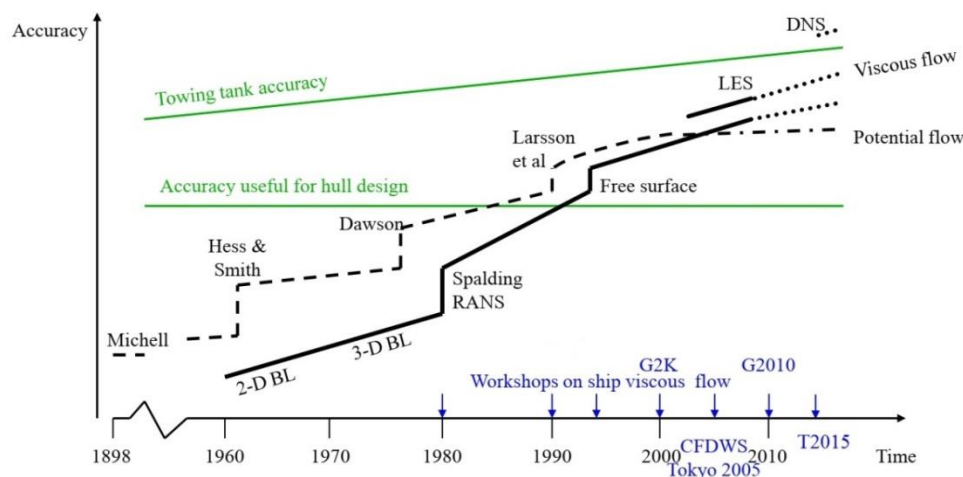


Figure 1.2 The development of CFD in ship hydrodynamics [51]

### 1.3.2 Propulsion

In the past three decades, the viscous RANS method begun to gain in popularity as well. The early attempts were applied on simplified propeller geometries such as the one considered in [68], where the propeller-shaft geometry was idealized based on infinite-pitch rectangular blades. The obtained results were compared to another solution based on lifting-surface method showing that the proposed approach could predict accurately the blade loadings including the viscous effect and revealed the ability to solve the viscous region in distinction from the inviscid-flow approach.

An early attempt to solve the propeller behind the ship was done based on combining the benefits of both BEM and RANS methods, hybrid RANS/BEM methods were consequently developed, in which the propulsor inflow is solved by using a viscous flow solver, while the propeller effect is represented by a body force model [70]. The obtained results were within a satisfying level of accuracy compared to the EFD data with a good prediction of flow details. Recently, the DES and LES methods are aggressively spreading due not only to the augmentation of the available computation power but also to their versatility in reproducing accurately the intrinsic flow features.

The review of the state-of-the-art in ship propulsion whether in open water or working behind the ship shows that the viscous flow CFD-based method is gaining more popularity and rather becoming a common practice tool for engineers. The achieved level of accuracy of the numerical solutions obtained is more than sufficient for design purposes or for propeller design optimization.

### 1.3.3 Seakeeping

Studying the ship behavior in waves is an important issue for the initial design stage. The added resistance in waves is crucially important to be taken into consideration for an accurate ship powering estimation, as well as to satisfy the new powering requirements imposed by the Energy Efficiency Design Index (EEDI) and Energy Efficiency Operational Indicator (EEOI), which are regulated by the IMO and Marine Environment Protection Committee (MEPC). From the safety point of view, severe ship motions in waves may have a considerable influence on the ship stability and operability. Many researchers have developed approaches to predict ship performance in waves using EFD, potential flow solvers and viscous-based methods.

The experimental approach was the fundament of predicting the seakeeping performances along with the analytical methods till the early 1970s. Experiments are usually performed for the ship models moving either in regular or in irregular waves artificially generated by hydraulically-powered wave makers. Seakeeping tests are extremely expensive especially due to the prohibitive costs of the onset equipment. Aside of that, because the number of the personnel involved in such an experiment is larger than usual, the human resources costs are also high. Last, but not the least, the experimental investigation is expensive because of the long waiting periods required between tests until the water has to completely calm down and come back to the initial rest condition again. The waiting periods are especially long in standard towing tanks. Aside of that, depending of the number of the degrees of freedom of the model and the sea state, the scope of the experiments is usually complicated considering the fact that many parameters need to be varied, e.g. wave length, wave height, angle of encounter, ship speed, draught and trim, metacentric height etc. [14].

The potential flow-based methods either linear or nonlinear were the most frequently used method in the theoretical seakeeping investigation for the past five decades because of its simplicity and efficiency in terms of the CPU time needed to be performed at a satisfactory level of accuracy. The linear potential flow seakeeping solvers based on the strip theory, source distribution method, panel method and more recently enhanced unified theory, were widely used by ship researchers [82]; but because of limitations of the models, the solutions had some drawbacks determined mainly by the neglected viscous effect, otherwise very important for the phenomenon in itself.

Recently, as computational facilities have become more powerful and more accessible, CFD tools are commonly used to predict not only the added resistance, but also the ship motions in waves of different characteristics. They have proven obvious advantages over the potential codes as they can deal directly with large amplitude ship motions and nonlinear flow phenomena such as breaking waves and green water embarking, without explicit approximations and empirical value corrections [83]. The largest majority of the seakeeping computations conducted nowadays are performed based on the URANSE solvers, whereas only a few simulations are based on the LES and DES approaches. The capturing of the free-surface is made based either on the VOF method or on the level set method. Incoming waves are mainly assumed as being linear and enforced on the domain boundaries.



Structured or unstructured multi-block or overset grids are used for the numerical study of the ship motions. Numerical methods mainly use second order discretization schemes for spatial and temporal terms. High performance computers are more and more frequently used in the simulations, a fact which allows the use of small grid sizes at the free-surface and inside the boundary layer as well as smaller time steps aimed to capture the motions in waves more accurately [35].

CFD methods are now applied to a wide variety of seakeeping problems, including added resistance and motions in waves, roll decay, parametric rolling, and to violent and complex flows such as green water, sloshing, slamming, water embarking and water entry. The ability of CFD to simulate the free running vessels in waves has been improved significantly through the past decade, opening up the possibility of applying CFD to the complex problem of a ship maneuvering in waves [96].

### **1.3.4 Maneuvering**

Maneuverability of a ship has a very significant influence on the efficiency and safety of maritime transportation in general. The maneuvering quality of a ship has to be assessed in the various design stages and after the ship is built to insure that the quality of the designed ship is compatible with the requirements of the IMO Maritime Safety Committee. This assessment can be done based on experimental tests, mathematical models or a combination of both. Experimental methods for ship maneuvering are done for model scales in radio-controlled model basins or using radio-controlled models in lakes and large reservoir [97]. Though model testing is always considered as accurate as physical tests, unlike resistance and propulsion tests, the scale effect in maneuvering is quite significant and requires special treatment due to the fact that the forces and moments on the hull are highly dominated by the viscous effect and flow separation. Obviously, the most accurate results will be those predicted in the full scale ships in the sea trials; nevertheless, imposing modifications after the ship is delivered is extremely difficult. The mathematical models can be divided in two categories; the first is using Taylor series expansion for hydrodynamic forces and moments about a suitable initial condition [98]. This approach is suitable for computer simulations, since it contains the hydrodynamic added mass and damping coefficients that are necessary in predicting the maneuvering characteristics of a marine vehicle. The second is the response or modular model; in which, the hydrodynamic forces and moments are divided in three components for the bare hull, rudder and propeller. This approach investigates the responses of the ship motion due to the rudder action to solve the course keeping problems [98]. In practice, there also existed some series to predict maneuvering performance of a ship, such as the one presented in [99]. An early commonly used method for predicting the turning and steering of a ship is to use equations of motion with experimentally determined coefficients. Once these coefficients are determined for a specific ship design, equations of motion are used to simulate the dynamic behavior and controllability of that ship in various operating conditions [97]. This Coefficient based predictions have been used in the selection of rudder size and steering control systems, and in estimating the turning characteristics of ships [100].

Numerically, the simplest approach to body force computations is the use of regression formulae based on slender-body theory, but with empirical coefficients found from analyzing various model experiments, e.g. [101]. The next more sophisticated approach would be to apply slender-body methods directly, deriving the added mass terms for each strip from analytical or BEM computations [14].

One of the main advantages of CFD is its ability to provide information about hydrodynamic loads and motions of the vessel together with detailed flow field information, which can help to understand the flow physics related to maneuvering. Another advantage is that this type of simulation does not rely on model testing with physical scale models, which means that for instance the hull form or the rudder can be changed relatively easy. This is useful in the early design phase where CFD can help to investigate maneuvering related issues and help to improve the design. Therefore, CFD is used ranging from detailed flow studies (to learn about the features of the flow field) for prediction of hydrodynamic forces and moments to direct simulation of maneuvers. This applies to both surface ships and submarines. It seems that in addition to the traditional RANS approach, also DES and DDES have started to show up in practical applications [108].

## 1.4 Scope and Objectives

The general scope of this thesis is to study numerically the ship hull hydrodynamic performances in different operating conditions. Nonetheless, an experimental validation of the numerical computed solutions is provided within the limits of the existing experimental facilities in the laboratory the thesis was carried out. The rest of validations were done based on experimental data provided for several benchmarking cases by the most appreciated hydrodynamic labs in the world, whose data are freely provided in the public domain. The red wire of the present work was to develop several robust and reliable methods to simulate various ship hydrodynamic problems using the CFD tools as a complementary or even as an alternative method to the experimental and empirical approaches. Viscous flow solver is utilized for this purpose, based on the RANSE, either in steady or unsteady regimes, depending on the problem of concern. A thorough investigation for the physical hydrodynamic phenomena in each case study is included, such as: velocities, pressure, free-surface, turbulence, boundary layer, vorticity, motions and general flow visualization, to provide a proper understanding for each case, and discuss upon the credibility and/or finding practical solutions for the given problems of interest. The ultimate goal was to investigate the capabilities and limitations of the CFD methods to simulate accurately the ship performances related to the: hydrodynamic resistance, powering, seakeeping. The numerical solutions are rigorously evaluated through systematic verification and validation procedures to assess the numerical uncertainties and to account for the errors associated in the numerical approach, to demonstrate, not just the accuracy of the numerical model, but also its robustness.

To achieve this purpose, extensive numerical studies are performed for the selected types of ships, which can be categorized based on type as commercial and special purpose ships, and based on mode of operation as slow and fast ships. The present study is aimed at complying with the previous researches in the field, as previously described in the literature review, and providing, when necessary, alternative and more simplified solutions for some problems.

Since the scope of this research work is sufficiently broad and rather challenging to cover entirely all the associated topics, the following main objectives will be considered during the preparation of the present thesis, to make the problem understandable for the reader. The thesis objectives can therefore be simply outlined as follows:

1. Ship resistance. Studies on:
  - i. the bare hull ship resistance for fixed and free sinkage and trim conditions;
  - ii. the effect of special appendages on the ship resistance and the wake flow in the stern, such as rudders and energy saving devices (ESD);

- iii. the fully appended ship to investigate the capability of the numerical model to predict the influence of the appendages on the flow around the hull;
  - iv. the integration between experimental and numerical approaches to account for the banking effect for the fast ships in towing tank
2. Ship propulsion. Studies on:
    - i. propeller performance in open water;
    - ii. propeller performance behind the ship using two different approaches, including the body force method and fully discretized propeller;
    - iii. the influence of the ESD on the propulsion efficiency;
    - iv. the interaction between ship, propeller and rudder;
  3. Ship seakeeping. Studies on:
    - i. seakeeping performance in speed diffraction problem;
    - ii. seakeeping performance of ship hull in different sailing conditions, including vertical motions and added resistance in waves;
    - iii. local flow assessment during ship sailing in waves and its influence of the flow characteristics;
    - iv. the viscous effect on the roll decay of the ship at different roll angles, including the effect of bilge keels;

## 1.5 Structure of the Thesis

This thesis is structured in seven chapters; the review, which includes an introduction and a background survey of the most relevant issues that shape the essence problem, accompanied by a historical review of the most significant previous researches in the field, are given in the first chapter.

The second chapter is devoted to the mathematical model that describes the physics behaving the phenomena studied in the thesis. The chapter includes the numerical representation of the governing equations and solution algorithms and finally, the basic procedures for the solution process of a general CFD approach in ship hydrodynamic.

Since the CFD is a numerical method that is subjected to the presence of errors and uncertainties, the error classification and the systematic verification and validation process are presented in Chapter III, with a special focus on the possible techniques and the main aspects to reduce or mitigate the numerical errors. A special concern regarding the grid generation for an unstructured grid solvers is covered to ensure the grid similarity during the simulations.

The numerical solutions are presented and discussed starting from chapter four, which includes the results for ship resistance computations. The first study includes a detailed investigation of the JBC, which includes an ESD between the hull and propeller to enhance uniformity of the wake inflow into the propeller. The study includes analyses for the resistance, ship motions, free-surface configuration and wake flow inner particularities for the ship with and without the ESD; besides, a detailed investigation of the effect of the ESD on the total resistance is carried out.

The second part of the chapter includes a numerical simulation for the KVLCC2 hull model to compute the bare hull ship resistance and the free-surface topology for a fixed and free sinkage and trim conditions. The results are presented for the computed forces, velocity and pressure contours on the hull and the wake, and finally, the free-surface flow in the near and far-field region with respect to the hull is detailed. The influence of the rudder existence at the aft of the ship is also investigated for different ship speeds.

Since both ships can be included in the high block-coefficient and slow speed ship category, a third study is applied on the surface combatant DTMB ship model, which can be considered as a medium-to-high speed ship. The scope of the investigation is to assess the accuracy of the numerical model for the high speed ships and to set the base for the appended ship resistance simulations which are applied specifically on the DTMB ship in the end of this chapter. Both studies are concerned with the forces, motions, free-surface and local flow around the hull and particularly the appendages.

The final part of the fourth chapter describes the validation of the numerical results based on the experimental work performed by the author in the towing tank. The experiment is carried out for the DTMB ship hull to assess and validate the numerical solutions from the global hydrodynamic forces and free-surface topology point of view. The tank banking effect is also investigated and its influence on the ship resistance and free-surface reflections is covered experimentally and numerically.

The fifth chapter contains the propulsion simulations divided into two sections. The first section of this chapter covers the Propeller Open Water (POW) simulations for the model propellers of the JBC ship. The study stands as a basic step to predict the open water performance of the propeller to use further in the self-propulsion simulations. In this study, a special focus is devoted to the accurate estimation of the forces and moments acting on the propeller, as well as to the distributions of pressure, velocity, turbulent kinetic energy on the propeller blades. Consideration is also given to the vortices formation process. The second section includes the self-propulsion performance estimation of the JBC propeller for two cases when the ship is equipped or not with the ESD. Two different approaches are used to solve this problem based on the body force method and fully discretized propeller.

The second part includes similar analysis for the open water performance of the KVLCC2 propeller model using different turbulence models based on RANS and Hybrid RANS/LES models to have a proper representation of the wake flow of the propeller and better understanding of the vortices formation. Later, the interaction between the hull, propeller and rudder is numerically studied and discussed for the KVLCC2 ship based on the body force method and fully discretized propeller.

The sixth chapter is covering the seakeeping simulation for the DTMB ship in regular head waves. Two different scenarios are analyzed for this particular hull, including speed diffraction problem, when all the motions of the ship are restrained, while the second is presented for radiation problem including 3-DOF, surge, heave and pitch. A special consideration for the roll motion is also analyzed for the same ship in the roll decay condition in calm water. The roll decay is computed for different initial roll angles and compared with the existent experimental data. The effect of numerical parameters on the accuracy of the roll decay simulation is investigated, along with the speed effect on the roll damping process and free-surface prediction during roll damping process. Finally, a consistent study is focused on the viscous flow interaction between the hull and bilge keels in order to understand the viscous mechanism of damping.

The final conclusions, the personal contribution as well as the steps to be taken in a future work are summarized in chapter seven.

Appendix A gives a general overview about the solution method in ship hydrodynamic viscous flow applications based on the RANSE approach, with a general description of the mostly employed techniques in terms of the: spatial and temporal discretization methods, grid generation, free-surface definition (interface capturing/tracking), turbulence modeling, motion adaptation, and boundary conditions formulation.



## Chapter II

# Mathematical Model

Since the CFD method is basically a numerical representation of a physical problem, it is important to turn the focus now on the mathematical model representation for the flow solver used in all the various numerical solutions obtained in this thesis.

The numerical solver used exclusively in all the numerical simulations whose results will be presented in the following chapters of this dissertation is the ISIS-CFD viscous flow solver of the commercial software FINE<sup>TM</sup>/Marine available under the NUMECA suite. The solver is created by EMN "Equipe Modélisation Numérique", i.e. the Department of the Fluid mechanics Laboratory and developed by Ecole Centrale de Nantes and Centre National de la Recherche Scientifique CNRS [88, 109]. It is based on the finite volume method to build the spatial discretization of the transport equation in order to solve the incompressible, unsteady Navier-Stokes equation. The spatial discretization is face-based which constructs the fluxes face by face, giving the solver a flexibility to use unstructured meshes with non-overlapping control volumes bounded by an arbitrary number of arbitrarily-shaped faces. The temporal discretization is enforced through a cell centered implicit second order three-level scheme. The velocity and pressure coupling is achieved through a Rhie and Chow SIMPLE algorithm, in which the velocity field is obtained from the momentum conservation equations and the pressure field is extracted from the mass conservation constraint, or continuity equation, transformed into a pressure-equation [40]. Turbulent flows are treated by introducing additional transport equations for modeled variables in the same principle as the momentum equation and they are discretized and solved accordingly. A variety of turbulent closure models are available such as the eddy viscosity models including the one-equation Spalart-Allmaras model, two-equation standard  $k-\epsilon$  and the standard  $k-\omega$  Wilcox model, Menter's  $k-\omega$  baseline and SST models. One Algebraic Reynolds Stress models is also available represented in the EASM model. Finally, hybrid models are also available such as DES models and most recently the DDES and IDDES were introduced starting from version FINE<sup>TM</sup>/Marine 8.1. Gradients are computed based on a Gauss's theorem approach. Formal first-order and second-order accuracy are achieved, respectively, through non-orthogonal corrections and piecewise linear upwind stabilizing approach for inviscid fluxes. Central difference scheme is used for viscous fluxes to insure a first-order formal accuracy. The free-surface is modeled using a multi-phase flow approach applying the volume of fluid VOF free-surface capturing technique. Incompressible and non-miscible flow phases are modeled through the use of conservation equations for each volume fraction of phase/fluid [88]. Propeller modeling is allowed based on both, the body force method solved based on the infinite-blade actuator disk; besides, a fully discretized propeller can also be handled with the aid of sliding or overset grid.

Governing equations and all the related mathematical modeling of the solver, turbulence closure equations for  $k-\omega$  and EASM models, general boundary conditions are given in the following sections. All the numerical details including their applications and mathematical representation in the solver can be found with complete details provided by Queutey and Visonneau in [109].

## 2.1 Governing Equations

The RANS equations for incompressible flows including external forces, the averaged continuity and momentum equations can be written in tensor form, in the Cartesian coordinate system as

$$\frac{\partial(\rho\bar{u}_i)}{\partial x_i} = 0 \quad (2.18)$$

$$\frac{\partial(\rho\bar{u}_i)}{\partial t} + \frac{\partial}{\partial x_j}(\rho\bar{u}_i\bar{u}_j + \rho\overline{u'_i u'_j}) = -\frac{\partial\bar{p}}{\partial x_i} + \frac{\partial\bar{\tau}_{ij}}{\partial x_j} \quad (2.19)$$

where  $\bar{u}_i$  is the relative averaged velocity vector of flow between the fluid and the control volume,  $\overline{u'_i u'_j}$  is the Reynolds stresses,  $\bar{p}$  is the mean pressure and  $\bar{\tau}_{ij}$  is the mean viscous stress tensor components for Newtonian fluid under the incompressible flow assumption, and it can be expressed as

$$\bar{\tau}_{ij} = \mu \left( \frac{\partial\bar{u}_i}{\partial x_j} + \frac{\partial\bar{u}_j}{\partial x_i} \right) \quad (2.20)$$

## 2.3 Boundary Conditions

The NSE is as second-order partial differential equations. In order to solve this system of equations, it is necessary to define the initial conditions on all the boundaries of the computational domain. The unknown variables in the domain must be clearly defined, such as the three components of velocity,  $u, v, w$ , the pressure  $p$  and the turbulent model unknown variables, such as in case of the two-equation eddy viscosity models it stands for turbulent kinetic energy  $K$  and turbulent dissipation  $\varepsilon$  or dissipation rate  $\omega$ .

It is worth mentioning that boundary conditions in ship hydrodynamic are dependent of the type of simulation performed; however, there are generic boundary conditions that can be applied on the main boundaries that must be included in the computational domain, such as the solid body (hull), free-surface and far-field. There are also other boundary conditions that are specific to the simulations such as the wave generators in the inlet for seakeeping simulations or the specific boundary conditions for sliding or overset grids.

In the following context, an outline of the generic boundary conditions is given for each boundary individually, while the specific boundary conditions are going to be noted in particular regarding the type of simulation performed, as for seakeeping, sliding grids or other simulations that will be presented in the following chapters.

### – Solid Body (Ship Hull)

As a consequence of the viscous interaction between the submerged part of the hull and fluid, the moving hull is causing a disturbance on the molecular level. Molecules from one phase interact with another phase due to ship motion, colliding with the molecules of the other phase. The phases are thus combined in a very thin layer, and the tangential velocity of the molecules is transferred from one side to another. The velocity difference between the two phases is smoothed out, and basically it is assumed that the difference is equal to zero, which means that the fluid is attached to the solid surface. This is known in the CFD field as the “no-slip” condition which can mathematically be expressed as

$$u = v = w = 0 \quad (2.41)$$

In general, the ship hull is not the only solid wall included in the domain, there are other surfaces that are treated as a solid wall, such as the seabed and banks, which are very common to be found in restricted water channels and depth simulations, the corresponding boundary condition could be written as

$$u = -U \text{ \& } v = w = 0 \quad (2.42)$$

where these surfaces are assumed to be moving backward with respect to the ship speed  $U$ .

### – Free-Surface

The aforementioned no-slip condition is applicable for both air and water parts, though the density of air is very much less than that in water. As a result for the molecular interchange at the interface between air and water, both will gain the same speed at the free-surface. Besides, the equilibrium of the tangential forces at the interface must be maintained

$$\begin{aligned} \sigma_{(ns)_w} &= \sigma_{(ns)_a} \\ \sigma_{(nt)_w} &= \sigma_{(nt)_a} \end{aligned} \quad (2.43)$$

where  $w$  and  $a$  refer to water and air, respectively, and  $s, t, n$  represent a local Cartesian coordinate system with  $n$  normal to the surface [27]. The effect of surface tension  $\Delta p_\gamma$  should be also taken into consideration; hence, the normal force equilibrium that represents the dynamic boundary condition on the free-surface is given by

$$(\sigma_{nn} - p)_w = (\sigma_{nn} - p)_a + \Delta p_\gamma \quad (2.44)$$

However, the viscous stresses are usually very small and can be neglected. Thus, the inviscid dynamic boundary is basically transformed into a water surface pressure as

$$p = p_a - \Delta p_\gamma \quad (2.45)$$

where  $\Delta p_\gamma$  expresses the pressure jump due to surface tension and can be defined as

$$\Delta p_\gamma = \gamma \left( \frac{1}{r_1} + \frac{1}{r_2} \right) \quad (2.46)$$

where  $\gamma$  is the surface tension and  $r_1$  and  $r_2$  are the principal radii of curvature of the free-surface [27].

The kinematic condition on the surface also must be fulfilled, where it indicates that there is no flow through the surface. This is satisfied if the vertical velocity of a water particle moving along the surface are be equal to the total time derivative of the wave as [27]

$$w = \frac{d\zeta}{dt} \quad (2.47)$$

where  $\zeta = \zeta(x, y)$  is the equation for the free surface.

As previously mentioned in the interface modeling section that the new techniques in the air-water interface modeling that are used recently, such as level set or VOF methods, do not explicitly enforce these boundary conditions; however, the conditions are satisfied automatically from the implementation of the indicator function.

### – Infinity

Despite the fact that the computational domain is usually bounded, it is common practice to consider the flow domain to be infinite at one or more boundaries. Hence, the boundary condition can be applied based on the assumption that the flow at the infinity is not disturbed such that



$$u = U, v = w = 0, p = p_\infty \quad (2.48)$$

where  $p_\infty$  represents the undisturbed pressure.

It is worth mentioning that these are the mathematical boundary conditions. Since the computational domain is always limited in numerical methods, artificial numerical boundaries must be introduced, where the pressure and velocities, or their derivatives in one direction, will have to be essentially identified.

### – **The Turbulence Model**

The vast majority of the numerical simulations performed in this thesis used mainly the  $k - \omega$  SST model or EASM after proving their capabilities of giving a reasonable balance between the accuracy and computational cost. Though some other turbulence closure models were investigated, as it will be introduced in Chapter V, these models were the ones selected for the rest of the numerical simulations to be followed. For this reason, the boundary conditions for the default free-stream values of the turbulent kinetic energy, turbulent viscosity and the dissipation rate, which are applicable for both models  $k - \omega$  SST and EASM, can be expressed mathematically as

$$K_\infty = \lambda \frac{\mu_{t_\infty} \omega_\infty}{\rho}; \omega_\infty = \lambda \frac{U_\infty}{L} \& \mu_{t_\infty} = 10^{-3} \mu_t \quad (2.49)$$

where  $L$  and  $U_\infty$  are the characteristic length and a characteristic velocity of the simulation, respectively. The factor of proportionality  $\lambda$  can be chosen between 1 and 10. Default value is chosen as  $\lambda = 1$  [110].

Wall boundary conditions are given by the following equations

$$K = 0 \& \omega = 10 \frac{6\mu}{\beta \rho (\Delta y)^2} \quad (2.50)$$

where  $\Delta y$  is the distance of the first point away from the wall, such that  $y^+ < 1$ .

In addition to all the aforementioned conditions, there are other conditions that might be considered general for numerical simulations in viscous ship hydrodynamic solvers such as the outflow and the symmetry boundary conditions.

In the outflow boundary condition, it is common practice to set the derivatives in the longitudinal direction for all unknowns to zero. This condition insures that the flow leaving the domain must preserve the continuity of the flow inside the entire domain. The longitudinal derivatives are in fact not essentially zero, but this boundary condition is proposed to prevent upstream propagation of any reflections or disturbances that can be created by the numerical method. Numerical experiments show that these boundary conditions affect results only in a small local region near the outlet [14].

At the symmetry planes, due to the fact that the normal derivatives of the tangential velocities and the shear stresses vanish, the normal velocity and all the derivatives in the normal direction are basically set to zero.

## 2.4 CFD Process

The generic procedures for performing a numerical simulation for a general ship hydrodynamic performance are illustrated in Fig. 2.1. The outlined hierarchy shows that the CFD process is decomposed mainly of three major steps: the first is the computational set up process, which can be categorized in this context with respect to the numerical methods from Chapter II under the modeling process; while the second stands for the execution of the numerical solution of the presented model; and finally, the third is for the assessment and

evaluation of the numerical solution. Worth mentioning that the sub steps included within the presented hierarchy might add or exclude one or two more steps or might slightly differ based on the problem of concern; nevertheless, this structure was chosen to be as general and possible to be suitable for the four fields of ship hydrodynamics that will be covered in this thesis, i.e. resistance, propulsion, seakeeping and maneuvering.

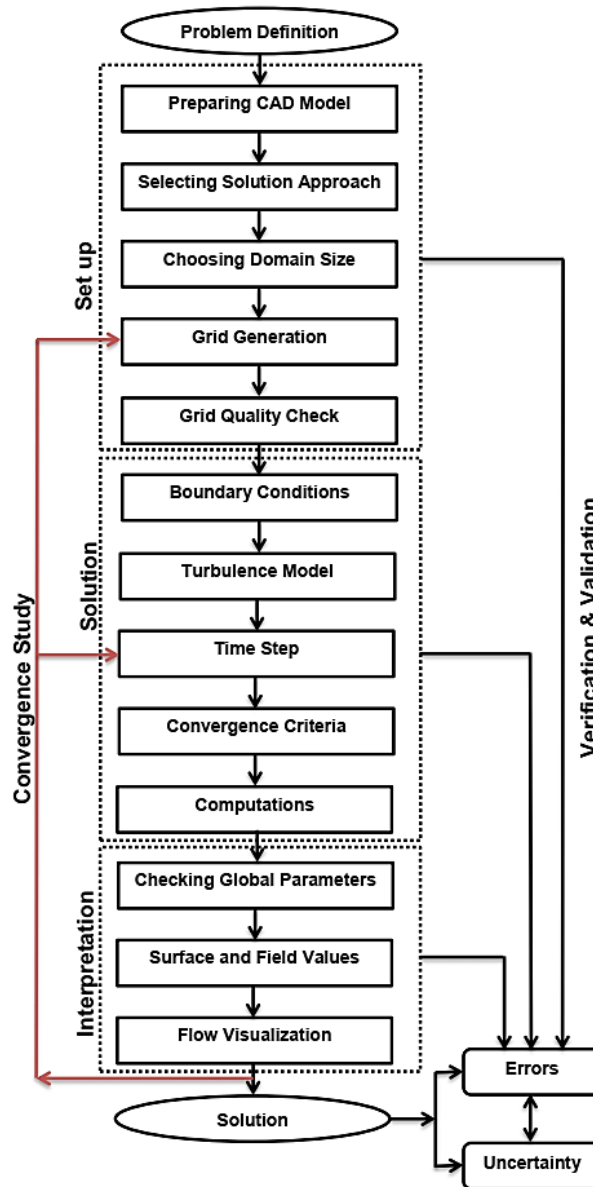


**Figure 2.1** General CFD process [60]

Prior to performing any of these stages, a proper definition for the problem is essential, since each and every problem in ship hydrodynamic require special considerations, which may influence the entire step coming afterwards. After establishing a proper definition for the problem, the three main stages can be broken down as follows:

1. Solution set up, which involves:
  - i. *Preparing the CAD model.*
  - ii. *Selecting the solution approach;*
  - iii. *Selecting the domain size;*
  - iv. *Grid generation;*
  - v. *Grid quality check;*

2. Preparing and performing the numerical solution, which includes:
  - vi. *Boundary condition;*
  - vii. *Choosing a proper turbulence model,*
  - viii. *Choosing a proper time step;*
  - ix. *Selecting the convergence criteria;*
  - x. *Performing the computation.*
3. Solution assessment or checking the numerical results, which include:
  - xi. *Checking global parameters;*
  - xii. *Checking surface and field parameters;*
  - xiii. *Flow visualization.*

The next step after this final stage is to assess the numerical uncertainties, which requires the execution of the quantitative verification and validation study. Since this step is crucially important and rather becoming essential in all of the recent numerical simulations, Chapter III is describing the basic procedures for performing this study, describing in brief the available standard procedures from the literature, and how it is applied particularly in this thesis.

## Chapter III

# Verification and Validation

Investigation of CFD errors is crucially important for the consistency and accuracy of any numerical solution. Despite the fact that the recent maturity in the numerical methods have led to high quality solutions which can provide a very good interpretation for the physical phenomenon, there are always approximations and assumptions that might include errors and uncertainties. Theoretically, solving the full NSE can provide superior results for almost all flow phenomena; unfortunately, it is not feasible to perform this operation for most of marine applications, as described clearly in Chapter II. The applicable solution for this problem is to use the filtered NSE either in space or time. Thus, the CFD user must be aware of the main steps followed to perform a numerical simulation in order to understand the different levels of errors included in the numerical method and to be able to judge reasonably the validity of the used method. The principle procedures to model the physical problem in general can be visualized in Fig. 4.1, where the sequence of the numerical solution starting from the physical problem ending with the obtained results is illustrated. Consequently, each step may result in one or more level of errors as a result for the different approximations and assumptions involved.

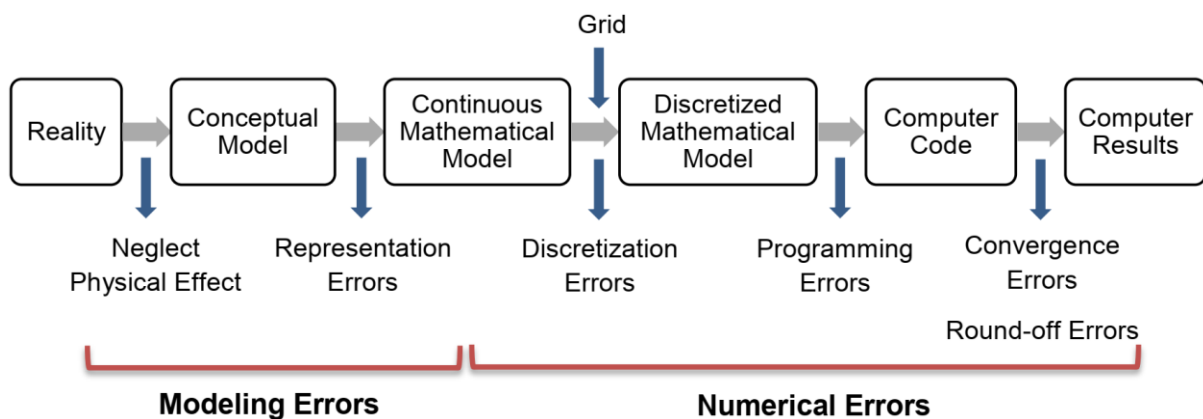


**Figure 3.1** Sources of errors in CFD results [27]

As it was formerly introduced in the previous chapters that it is very important to assess the numerical solution with a physically measured data from towing tank or sea trials, for many years this process was conducted through direct comparison between CFD and EFD data. Though this method is a straightforward and logic from one perspective; it remains deceiving, since the numerical errors as we previously mentioned may tend to interact mathematically and eliminate one another. This may pose a lack of confidence in the numerical solution even when it shows a good agreement with the experimental data. One may ask, is it really a result for a high quality solution, or just the different types of errors were eliminated? From this point systematic procedures were required to judge the numerical solution to investigate this problem. A consistent effort was paid in the past two decades to develop standard procedures for verification and validation of the numerical solutions. In 1998, the American Institute of Aeronautics and Astronautics (AIAA) introduced one of the milestone standards for verification and validation for CFD simulations [111]; besides, Patrick Roache in 1998 also presented his fundamental reference book *Verification and Validation in Computational Science and Engineering* [112]. Other efforts may be

recognized in the early stage in the last decade of the 20<sup>th</sup> century; however, these remarkable references build the basic foundation for the verification and validation standard procedures that are still being improved until nowadays.

### 3.1 Verification and Validation Concept

In the spirit of the original comparison concept, the simulation data which can be indicated by the symbol  $S$  is compared to the experimental data  $D$ ; both are representation of the true value  $T$ . Fundamentally, the error  $\delta$  in this case can simply be defined as the difference between simulation or experimental data and the true value. Regardless of its simple concept in definition, it is difficult to define this error as it is basically unknown, so it is usually estimated. This estimate produces another question regarding how accurate this estimate is. For this reason, the uncertainty  $U$  was introduced, which indicates that the estimate of an error  $\delta$  is bounded by the uncertainty interval  $\pm U$  that contains the true value 95 times out of 100. The uncertainty interval can only indicate the magnitude of the error  $\delta$  not its sign. Yet, this is not happening always, because in some cases when there is enough information available regarding the performed simulation, both magnitude and sign can be estimated and used as correction values for the obtained results.

### 3.2 Verification Methodology

According to the aforementioned concept for verification and validation process, the numerical uncertainties and errors can occur due to different sources in the numerical solution such as the discretization grid, time step, iterative method applied by the CFD code and any other parameter that might be related to the numerical solution including round of errors or statistical data sampling, etc. In general, there are two levels for the verification process a CFD user must perform to make sure his numerical solution can be reliable, code verification and solution verification. The former is concerned with verifying the CFD solver itself to insure that it solves the equation correctly regardless of the user's interference, whereas the latter is concerned with the application of the solver in the numerical simulation, which might be affected by the user's input parameters such as the choice of the grid size or time step, etc. It is worth mentioning that the solution verification is the only one covered in all the studies performed in this thesis, since the ISIS\_CFD code was thoroughly verified in multiple occasions such as the in the different versions of the International Workshops on CFD in Naval Hydrodynamics, SIMMAN Workshops for Ship Maneuvering Simulation Methods and other well recognized workshops and researches, as previously discussed in details in Chapter I.

Convergence studies are usually achieved through a minimum of three solutions  $m = 3$  to evaluate the convergence based on the input parameters, while  $m > 3$  is usually required. The three levels are usually defined as coarse medium and fine. Principally, the finest solution is considered the most accurate. The difference between the solutions in the refinement levels can give us an indication about the solution behavior. For example, assuming there are three solutions, the simulation results obtained can be identified as  $\hat{S}_{i,1}, \hat{S}_{i,2}, \hat{S}_{i,3}$  representing respectively, the simulation results for fine, medium and coarse mesh. Conceptually, the finer solution is more accurate than the coarser; thus, the changes between the solutions is usually referred to the finer one computed as follows

$$\varepsilon_{i,21} = \hat{S}_{i,2} - \hat{S}_{i,1} \ \& \ \varepsilon_{i,32} = \hat{S}_{i,3} - \hat{S}_{i,2} \quad (3.14)$$

and they can be used to define the convergence ratio

$$R_i = \frac{\varepsilon_{i,21}}{\varepsilon_{i,32}} \quad (3.15)$$

If the solution is converging, the difference between the fine and medium grids should be less than that between medium and coarse. Eq. (3.15) can lead to three possible convergence conditions

- i. Monotonic convergence:  $0 < R_i < 1$
- ii. Oscillatory convergence:  $R_i < 0$
- iii. Divergence:  $R_i > 1$

For the first condition, the uncertainties and errors can be estimated based on one of the generic methods, such as generalized Richardson Extrapolation method. For condition (ii), uncertainties are estimated simply by implementing the oscillatory concept from the iterative uncertainty based on oscillation maximums  $S_U$  and minimums  $S_L$ ; which mean that a general uncertainty  $U_K$  for any convergence parameter such as grid, time step or any other input value can be expressed as  $U_K = \frac{1}{2}(S_U - S_L)$ . It is worth mentioning that in this condition it may be deceiving only three levels to judge the convergence or the divergence of the solution, and it is advised in this case to use  $m > 3$ . Finally, for condition (iii), errors and uncertainties cannot be estimated [114, 115].

### 3.2.1 Generalized Richardson Extrapolation (RE)

For three solutions, when the monotonic convergence is achieved with respect to condition (i) of Eq. (3.15), errors can be estimated based on the leading term  $\delta_{RE_{i,1}}^*$  according to Eq. (3.16) based on the solution order of accuracy  $p_i$  and grid refinement ratio  $r_i$  as it is expressed in Eq. (3.17) as follows

$$\delta_{RE_{i,1}}^* = \frac{\varepsilon_{i,21}}{r^{p_i} - 1} \quad (3.16)$$

$$p_i = \frac{\ln(\varepsilon_{i,32}/\varepsilon_{i,21})}{\ln(r_i)} \quad (3.17)$$

### 3.2.2 Estimating Errors and Uncertainties with Correction Factor

The correction factor concept was introduced based on different verification studies and analytical benchmarks applied for 1D wave equation, 2D Laplace equation and Blasius boundary layer [114]. The concept can be used to define the distance of the solution from the asymptotic range and to account for the higher order terms in the error estimates, which might be disregarded in RE method. The principle is to multiply the error obtained from the RE method, which is computed based on one-term order of accuracy and far from the asymptotic range, in order to improve the error estimate. Hence, the error according to the correction factor  $C_i$  with respect to Eq. (3.16) is defined as

$$\delta_{i,1}^* = C_i \delta_{RE_{i,1}}^* = C_i \left( \frac{\varepsilon_{i,21}}{r^{p_i} - 1} \right) \quad (3.20)$$

where  $C_i$  is the correction factor and it can be estimated from Eq. (3.17) by simply replacing the estimated order of accuracy  $p_i$  with the improved estimate  $p_{i_{est}}$

$$C_i = \frac{r^{p_i} - 1}{r^{p_{i_{est}}} - 1} \quad (3.21)$$

### 3.2.3 Estimating Uncertainties with Factor of Safety

An alternative approach of the correction factor is to use the factor of safety  $F_s$  that was proposed by Roache [112, 117]. It can similarly be used to define the uncertainty  $U_i$  based on the error estimate from RE as

$$U_i = F_s \left| \delta_{RE_{i,1}}^* \right| \quad (3.26)$$

Also, the factor of safety approach can be used for situations where the solution is corrected with an error estimate based on the RE method as

$$U_i = (F_s - 1) \left| \delta_{RE_{i,1}}^* \right| \quad (3.27)$$

The choice of the value for the factor of safety is ambiguous; however, it is recommended to use the exact value for factor of safety as  $F_s = 1.25$  for systematically performed convergence studies and  $F_s = 3$  for cases when only two grids are used and the accuracy is set to the theoretical order of accuracy  $p_{th}$  [114, 119].

## 3.3 Validation Methodology

After the verification process is conducted and all the associated numerical uncertainties and errors are estimated, the validation process takes place, which is aimed at assessing the modeling uncertainties and errors through comparison with benchmark data, basically obtained from experiment or sea trials. The basic concept is to correlate the error  $E$ , which was previously introduced in Eq. (3.9) with the validation uncertainty  $U_V$  from one side, and the required level of validation  $U_{reqd}$  on the other side. Here,  $U_{reqd}$  is selected for practical application based on the level of accuracy required for a certain type of simulation, which can be established based on the common level of accuracy for this type of simulation from previously collected data, for example as in the ship hydrodynamic workshops. The combination between the three variables, just assuming that they are not matching, can lead us to six different scenarios as it was presented in [114, 115] as follows

- 1)  $|E| < U_V < U_{reqd}$
  - 2)  $|E| < U_{reqd} < U_V$
  - 3)  $U_{reqd} < |E| < U_V$
  - 4)  $U_V < |E| < U_{reqd}$
  - 5)  $U_V < U_{reqd} < |E|$
  - 6)  $U_{reqd} < U_V < |E|$
- (3.28)

In case 1, 2 and 3,  $|E| < U_V$  hence, the validation process is achieved at the  $U_V$  level which indicates that the comparison error is below the noise level. For this reason, it is not reasonable to improve the model assumptions in the CFD process in order to decrease the model uncertainty  $\delta_{SM}$ . Case 1 shows that the validation process is achieved at a level below  $U_{reqd}$  which means that from a programmatic point of view, the validation is successful.

In case 4, 5 and 6  $U_V < |E|$ , it means that comparison error is above the noise level. In this case it is feasible from the uncertainty point of view to use the sign and magnitude of  $E$  to estimate the modeling error  $\delta_{SM}$ . In this case it is more likely that  $E$  corresponds to modeling error, so in case if  $U_V \ll |E|$ , errors can be unambiguously determined. In case 4, validation is successful at the  $E$  level from a programmatic point of view as in case 1. The same

conditions are applicable for corrected error  $E_c$  which will be compared to  $U_{V_c}$ , except for the fact that  $E_c$  may be smaller or greater than  $E$ , while  $U_{V_c}$  is always less than  $U_V$ .

### 3.4 Unstructured Grid Generation for Verification and Validation Studies

In order to insure the geometrical grid similarity, the refinement process should be conducted following systematic steps. The basic variables that are controlled in this case are the initial cell size and the refinement diffusion depth. This method was applied successfully for unstructured grids generated by HEXPRESS™, as it was presented in [120, 121] and even for another similar grid generator as described in [122]. The basic steps can be demonstrated for a simplified configuration of a solid cube; an initial high quality grid is generated and then successively refined to obtain as geometrically similar grids as possible, executing the following steps:

- a. the initial cell size is reduced by imposing more divisions for the initial grid in (x-, y-, z-) directions;
- b. all the refinement levels for the geometry elements (curves and surfaces) are maintained unchanged;
- c. the refinement diffusion is increased to adapt to the required final grid size;
- d. finally, the number of levels for the viscous sub-layer are adapted to match the grid refinement.

The grids obtained, especially after the third step, are guaranteed to be geometrically similar. The resulted grids after the third step for a simple cube configuration are presented in Fig. 4.2, while the corresponding grid generation details are listed in Table 4.1.

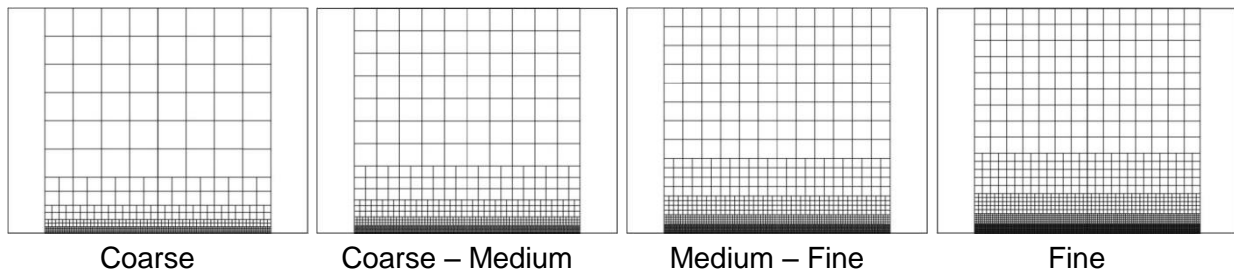


**Figure 3.2** Geometrically similar grid for a simple cube configuration

**Table 3.1** Geometrically similar grids parameters for a cube

Grid	Directional Subdivisions			Refinement Diffusion
	x	y	z	
Coarse	8	8	8	1
Coarse – Medium	10	10	10	2
Medium – Fine	12	12	12	3
Fine	14	14	14	4

It is worth mentioning that this sequence is followed for an ascending refinement approach; i.e. the coarsest grid is generated first then refined; while, a descending approach is also possible to be applied starting with the finest grid then coarsened gradually. The first approach is the one applied in this thesis, while the later was proposed and followed by some other researchers.

An example for geometrically similar grids generated based on the same principle for the Japan Bulk Carrier JBC is depicted in Fig. 4.3 showing the forepeak of the ship



highlighting the refinement criteria based on the previously described details in the cube example; nevertheless, the initial grid size in this case is refined by increasing the directional divisions with a value of 4 in each time instead of 2, while the refinement diffusion here starts with a value of 2 for the coarsest grid. Similarly, the criteria can be applied for any geometry or in case if the ship is equipped with appendages.

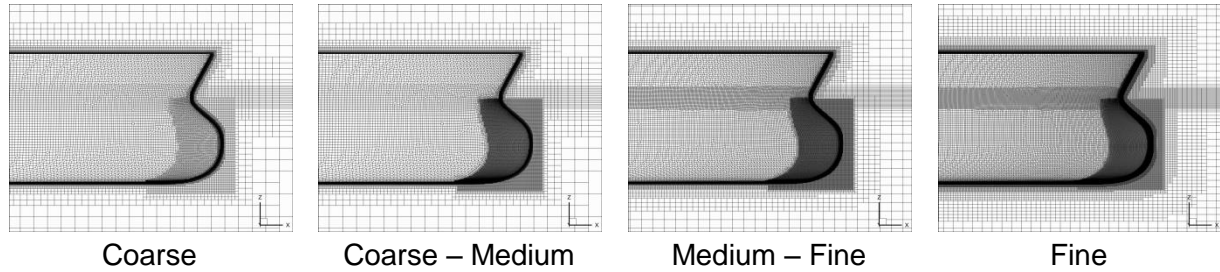


**Figure 3.3** Geometrically similar grids for the JBC ship model

After the grid similarity is insured, the other parameters of the numerical uncertainties such as the time step is handled in the solver by imposing proper refinement criteria to reduce the time step accordingly in order to examine its influence on the solution errors and uncertainties. Later after the results are obtained, analyzing the residuals and the iterative behavior of the solutions, the iterative and other sources of uncertainties can be easily applied. More details about the verification and validation studies will be given correspondingly for the simulations performed whose results are to be presented in the following chapters.

## Chapter IV

### Ship Resistance Performance

Ship resistance represents the principal parameter that must be predicted in the early design stage of the ship by means of numerical, statistical or experimental methods, as it was previously introduced in Chapter I. This chapter provides the ship resistance prediction for 3 ship models (JBC, KVLCC2 and DTMB).

#### 4.1 Japan Bulk Carrier (JBC)

The Japan Bulk Carrier (JBC) is a Capesize bulk carrier equipped with wake equalizing duct located upstream the propeller to work as an energy saving device (ESD). The ship model was introduced as a new design in the Tokyo 2015 Workshop on CFD in ship hydrodynamics (T2015) in order to assess the capability and accuracy of CFD methods to predict new concept designs, as previously described in Chapter I. The geometry of hull, duct, propeller and rudder are depicted in Figure 4.1, while the main particulars of the ship model and duct only are tabulated in Table 4.1, only resistance tests are considered in this chapter, the propeller performance is covered in Chapter V.

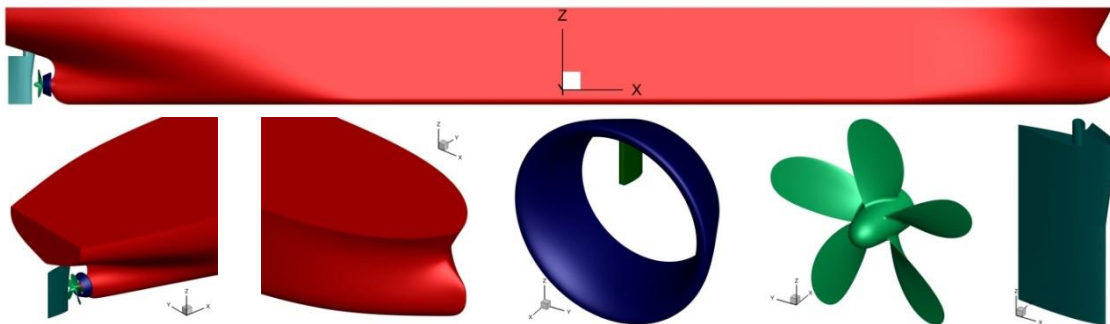


**Figure 4.1** JBC model geometry highlighting stern, fore, duct, propeller and rudder

**Table 4.1** Principal particulars of ship and duct

Particulars		Unit	Value
Ship	Length between Perpendiculars ( $L_{PP}$ )	[m]	7.0
	Beam ( $B$ )	[m]	1.125
	Depth ( $D$ )	[m]	0.625
	Draft ( $T$ )	[m]	0.4125
	Volumetric Displacement ( $\nabla$ )	[m <sup>3</sup> ]	2.787
	Wetted Surface Area ( $S_0$ ) (without ESD)	[m <sup>2</sup> ]	12.225
	Wetted Surface Area ( $S_0$ ) (with ESD)	[m <sup>2</sup> ]	12.272
	Block Coefficient ( $C_B$ )	[-]	0.858
	LCB ( $\%L_{PP}$ ), fwd+	[-]	-2.548
Duct	Duct Outlet Diameter ( $0.55D_p$ )	[m]	0.11165
	Duct Cord Length ( $0.3D_p$ )	[m]	0.0609
	Duct Angle of Attack	[Degree]	20
	Duct Foil Section	NACA4420	

### 4.1.1 Analysis Conditions

The numerical simulation performed for the JBC repeats the resistance towing tank conditions for the model towed in calm water at the design speed  $U=1.179$  m/s with a Froude number  $Fr=U/(gL_{pp})^{0.5}=0.142$  and Reynolds number  $Re=(UL_{pp})/\nu = 7.46E+6$ , where  $U$  represents the ship speed in m/s and  $\nu$  represents the water kinematic viscosity in  $m^2/s$ . Only two degrees of freedom for the vertical ship motions are included in both experimental and numerical studies, i.e. the axial translation in z-directions (heave, or in calm water resistance is called sinkage) and rotation around y-axis (pitch or trim), while all the other motions are locked. Two analysis conditions included based on the existence of the ESD where case 1 is assigned for the hull without the ESD, while case 2 is assigned for the model equipped with the ESD.

### 4.1.2 Domain & Boundary Conditions

The computational domain for all the resistance computations performed in this thesis is configured of a rectangular prism whose dimensions and boundary conditions are depicted in fig. 4.2. only half ship is represented in simulation to reduces simulation cost and effort.

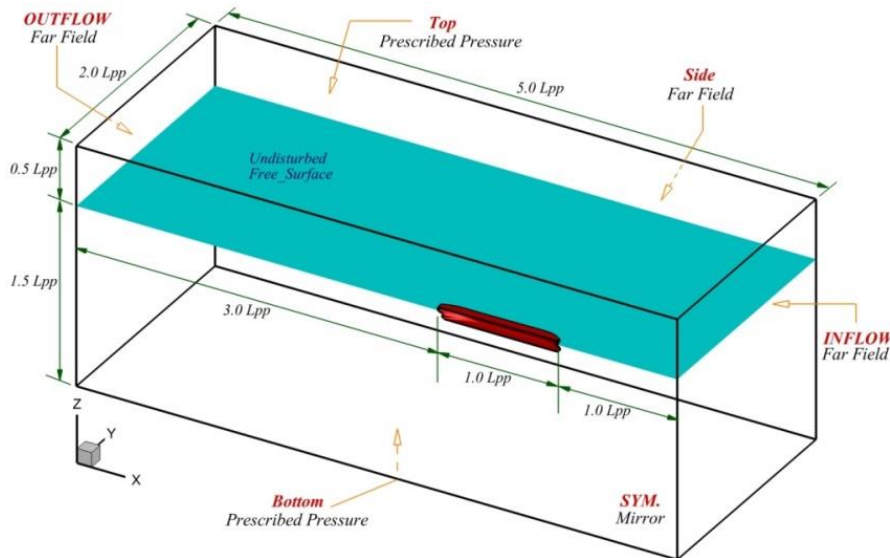
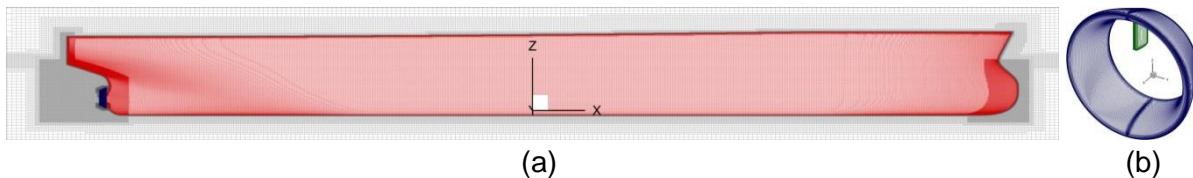
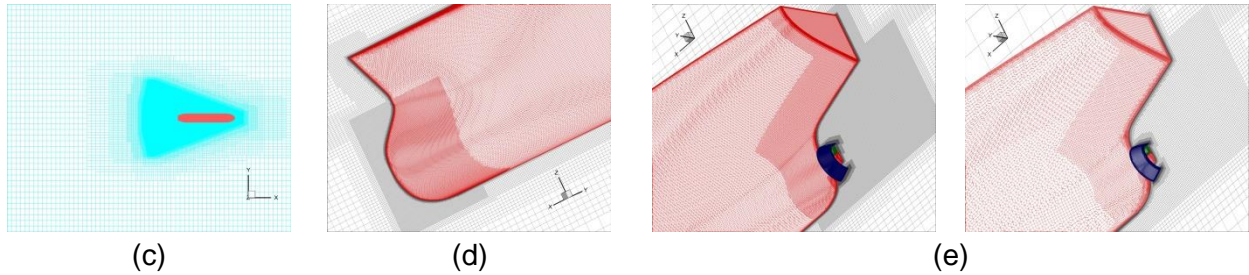


Figure 4.2 Computational domain, dimensions and boundary conditions

### 4.1.3 Computational Grids

Computational grids are generated by making use of the unstructured hexahedral grid generator HEXPRESS™ included in the Fine™/Marine package. Simulation grids are depicted in Fig. 4.3 while the grid details are represented in Table 4.3, where the M1 and M4 refers to the finest and coarsest grids, respectively.





**Figure 4.3** Computational grid, showing: (a) JBC with ESD, (b) duct and strut, (c) free-surface refinement, (d) fore and (e) stern comparison between fine and coarse grids

**Table 4.3** Computational grids

Ship Model	Grid Size (Million Cells)			
	M1	M2	M3	M4
JBC w/o. ESD	7.462	4.587	2.602	1.506
JBC w. ESD	9.670	5.881	3.583	2.107

#### 4.1.4 Simulation Strategy

The simulation is performed for 30 seconds to achieve a sufficient convergence for the forces and vertical motions. A quasi-static approach is imposed with second order convergence criteria and 10 nonlinear iterations, while the time step  $\Delta t$  is decided based on the ITTC recommended procedures.

#### 4.1.5 Resistance and Motion Results

The convergence is achieved after about 22 seconds of physical simulation time for total ship resistance and approximately 25 seconds for sinkage and trim motions. The results obtained for total ship resistance coefficient  $C_T = R_T/0.5\rho S_0 U^2$  are tabulated in Table 4.4, where S1 refers to the simulation results from the finest grid M1, while S4 refers to the results from M4 and finally, the error  $\varepsilon\%$  refers to the percentage difference between EFD and CFD results, such that  $\varepsilon\% = 100 \times (EFD - CFD)/EFD$ .

**Table 4.4**  $C_T$  results computed at  $T=30s$  Compared to EFD data [124]

EFD		JBC w/o. ESD		JBC w. ESD	
		$C_T = 4.289 \times 10^3$		$C_T = 4.263 \times 10^3$	
CFD	Turbulence model	EASM	$K-\omega$ SST	EASM	$K-\omega$ SST
	S1	4.231	4.169	4.282	4.131
	$\varepsilon\%$	1.36	2.80	-0.45	3.09
	S2	4.227	4.112	4.227	4.097
	$\varepsilon\%$	1.45	4.13	0.84	3.89
S3	4.224	4.087	4.206	4.055	
$\varepsilon\%$	1.52	4.71	1.33	4.88	
S4	4.179	4.014	4.088	3.970	
$\varepsilon\%$	2.57	6.42	4.11	6.87	

Similarly, the computed sinkage and trim had a reasonable agreement with the experimental data, regardless of the turbulence model used. Table 4.5 brings to attention the

comparison between the CFD results computed using the EASM model and the EFD data for the hull with and without ESD.

**Table 4.5** Sinkage and trim results computed at  $T=30s$  Compared to EFD data [124]

		Sinkage $\sigma$ (Upward +)		Trim $\tau$ (Bow Up +)	
		JBC w/o. ESD	JBC w. ESD	JBC w/o. ESD	JBC w. ESD
EFD		$\sigma=-0.086 \%L_{PP}$	$\sigma=-0.085 \%L_{PP}$	$\tau=-0.180 \%L_{PP}$	$\tau=-0.182 \%L_{PP}$
CFD	S1 $\varepsilon\%$	-0.0872 1.39	-0.0877 3.18	-0.178 1.11	-0.180 1.10
	S2 $\varepsilon\%$	-0.0878 2.09	-0.0902 6.12	-0.176 2.23	-0.176 3.13
	S3 $\varepsilon\%$	-0.0919 6.86	-0.0902 6.12	-0.172 4.45	-0.175 3.96
	S4 $\varepsilon\%$	-0.0922 7.21	-0.0903 6.23	-0.169 6.11	-0.173 4.95

### 4.1.6 Free-Surface Results

For validation purposes, in order to highlight the accuracy of predicting the free-surface in the current study, the free-surface results are compared to the EFD data [125] as shown in Fig. 4.5. The computed wave profile as well as the wave elevation shows a good agreement with the EFD data especially in the near field region close to the hull. The height of the obtained wave crest at the bow is over predicted with an approximate error 2.52% compared to the EFD.

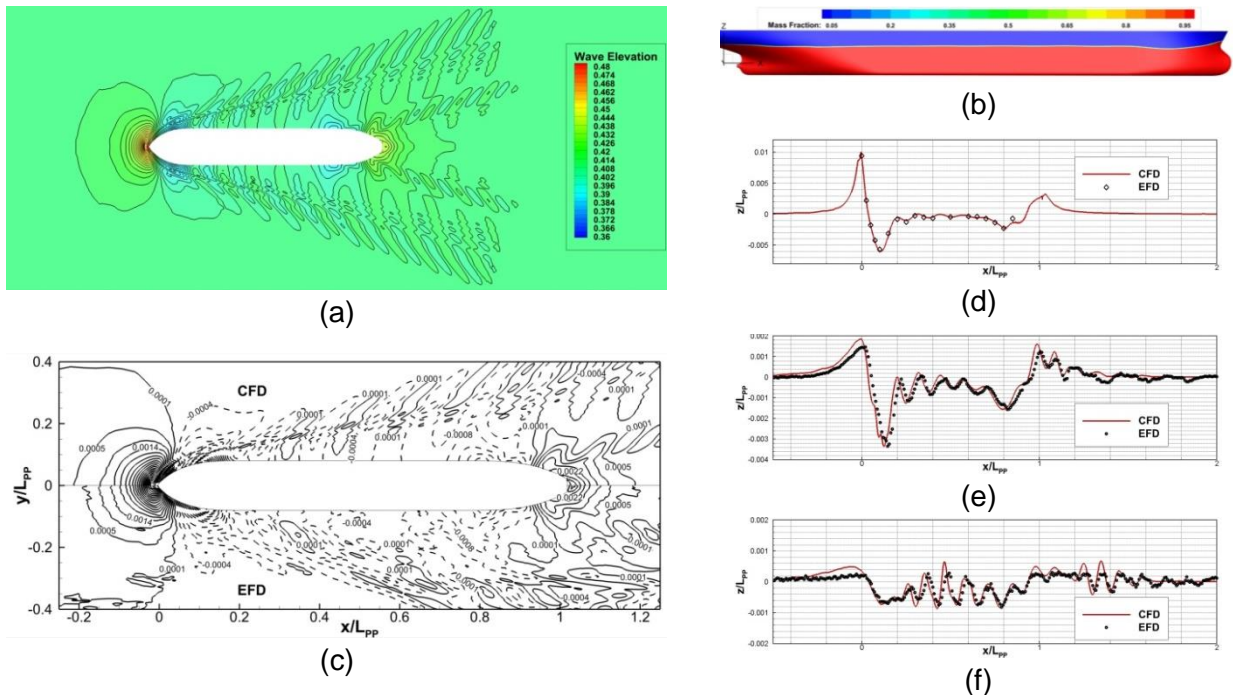


**Figure 4.5** Computed free-surface at  $T=30 s$ , showing: (a) free-surface configuration, (b) mass fraction, (c) CFD vs. EFD for the free-surface topology, (d, e and f) CFD vs. EFD for wave profile at the hull, at distances  $y/L_{PP}=0.1043$  and  $y/L_{PP} =0.19$ , respectively

### 4.1.7 Local Flow Results

The obtained results were checked from the forces point of view as well as from the wake flow quality. As previously mentioned, the EASM and  $K-\omega$  SST models, either the classic or modified, produced the best results. Fig. 4.7 shows the velocity contours for section S2 which is located at a distance 0.2625m from the A.P, for the ship without ESD.

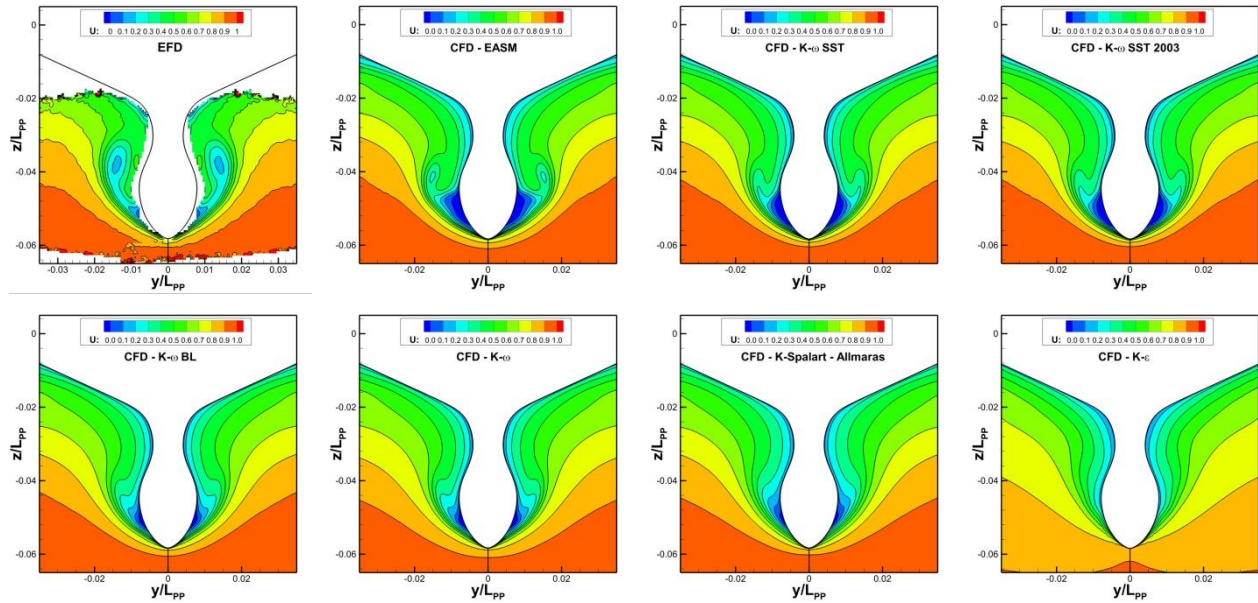


**Figure 4.7** EFD and CFD results for the axial velocity contours computed at  $T=30s$  for ship without ESD at section S2 using different turbulence models

Fig. 4.10 shows a comparison between the axial flow velocity contours in  $x$ -direction for the three sections S2, S4 located at distance 0.11m from the A.P. and S7 located at the A.P.

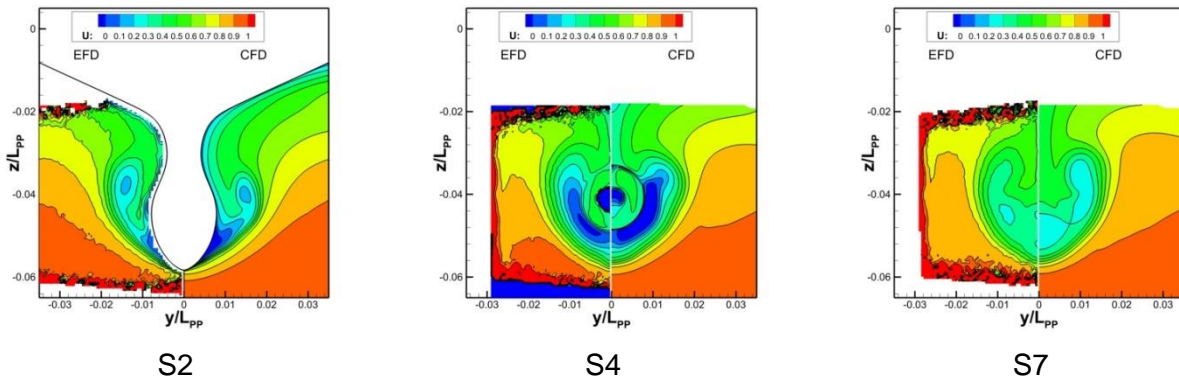


**Figure 4.10** Comparison between the streamwise velocity contours measured and computed at  $T=30 s$  using EASM turbulence model for ship with ESD for sections S2, S4 and S7

The computed vortical structures for the ship without ESD compared to the data provided in the Workshop as it can be found in [126] is depicted in Fig 4.11 for the second invariant  $Q$  criterion at an iso-surface  $Q^*=25$  colored by the non-dimensional helicity defined by

$$He = \frac{\vec{U} \cdot \vec{\Omega}}{|\vec{U}| \cdot |\vec{\Omega}|} \quad (4.2)$$

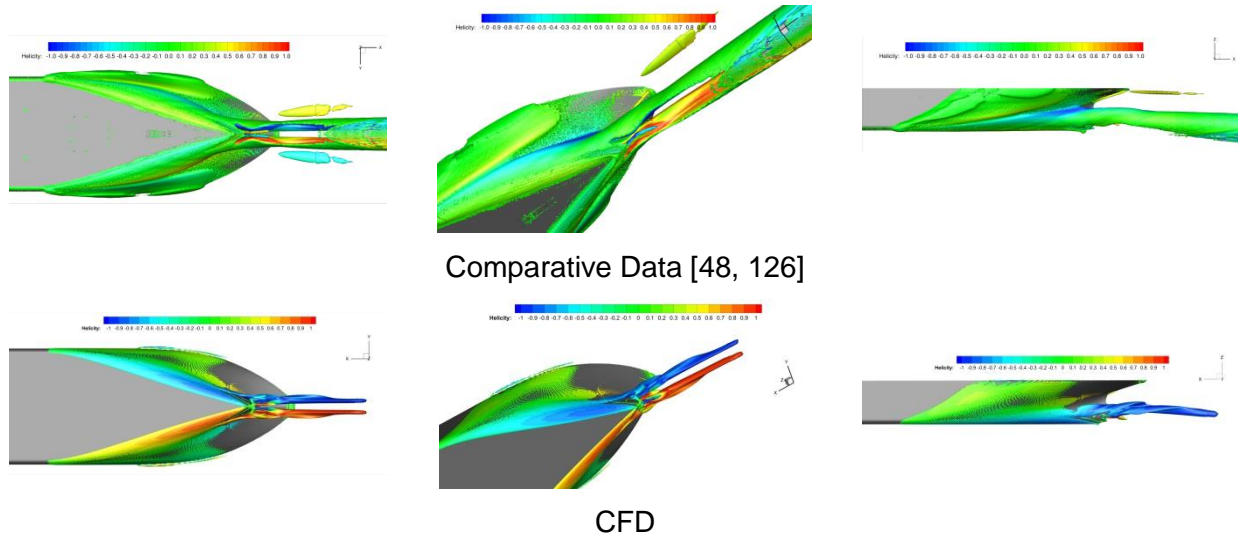


**Figure 4.11** Workshop data for the second invariant iso-surface  $Q^*=25$  colored by helicity and the corresponding CFD results computed at  $T=30$  s using EASM model

Finally, all the results obtained for the JBC ship model concerning the resistance, vertical motions, free-surface and local flow have been published in [132, 133].

## 4.2 KRISO Very Large Crude Carrier (KVLCC2)

The geometry of the KVLCC2 model showing the propeller and rudder is depicted in Fig. 4.12, while the principal dimensions of the 7.0 meters INSEAN model are tabulated in Table 4.8.

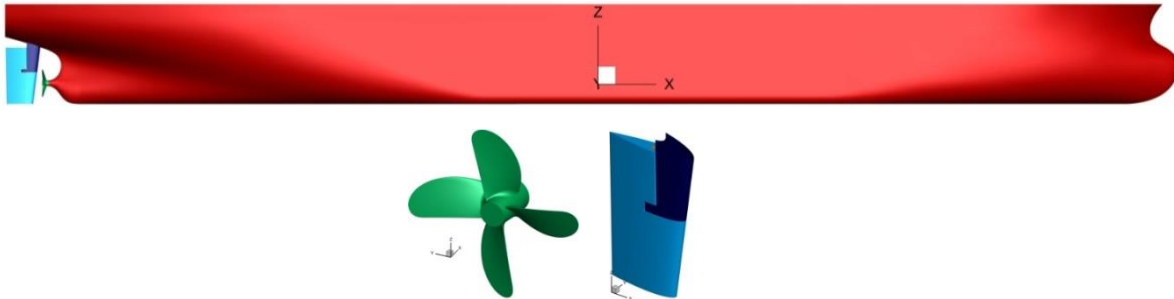


Figure 4.12 KVLCC2 model geometry highlighting propeller and rudder

Table 4.8 Principal particulars of ship and rudder

	Particulars	Unit	Value
Ship	Length between Perpendiculars ( $L_{PP}$ )	[m]	7.0
	Beam ( $B$ )	[m]	1.1688
	Depth ( $D$ )	[m]	0.6563
	Draft ( $T$ )	[m]	0.4550
	Volumetric Displacement ( $\nabla$ )	[m <sup>3</sup> ]	3.2724
	Block Coefficient ( $C_B$ )	[-]	0.8098
	Mid-ship section coefficient ( $C_M$ )	[-]	0.9980
Rudder	Rudder type	-	Horn
	Rudder area ( $S_R$ )	[m <sup>2</sup> ]	0.1308

### 4.2.1 Analysis Conditions

Table 4.9 summarizes the computational cases with the corresponding ship speed, Froude number and Reynolds number.

Table 4.9 Computational cases and corresponding ship speed parameters

Case Number	C1	C2	C3	C4	C5	C6
$U$ [m/s]	0.8370	0.9894	1.1411	1.1792	1.2173	1.2554
$Fr$ [-]	0.1010	0.1194	0.1377	0.1423	0.1469	0.1515
$Re$ [-] $\times 10^6$	3.5	4.1	4.8	4.9	5.1	5.2

### 4.2.2 Domain & Boundary Conditions

The computational domain dimensions and boundary conditions are imposed exactly similar to those given in section 4.1.2 for the JBC hull, the only difference is that the initial undisturbed free-surface level is set at the design draft of the KVLCC2 model at  $z=0.455$  m from the baseline.



### 4.2.3 Computational Grids

The details of the computational grids are given in table 4.9, while the stern area of the discretized domain can be visualized in Fig. 4.13 for both rudder configurations.

**Table 4.10** Computational grids for ship with and without rudder

Number of grid cells (M)	Bare Hull			With Rudder	
	M1	M2	M3	Simplified	Actual
	20.33	10.84	4.56	4.752	5.577

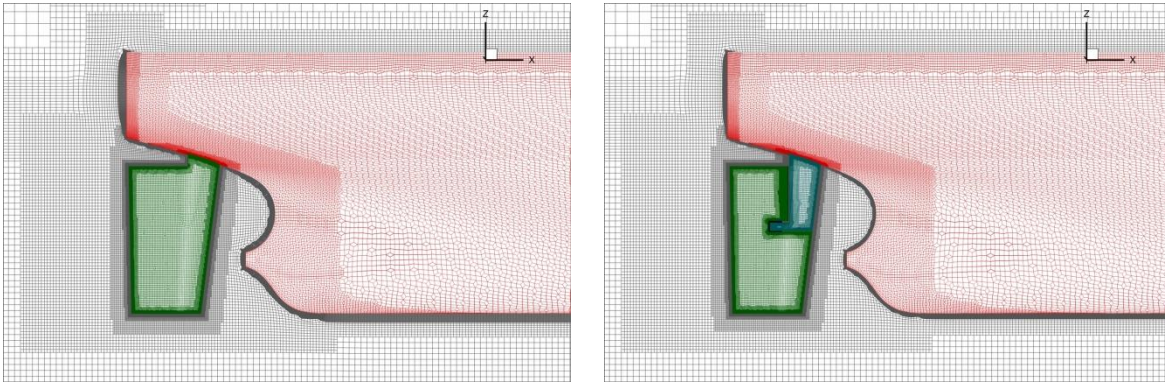


**Figure 4.13** Discretization grid for ship with simplified rudder (left) and actual rudder (right)

### 4.2.4 Resistance and Motion Results

The forces are obtained and compared to the EFD data for the grid convergence study as it can be observed in Fig. 4.14.

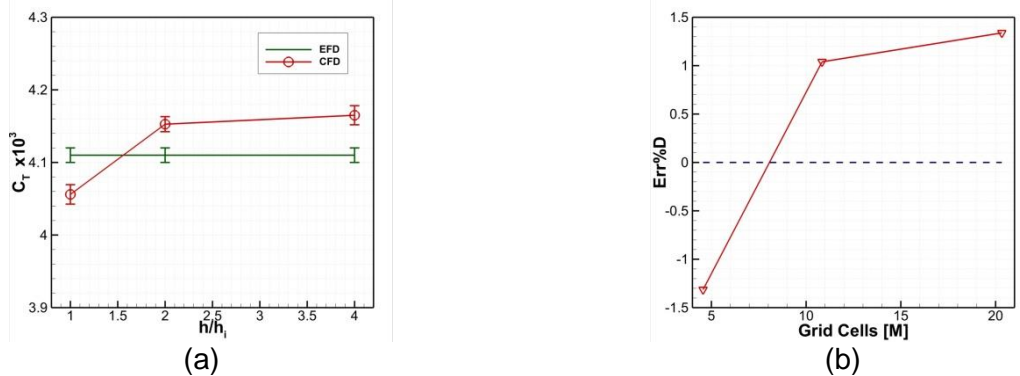


**Figure 4.14** Obtained results for ship without rudder: (a) Computed total resistance coefficient  $C_T$  compared to the EFD, (b) estimated error as a function of grid density

### 4.2.5 Free-Surface Results

Fig. 4.16 shows the qualitative validation of the free-surface pattern and two lateral sections distanced at  $y/L_{pp} = -0.0964$  and  $-0.1581$ , respectively, from the ship center-line. A very good resemblance can be observed from the comparison between the CFD results and the provided EFD data from the G2010 Workshop [47] and Kim et al. [138].

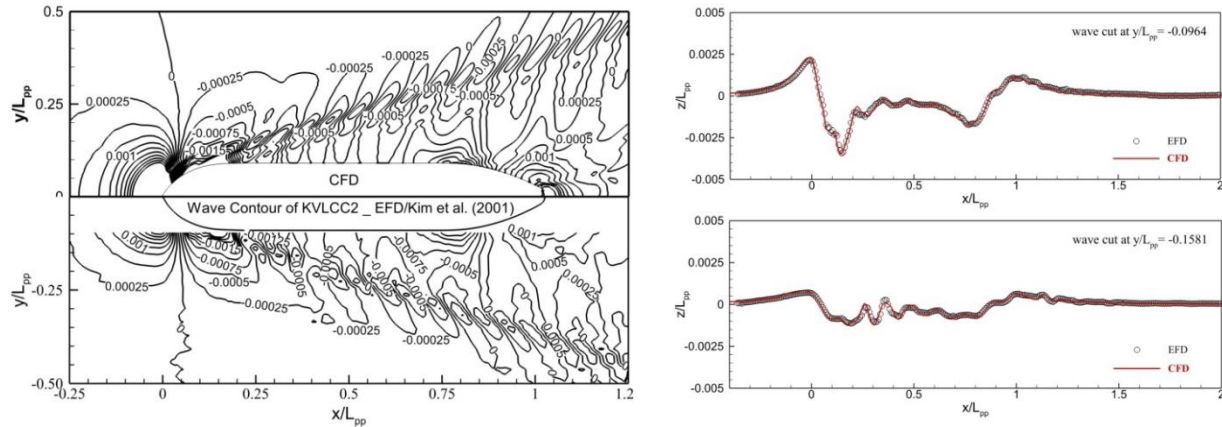


Figure 4.16 Free-surface topology (left), and wave cuts at  $y/L_{pp}=-0.0964$  and  $-0.1581$ (right)

### 4.2.6 Local Flow Results

Results are plotted in Fig. 4.17 compared to the experimental data showing a good agreement between CFD and EFD results.

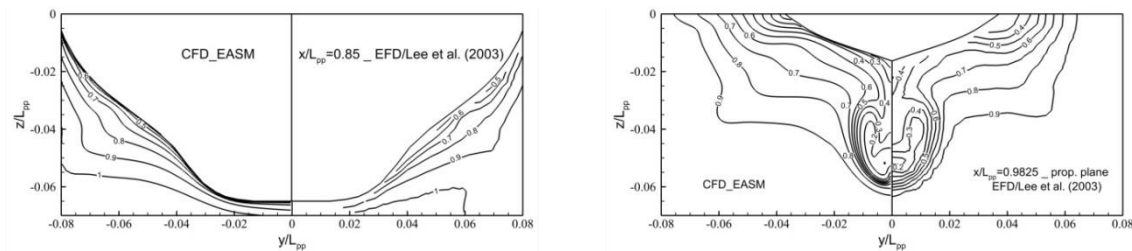


Figure 4.17 CFD vs. EFD streamwise velocity contours at sections:  $x/L_{pp}=0.85$  and  $0.9825$

Finally, all the results presented for the KVLCC2 ship model have been fully or partially published in [134].

### 4.3 David Taylor Model Basin (DTMB) Surface Combatant

The third ship to be analyzed in the resistance study is the US Navy surface combatant ship model known as the David Taylor Model Basin (DTMB). The appended model geometry is presented in Fig. 4.20, while the principal dimensions of the INSEAN and IIHR models used for ship resistance simulations are tabulated in Table 4.12 compared to the full scale ship.

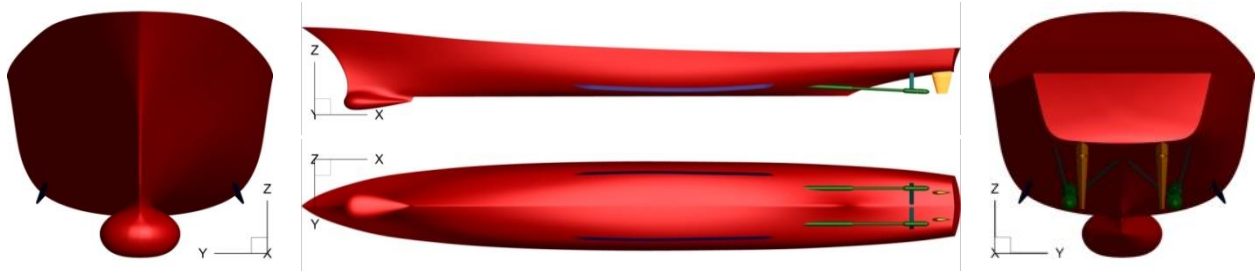


Figure 4.20 DTMB model geometry viewing: front, profile, bottom and rear

Table 4.12 DTMB ship models and full scale characteristics

Particulars	Unit	Full Scale	Model – INSEAN	Model – IIHR	Model – UGAL
Scale ( $\lambda$ )	-	1:1	1:24.830	1:46.558	1:44
Length of Waterline ( $L_{PP}$ )	[m]	142.0	5.719	3.048	3.232
Beam ( $B$ )	[m]	19.06	0.768	0.409	0.434
Depth ( $D$ )	[m]	10.98	0.442	0.236	0.25
Draft ( $T$ )	[m]	6.15	0.248	0.132	0.14
Volumetric Displacement ( $\nabla$ )	[m <sup>3</sup> ]	8424.4	0.554	0.0826	0.099
Wetted Surface Area ( $S$ )	[m <sup>2</sup> ]	2972.6	4.828	1.371	1.54
Block Coefficient ( $C_B$ )	-	0.507	0.507	0.507	0.507
Long. Position of C.O.G ( $x_{CG}$ ) from F.P.	[m]	71.676	2.887	1.539	1.629
Vertical Position of C.O.G ( $z_{CG}$ )	[m]	7.54	0.304	0.162	0.1718
LCB (% $L_{PP}$ ), fwd+	-	-0.683	-0.683	-0.683	-0.683

#### 4.3.1 Bare Hull Ship Model

The two models from INSEAN and IIHR are introduced and analyzed individually in the numerical simulation in order to predict the total ship resistance at three velocities that correspond to  $Fr=0.1$ , 0.28 and 0.41 in order to investigate the solution quality at different speeds (slow, medium and high speed sailing conditions).

##### 4.3.1.1 Analysis Conditions

The analysis conditions for the DTMB ship model for bare hull and fully appended ship can be subdivided in three simulation cases based on the ship speed as summarized in Table 4.13 showing the corresponding Froude and Reynolds numbers for both INSEAN and IIHR models.

**Table 4.13** Computational cases and corresponding ship speed parameters

Ship Model	Case Number	C1	C2	C3
Model – INSEAN	$U$ [m/s]	0.749	2.097	3.071
	$Fr$ [-]	0.1	0.28	0.41
	$Re$ [-] $\times 10^6$	2.154	6.030	8.830
Model – IIHR	$U$ [m/s]	0.547	1.531	2.242
	$Fr$ [-]	0.1	0.28	0.41
	$Re$ [-] $\times 10^6$	1.572	4.403	6.447

#### 4.3.1.2 Domain & Boundary Conditions

The computational domain dimensions and boundary conditions are imposed exactly similar to those given in section 4.1.2 for the JBC hull, the only difference is that the initial undisturbed free-surface level is set at the design draft of the DTMB model at  $z=0.248$  and  $0.132$  m from the baseline, for the INSEAN and IIHR models, respectively, corresponding to the design draft as represented in Table 4.12.

#### 4.3.1.3 Computational Grids

The grid configuration is represented in Fig. 21, showing the comparison between fine and coarse grid, free-surface, while Table 4.14 summarized the grid details.

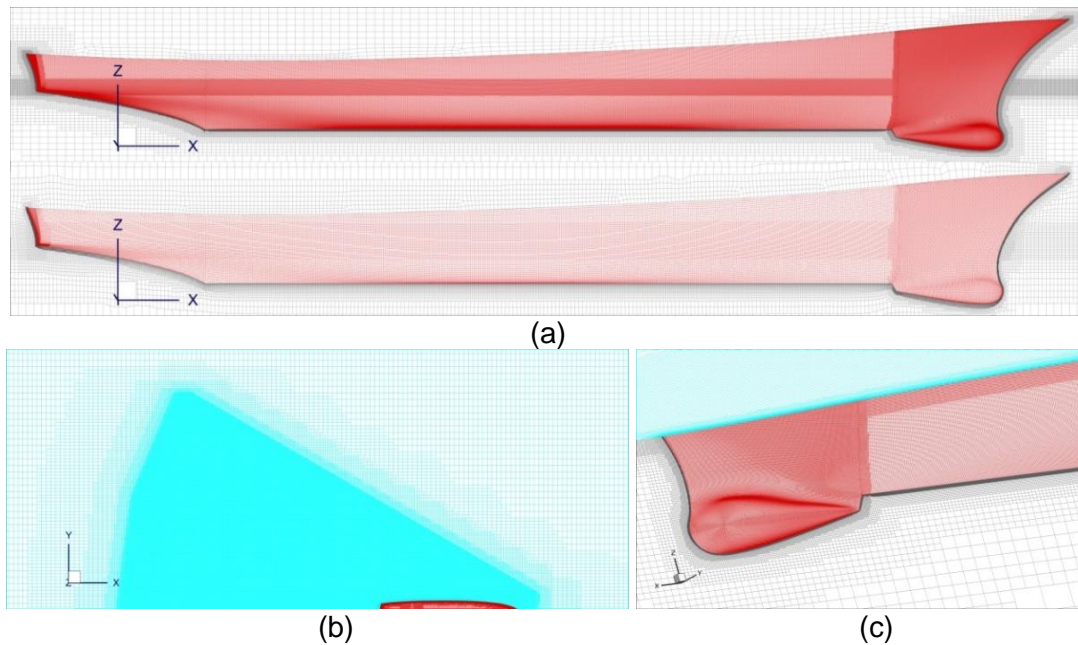


**Figure 4.21** Computational grids showing: (a) Fine and coarse grids, (b) free-surface refinement and (c) a forward section

**Table 4.14** Computational grids for ship based on the wall treatment modeling

Wall Condition	Number of grid cells (M)			
	M1	M2	M3	M4
WM	9.85	6.74	4.31	2.91
WR	16.55	10.17	6.81	4.34

### 4.3.1.4 Resistance and Motion Results

The forces are obtained and compared to the EFD data for the grid convergence study as it can be observed in Fig. 4.22, which reveals a proper agreement with the EFD data with an error range between 2.23% up to 6.74% for the slow the high speed case, respectively.

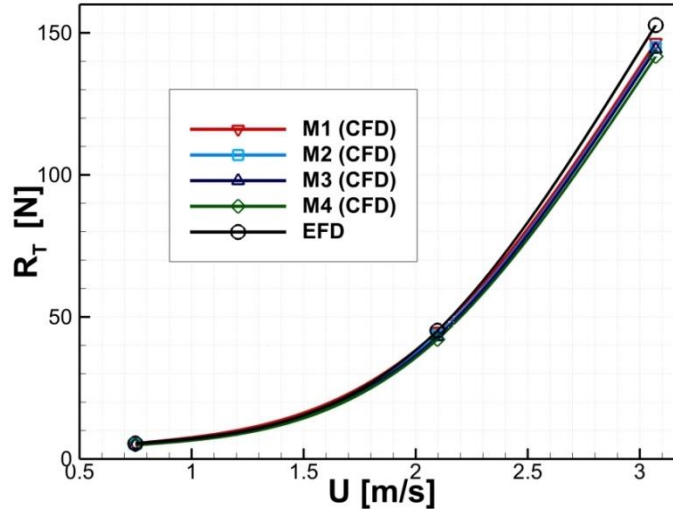


**Figure 4.22** Total resistance results based on the grid density

Ship motion results represent that the error for sinkage is within 0.55% and 9.77% , while for trim is within 1.18% and 9.4%. , which indicates the accuracy of the solution especially for fine grids.

### 4.3.1.5 Free-Surface Results

The comparison between the CFD results for the medium speed  $Fr=0.28$  and the corresponding EFD data reported in [130] is represented in Fig. 4.24 showing that the far-field wave height was slightly under predicted with 1.1%.

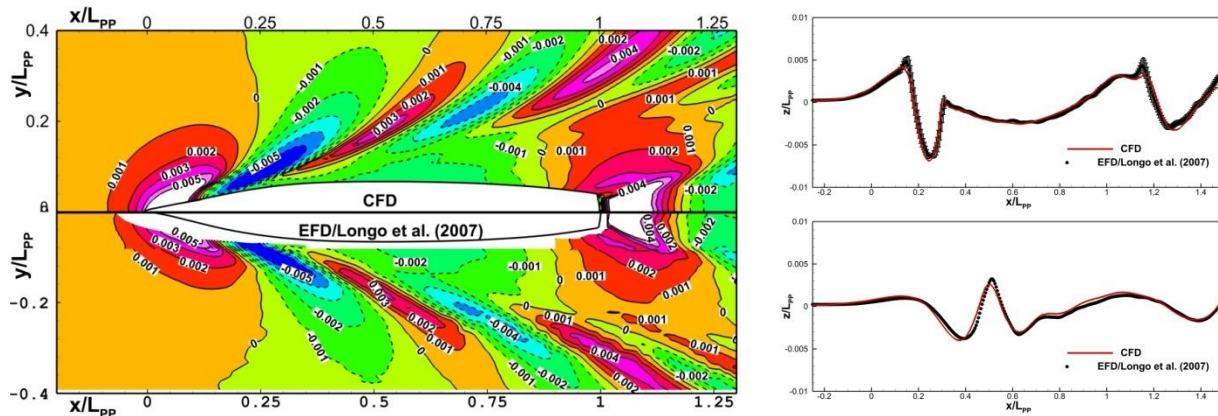


**Figure 4.24** Free-surface profile (left), and wave cuts at  $y/L_{pp}=0.082$  and  $y/L_{pp}=0.172$  (right)

### 4.3.1.6 Local Flow Results

Fig. 4.25 shows a comparison of different sections positioned at relative distances  $x/L_{pp}=0.1, 0.6, 0.935$  and finally  $1.1$  from the forward perpendicular. These positions represent

main checkpoint locations after the sonar dome, after the bottom rise, at the propeller position and the ship downstream, respectively.

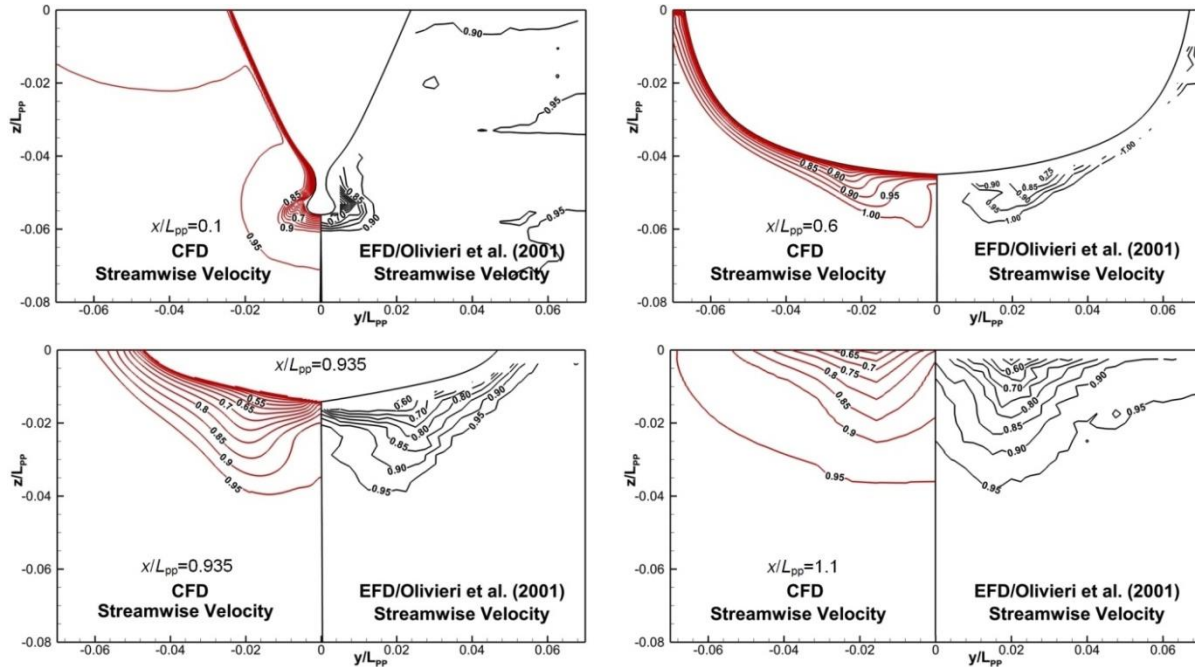


Figure 4.25 CFD vs. EFD streamwise velocity contours at different sections

### 4.3.2 Appended Hull Ship Model

The purpose of this analysis is to investigate the capability of the CFD method to assess accurately the total resistance and the local flow of the fully appended DTMB ship model with bilge keels, shafts, shaft brackets and tow rudders.

#### 4.3.2.1 Analysis Conditions

In this case, the INSEAN model with  $L_{pp}=5.72$  m is used in this simulation and compared with the same model results from the bare hull analysis.

#### 4.3.2.2 Domain & Boundary Conditions

The same domain configurations and boundary conditions for the bare hull are maintained unchanged in this analysis.

#### 4.3.2.3 Computational Grids

Four grids were generated to perform a grid dependent study and their density in millions of cells is summarized in Table 4.17, while the grid discretization is plotted in Fig. 4.26 showing the ship and the appendages refinements.

Table 4.17 Computational grids for ship based on the wall treatment modeling

Wall Condition	Number of grid cells (M)			
	M1	M2	M3	M4
WM	19.943	8.958	5.667	2.669
WR	26.757	16.605	9.022	3.634

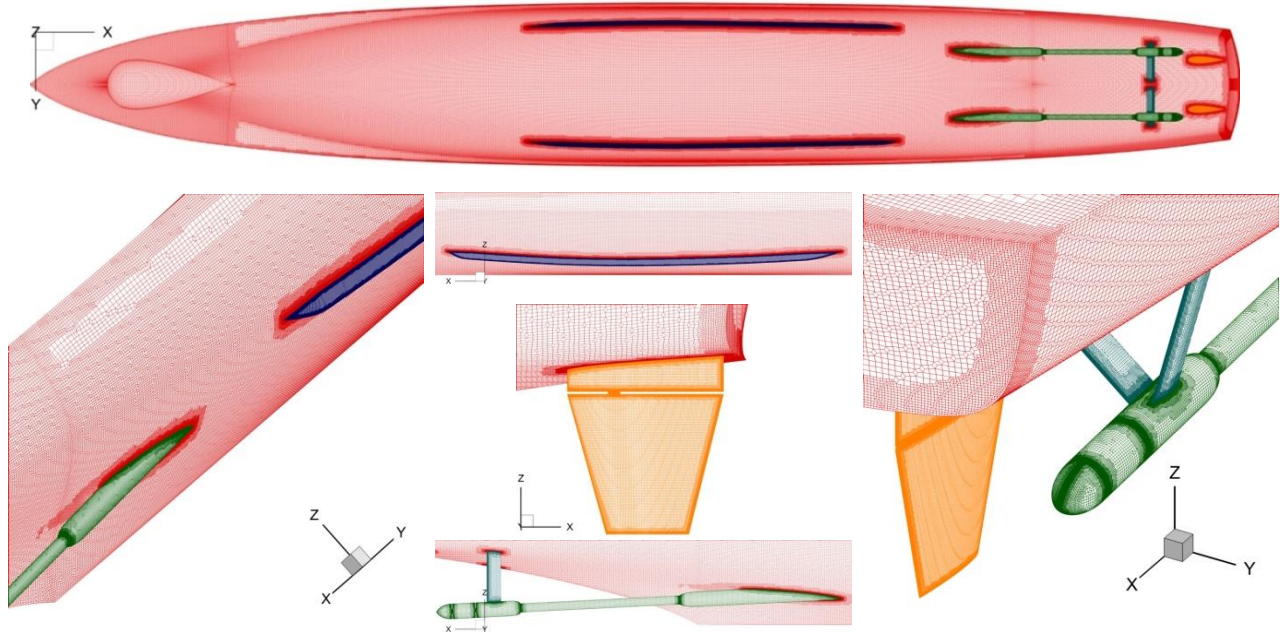


**Figure 4.26** Discretization grid highlighting the appendages refinement

#### 4.3.2.4 Resistance and Motion Results

The total resistance is obtained for the ship model with the appendages and represented in Table 4.18. One of the flexible features in the CFD modeling is regarding the fact that the solver can provide the drag on each appendage to highlight its influence on the total hull drag. This was introduced and compared for the different ship speed conditions and plotted in the pie chart represented in Fig. 4.27 in order to highlight the impact of each appendage on the total resistance computed.

**Table 4.18** Total resistance computed for the appended hull and appendages drag force

$Fr$	Hull Component Force [N]					
	Shaft	Shaft Brackets	Bilge Keel	Rudder	Bare Hull	Fully Appended
0.10	0.30	0.15	0.11	0.21	5.40	7.18
0.28	3.56	2.02	1.66	3.04	45.46	55.73
0.41	5.65	5.75	4.59	8.38	154.16	178.53

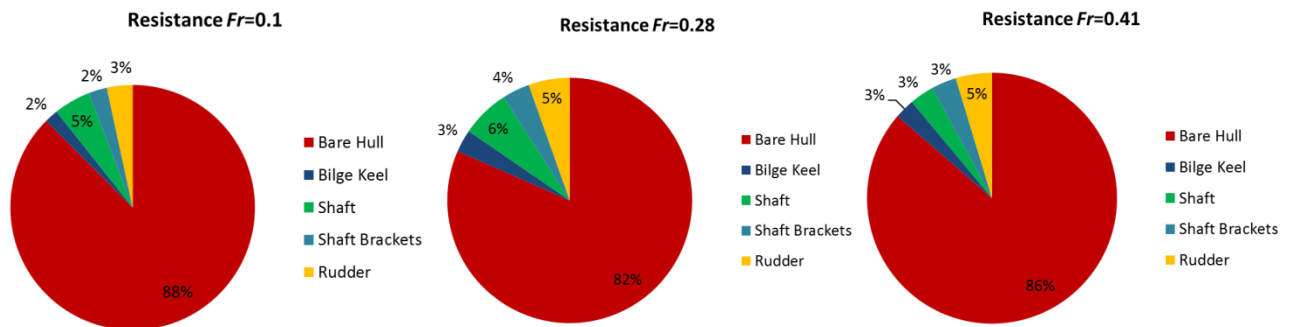


**Figure 4.27** Resistance results for the fully appended ship and hull components individually

**Table 4.19** Total resistance coefficient  $C_T$  computed for the bare hull component compared to EFD data [129]

Results	$C_T$ EFD	$C_T$ (WM), CFD		$C_T$ (WR), CFD	
		$k-\omega$ SST	EASM	$k-\omega$ SST	EASM
M1	$4.23 \times 10^{-3}$	4.361	4.334	4.049	4.092
$\varepsilon\%$		3.10	2.49	-4.28	-3.26
M2		$4.415 \times 10^{-3}$	$4.359 \times 10^{-3}$	$4.057 \times 10^{-3}$	$4.098 \times 10^{-3}$
$\varepsilon\%$		4.37	3.05	-4.09	-3.12
M3		$4.545 \times 10^{-3}$	$4.513 \times 10^{-3}$	$4.293 \times 10^{-3}$	$4.275 \times 10^{-3}$
$\varepsilon\%$		7.44	6.69	1.49	1.06
M4		4.561	$4.551 \times 10^{-3}$	$4.363 \times 10^{-3}$	$4.334 \times 10^{-3}$
$\varepsilon\%$		7.82	7.59	3.14	2.45

### 4.3.2.6 Local Flow Results

The flow around the DTMB is dominated by a strong combination of vortices starting from the flow separation at the sonar dome, where two layers of vortex tubes are generated, as it can be observed in Fig. 4.29 and 4.30; where the velocity contours at 11 equidistance sections at  $\Delta x/L_{pp}=0.1$  starting from the A.P. and heading downstream. Figure 4.29 represents the axial velocity contours and turbulent kinetic energy (TKE), while Fig. 4.30 shows the second  $Q$  invariant iso-surface  $Q^*=10$  colored by non-dimensional helicity for ship bottom and profile, comparing the bare and appended hull cases. From both pictures, nine main vortical formations can be observed and arranged as numbered on the figure as follows:

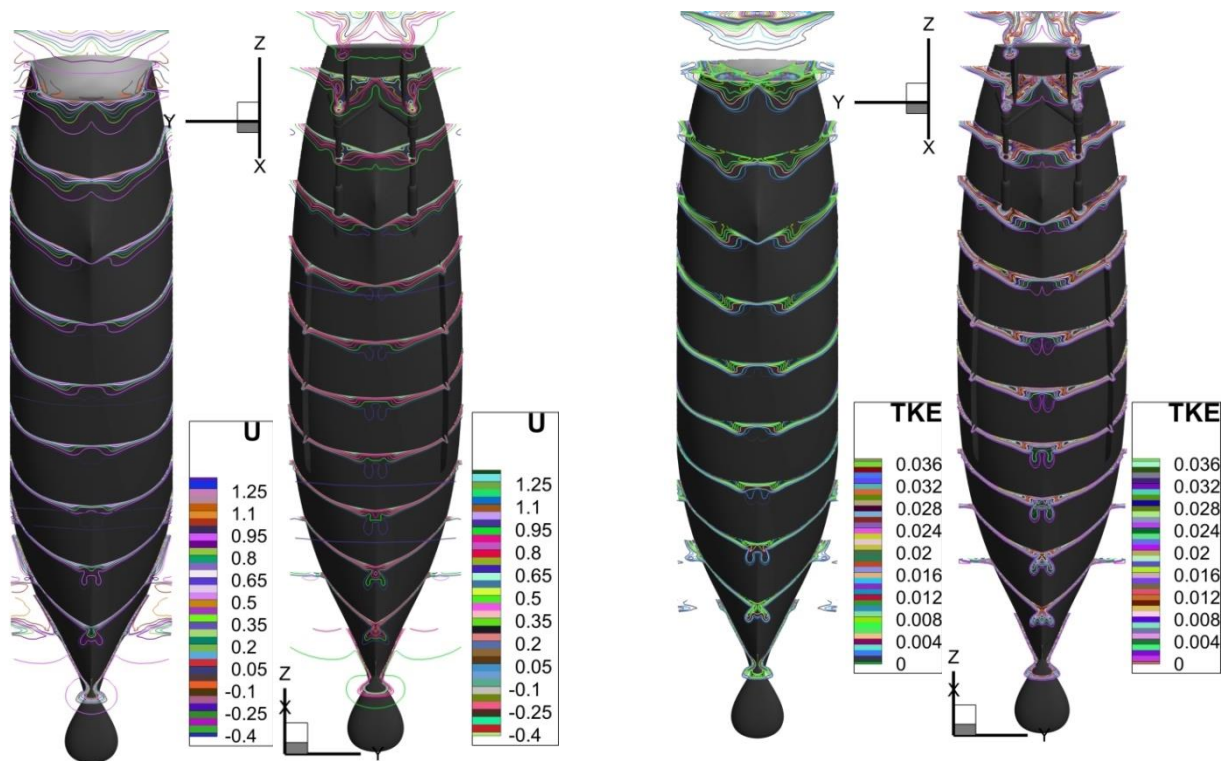


**Figure 4.29** Comparison between bare and appended hull for axial velocity contours (U) and



Turbulent Kinetic Energy (TKE)

1. Sonar Dome vortices (SDV);
2. Fore-Body Keel Vortices (FBKV);
3. Aft-Body Keel Vortices (ABKV);
4. Bottom-Shaft Vortices (BSV);
5. Bilge Keel Vortices (BKV);
6. Shaft Vortices (SV);
7. Rudder Tip Vortices (RTV);
8. Flow separation at the bottom-bracket intersection;
9. Flow separation at the Rudder-Hull intersection

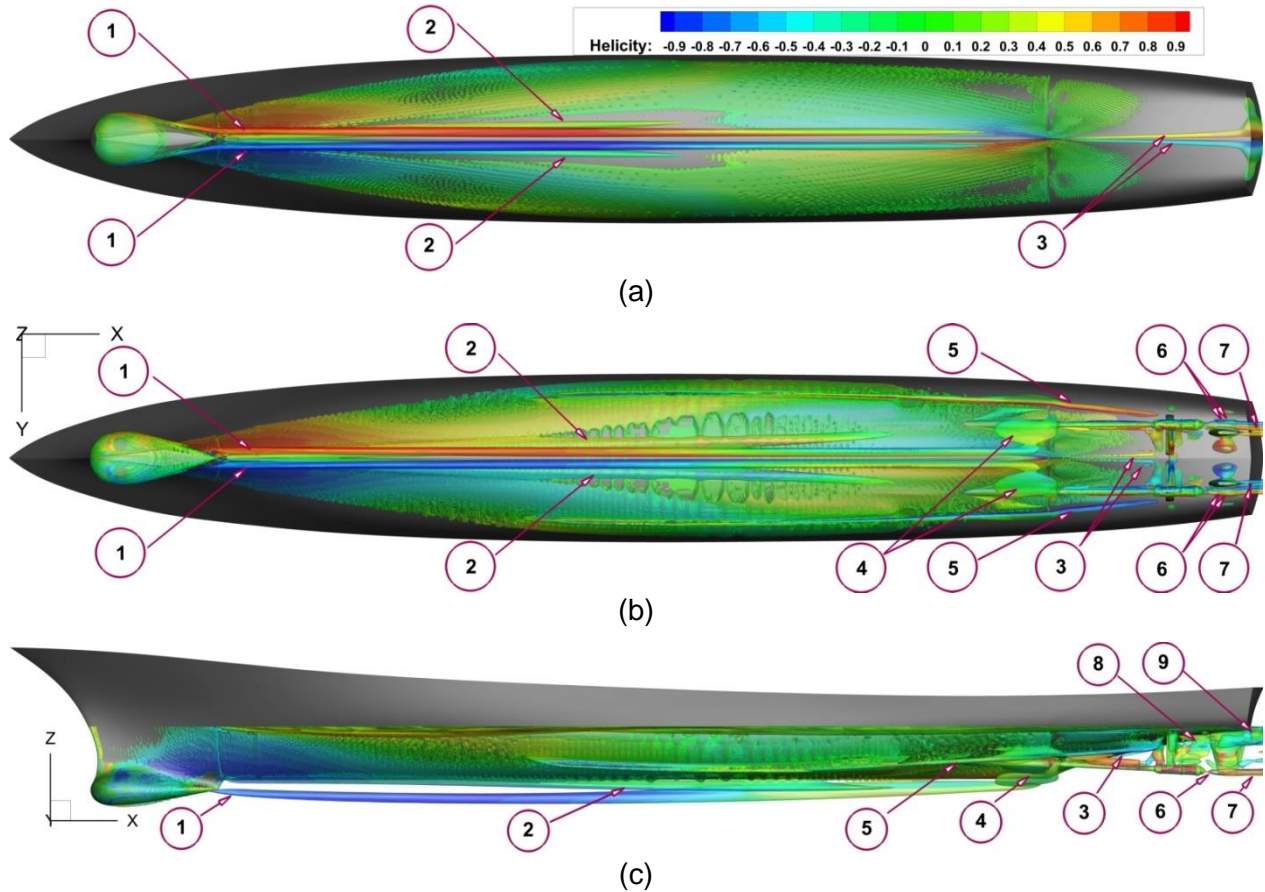


**Figure 4.30** Second invariant iso-surface  $Q^*=10$  colored by non-dimensional helicity bottom view: (a) Bare hull, (b) appended hull, and (c) appended hull profile

The results obtained for the bare hull ship model have been published in [135], while the simulation and results for the appended hull model are published in [136].

### 4.3.3 Experimental Test

An experimental test was planned and performed in the towing tank, on January, 16<sup>th</sup> 2019, aimed at predicting the total resistance, and free-surface configuration of the DTMB ship model. To make the problem more challenging, the speed range was selected to cover the medium-high speed range, starting from Froude number  $Fr=0.2$  up to  $Fr=0.44$  with a step  $\Delta Fr=0.04$  in every case. The reason behind choosing this range is to highlight the banking effect on the total resistance and the free-surface flow topology and wave height. To make this test possible, a geometrically similar model for the DTMB hull called “DTMB-UGAL” model with a scale of 1/44, which results in a reference length of  $L_{PP}=3.232$  m and design draft of 0.14 m, full characteristics can be found in Table 4.12. The speed range plan resulted in seven test cases based on the ship speed as listed in Table 4.21 showing the corresponding Froude and Reynolds numbers for every case.

**Table 4.21** Test cases and corresponding ship speed parameters

Case Number	C1	C2	C3	C4	C5	C6	C7
$U$ [m/s]	1.126	1.351	1.577	1.802	2.027	2.252	2.477
$Fr$ [-]	0.20	0.24	0.28	0.32	0.36	0.40	0.44
$Re$ [-] $\times 10^6$	3.46	4.15	4.84	5.53	6.22	6.91	7.60

#### 4.3.3.2 Resistance Measurements

The total, frictional and residual resistance coefficients are estimated based on the ITTC 57 method, according to the equations

$$R_T = R_F + R_R \quad (4.1)$$

$$C_T = \frac{R_T}{0.5\rho U^2 S}$$

$$C_T = C_F + C_R$$

$$C_R = C_T - C_F \quad (4.2)$$

$$C_F = \frac{0.075}{(\log Rn - 2)^2}$$

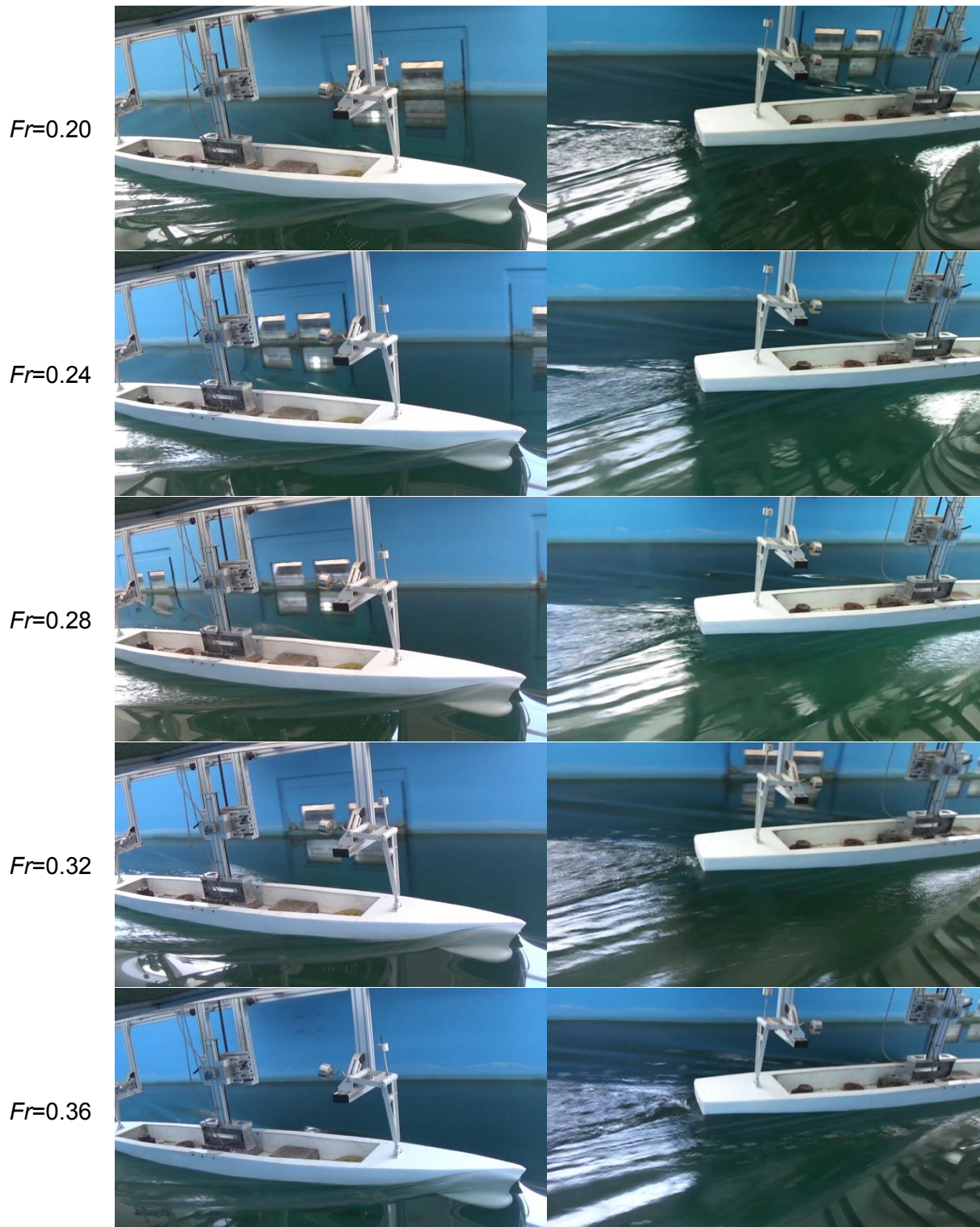
where  $R_T$  refers to the total ship resistance,  $R_F$  stands for the frictional resistance and  $R_R$  being the residuary resistance; similarly for the resistance coefficients  $C_T$ ,  $C_F$  and  $C_R$  represents, total, frictional and residuary resistance coefficients, respectively.

**Table 4.22.** Measured total resistance and corresponding resistance coefficients

Test	Time	$U$ [m/s]	$R_T$ [N]	$Fr$	$C_T$	$C_F$	$C_R$
1	10:40	1.126	5.177	0.200	5.308	3.640	1.667
2	11:30	1.351	7.357	0.240	5.240	3.517	1.723
3	12:30	1.577	10.379	0.280	5.425	3.417	2.008
4	13:30	1.802	13.580	0.320	5.436	3.334	2.102
5	14:30	2.027	17.534	0.360	5.547	3.264	2.284
6	16:35	2.252	25.668	0.400	6.579	3.202	3.377
7	17:40	2.477	35.109	0.440	7.438	3.148	4.290

### 4.3.3.3 Free-Surface Measurements

The wave profile at the ship extremities is continuously monitored by the means of two cameras to capture the wave profile in the vicinity of model and any possible green-water effect, as previously indicated. Several snapshots are captured for the wave profiles near the ship hull during the test and are brought to attention in in figure 4.32.



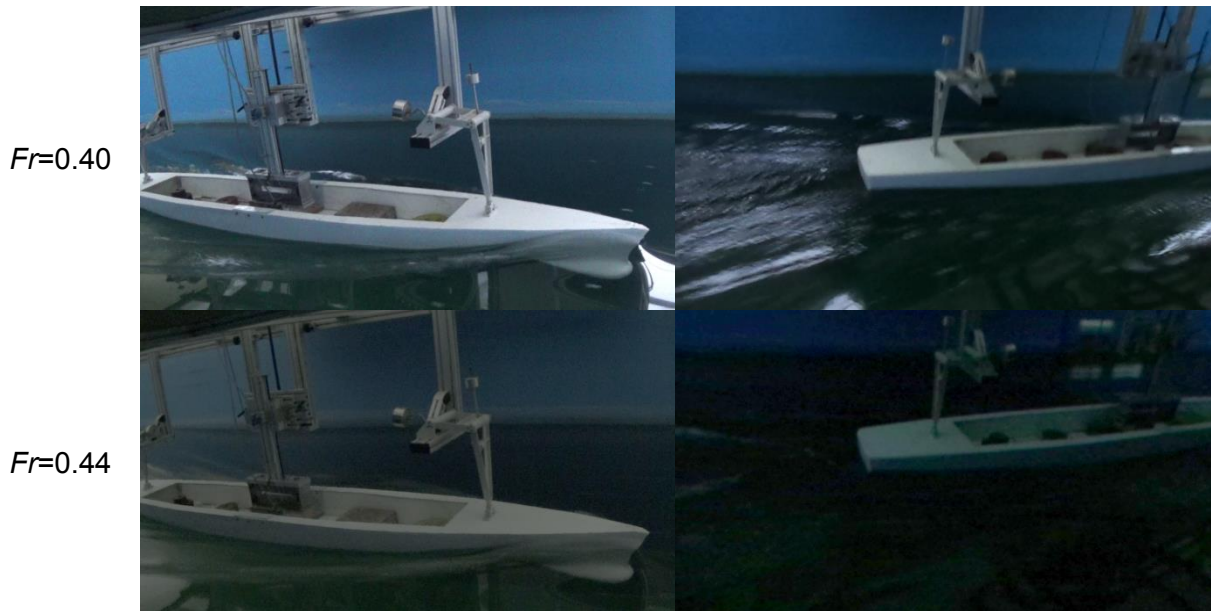


**Figure 4.32** Free-surface topology at ship extremities during the test: bow (left), stern (right)

#### 4.3.3.4 Measurements Validation

In order to investigate the accuracy of the measured results in the experiment, a simple comparison between the measured resistance in the towing tank for Model – UGAL and Model – INSEAN was performed after the data extrapolation procedure corresponding to the ITTC57 recommended procedures. This comparison is presented in Table 4.23 which shows that the tank experiment complies from the total force perspective, especially for the higher speed conditions, while for the lowest speeds, the error range is recognizable. Overall, the average error obtained in this comparison is still within 5.42%, which may be considered acceptable in the view of the aforementioned factors.

**Table 4.23** Extrapolated data from the UGAL model to the INSEAN model scale

$Fr$	Total Resistance $R_T$ [N]		$\varepsilon\%$
	Model – UGAL	Model – INSEAN	
0.2	25.39	22.58	-12.45
0.24	36.24	33.76	-7.36
0.28	51.61	48.82	-5.71
0.32	67.81	65.88	-2.93
0.36	88.04	88.70	0.75
0.4	131.28	136.35	3.72
0.44	181.58	191.23	5.05
<b>Average <math> \varepsilon\% </math></b>			<b>5.42</b>

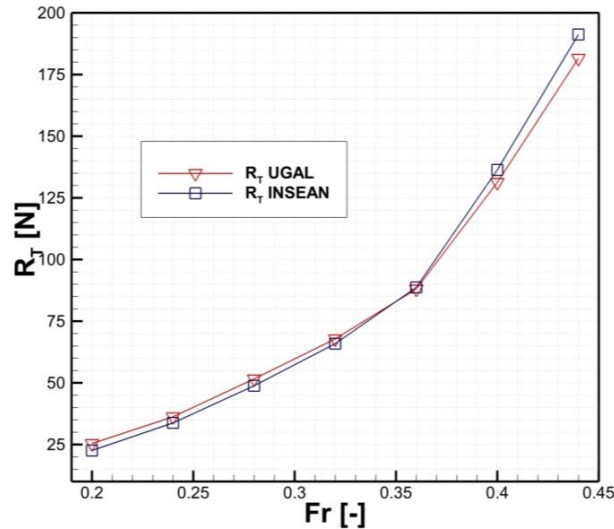


Figure 4.33 Extrapolated data of the UGAL – Model compared to INSEAN – Model [129]

### 4.3.3.5 CFD Approach

#### - Resistance Comparison

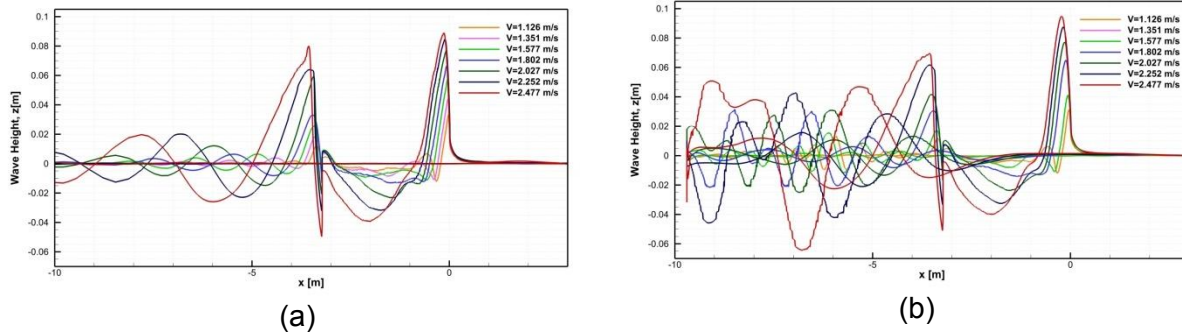
The total resistance force is numerically predicted and compared to the EFD data obtained from the experiment. This comparison is qualitatively described in Table 4.24 for the three simulation conditions. The comparison shows that the agreement between the EFD data and the CFD results is reasonable as the average error for the three simulation cases is slightly above 4.0%, which makes it more than acceptable. And also it remains within the error range obtained for the comparison made after results extrapolation that was presented in Table 4.23.

Table 4.24 Total resistance comparison between CFD and EFD results

U [m/s]	Total Resistance $R_T$ [N]				Error		
	CFD (GD)	CFD (DW)	CFD (AW)	EFD	$\varepsilon_{GD-EFD}\%$	$\varepsilon_{DW-EFD}\%$	$\varepsilon_{AW-EFD}\%$
1.126	4.910	4.947	4.950	5.177	5.157	4.443	4.385
1.351	6.850	6.881	6.941	7.357	6.891	6.470	5.654
1.577	9.696	9.814	9.830	10.379	6.581	5.444	5.290
1.802	12.973	13.176	13.164	13.580	4.470	2.975	3.063
2.027	17.194	17.458	17.468	17.534	1.939	0.433	0.376
2.252	25.846	26.492	26.528	25.668	-0.693	-3.210	-3.350
2.477	36.308	37.292	37.422	35.109	-3.415	-6.218	-6.588
<b>Average <math> \varepsilon\% </math></b>					<b>4.164</b>	<b>4.170</b>	<b>4.101</b>

#### - Free-Surface Results

The wave elevation diagram can also be visualized in Fig. 4.35 for the simulation cases combining the wave profile at the hull and at the side boundary. Evidently, due to the water reflection at the tank walls, another wave is generated.



**Figure 4.35** Wave elevation diagram: (a) general domain, (b) active walls domain

Continuously, the comparison represented in Fig. 4.36 shows the computed and the measured free-surface at the bow and the stern of the model. The CFD results resemble qualitatively well compared to the EFD data.

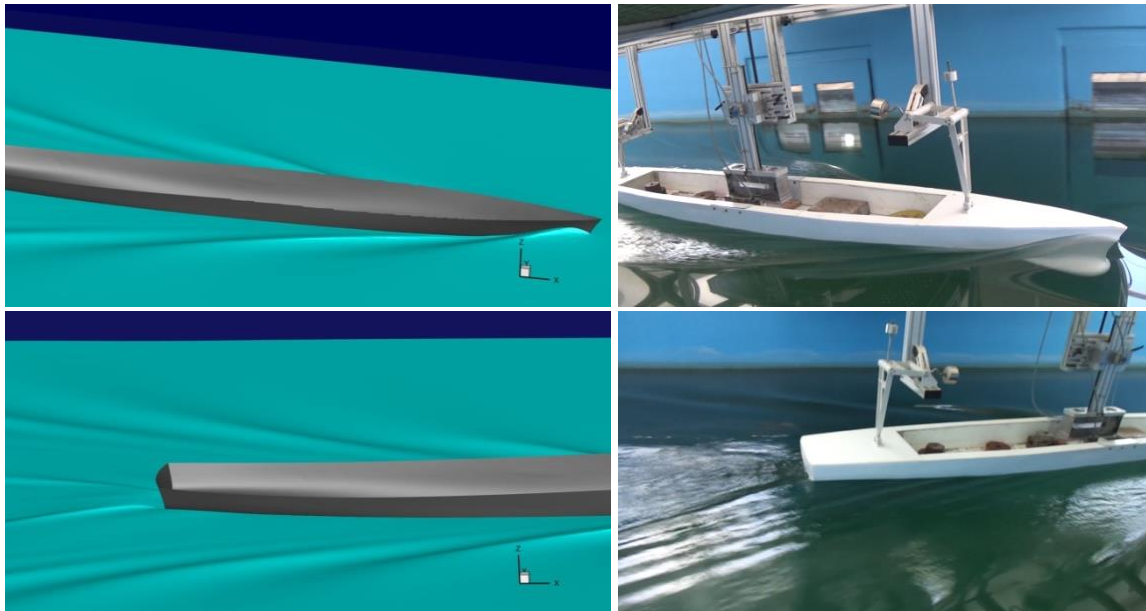


**Figure 4.36** The numerically predicted against the measured free-surface profile at model extremities

Finally, it is important to mention that all the results reported earlier for the experimental and numerical approach for this study have been fully published in [137].



## Chapter V

# Ship Propulsion Performance

Ship propulsion performance, also referred to as ship powering performance, is one of the most important aspects considered in ship hydrodynamics in the initial design stage of a ship. It comes directly after ship resistance prediction in order to establish the powering arrangement of the ship.

### 5.1 Propulsion Performance of the JBC

The JBC ship model continues for this simulation, taking advantage of the available EFD data in the public domain in order to validate the numerical results compared to the available experimental data provided by the NMRI from the Tokyo 2015 Workshop [48]. The analysis is covering three main aspects regarding the propulsion performance, which are: the propeller performance in open water (POW), the nominal flow analysis and finally, the self-propulsion performance for the propeller working in the wake domain behind the ship.

#### 5.1.1 Propulsion Performance in Open Water

The characteristic dimensions of the propeller are tabulated in Table 5.1.

**Table 5.1** Principal characteristics and parameters of the JBC propeller

Parameter	Value
Diameter, $D_p$ [m]	0.203
Boss ratio, $D_T/D_p$	0.18
Pitch ratio, $P/D_p$	0.75
Expanded area ratio, $A_E/A_0$	0.5
Number of blades, $Z$	5
Blade section	AU
Direction of rotation	Clockwise
Angle of rake	5°
Maximum blade width ratio	0.2262
Blade thickness ratio	0.05
Propeller Location from A.P., $x/L_{pp}$	0.014497
Propeller Location from base line, $z/L_{pp}$	0.018507

##### 5.1.1.1 Analysis Conditions

The propeller is analyzed in a mono-fluid condition with only water flow is considered in the simulation. Eight simulations with 8 advance speeds are performed to generate the propeller performance curves. All the eight speeds are investigated using the EASM for turbulent flow treatment to ensure better flow characteristics; however, two speeds are analyzed using an advanced turbulence model such as the DES model for comparison.



**Table 5.2** POW simulation cases and flow parameters

Simulation Case	C1	C2	C3	C4	C5	C6	C7	C8
$J$	0.1	0.2	0.3	0.4	0.5	0.6	0.7	0.8
$n$ [rpm]	3485.0	1742.0	1162.0	871.0	697.0	581.0	489.0	436.0
Equivalent Speed, $U_{eq}$ [m/s]	25.96	13.01	8.72	6.59	5.32	4.48	3.89	3.45
$Re * 10^5$	23.82	11.94	8.01	6.04	4.88	4.11	3.57	3.17

**5.1.1.2 Domain & Boundary Conditions**

The domain and boundary conditions are represented in Fig 5.1. Since the local flow wake is of an extreme importance in this case to understand the flow mechanism in the wake, an isotropic cylindrical refinement zone is imposed in the vicinity of the propeller as represented in Fig. 5.1. The boundary layer is considered in this simulation, maintaining the  $y^+$  values for all the no slip walls less than unity.

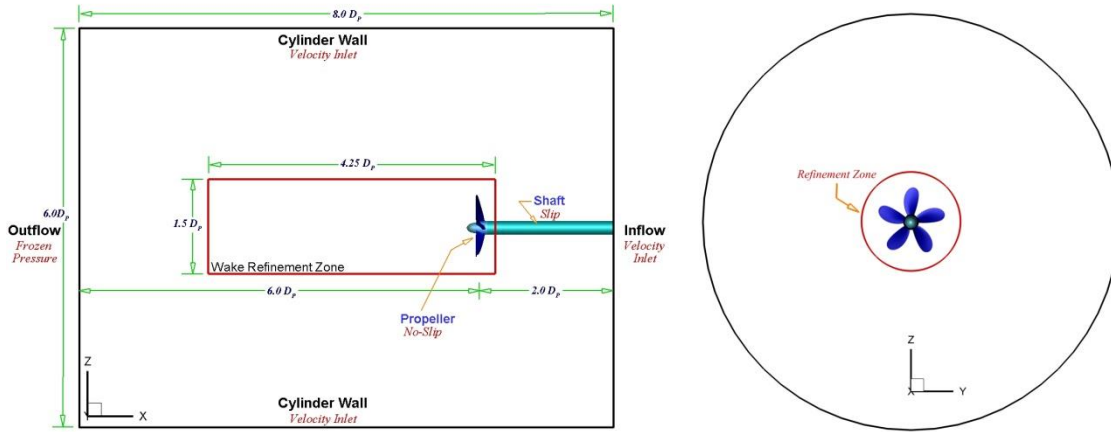


**Figure 5.1** Simulation domain dimensions and boundary conditions in x-z and y-z view

**5.1.1.3 Computational Grids**

The grid details are listed in Table 5.3, while the discretization grid configuration can be visualized in Fig. 5.2, showing the propeller blades, shaft and refinement zone.

**Table 5.3** Computational grids

Propeller Grid	Grid Size (Million Cells)			
	M1	M2	M3	M4
$y^+$	3.05	7.5	19.7	34.63
	1.26	0.92	0.68	0.46

**5.1.1.4 Simulation Strategy**

The analysis is performed for 5 seconds in each simulation case to ensure a sufficient convergence for the thrust and torque. Unsteady simulation with second order convergence criteria and 5 nonlinear iterations, while the time step  $\Delta t$  is decided to provide 100 time steps per propeller rotation according to the common practice from previous simulations based on the rotating frame approach, as proposed in the theoretical manual for the solver [110]. Once the convergence is achieved, the thrust and torque are recorded for every case and compared with the available EFD data [48].

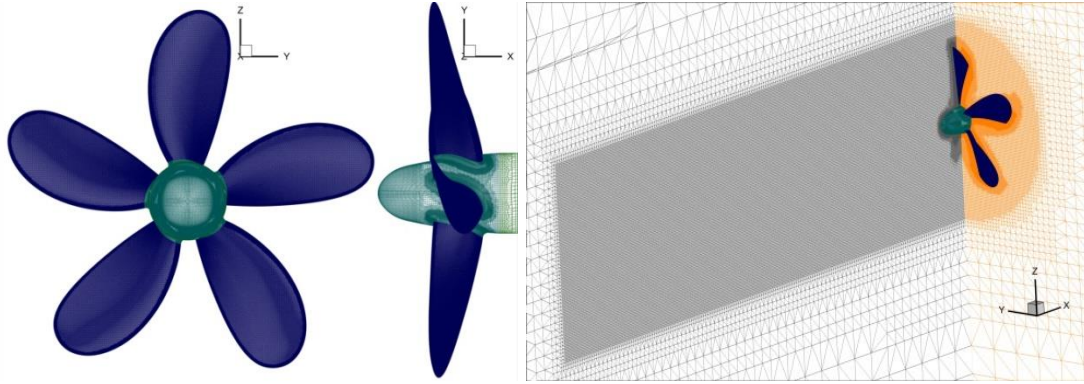


**Figure 5.2** Discretization grids for the finest grid illustrating blades grid and refinement zone

### 5.1.1.5 Thrust and Torque Results

The numerically obtained results for the thrust coefficient  $K_T$ , torque coefficients  $K_Q$  and the propeller open water efficiency  $\eta_o$  are computed for each advance coefficient based on the equations:

$$K_T = \frac{T}{\rho n^2 D_p^4} \quad (5.1)$$

$$K_Q = \frac{Q}{\rho n^2 D_p^5} \quad (5.2)$$

$$\eta_o = \frac{1}{2\pi} \frac{K_T}{K_Q} J \quad (5.3)$$

The results obtained for the propulsion coefficients are compared with the EFD data provided in [48, ] as plotted in Fig. 5.3; showing a reasonable agreement for the coarse grids and good agreement for the fines grids.

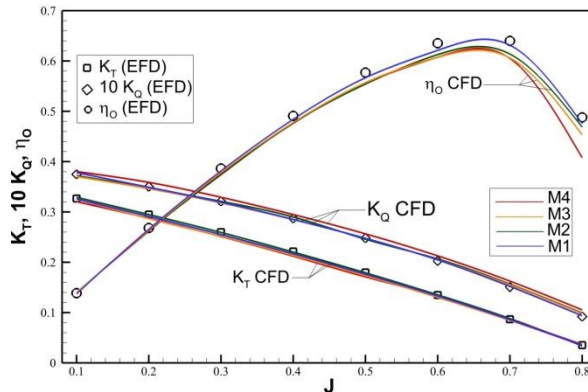


**Figure 5.3** Thrust coefficient  $K_T$ , torque coefficient  $K_Q$  and propeller open water efficiency  $\eta$  curves compared to EFD data [48, 125]

### 5.1.1.6 Wake Flow Analysis

The wake flow of the propeller is analyzed using two different turbulence models; the EASM and the DES models. One of the most important characteristics of the flow downstream of the propeller is the vortex formations, which should be well understood to get an insight into the

flow development in the wake zone. The vortices formation can be expressed by the second invariant Q criterion, as previously described in Chapter IV, as it is illustrated in Fig. 5.6 and 5.7 showing that the vortical tubes are starting due to the propeller rotation as the flow leaves the propeller tip causing the tip vortices. Close at the root of the blade, another helical tube formation can be observed resulting from the propeller rotation and flow separation at the blade root, as it can be noticed in Fig. 5.6.

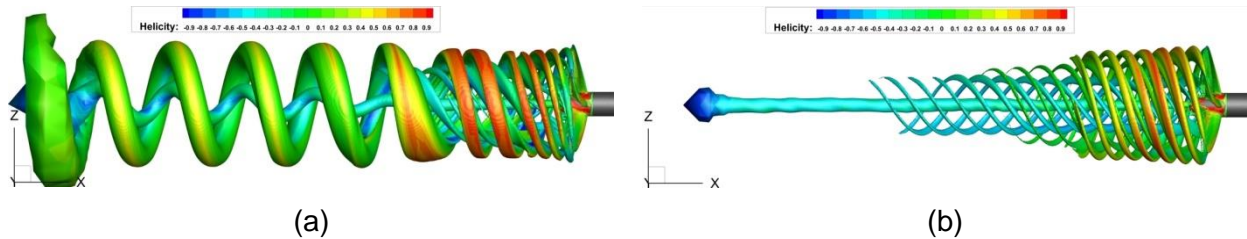


**Figure 5.6** Vortical structure of the wake flow computed at T=5 sec. for: (a)  $J=0.3$ , (b)  $J=0.6$

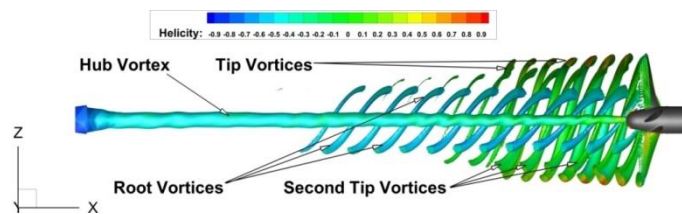


**Figure 5.7** Longitudinal cut in the vortical structure of the wake flow at  $J=0.6$

Finally, it is worth mentioning that the results reported in the previous sections have been partially or fully published in the conference paper by the author reported in [142].

The next sections are covering the study of the propeller working the ship wake based on the body force method and the fully discretized propeller using the sliding grid technique.

### 5.1.2 Self-Propulsion Simulation

The self-propulsion simulation in this study is aimed at predicting the self-propulsion point for the propeller, which can be defined as the propulsion condition when the propeller thrust is equal to the total ship drag obtained in the simple resistance test, a relation that can be mathematically expressed as  $T=R_T$ . Because the ship is usually towed in the tank by the carriage, as presented in Chapter V, sometimes the propeller thrust is not sufficient to provide the required thrust to overcome the total resistance of the model in the self-propulsion test. Thus, an extra force is added to help the propeller to overcome the total drag of the ship. This force is called the Shear Force correction (*SFC*), and can be estimated based on the formula;  $SFC=R_T-T$ . The data provided from the Tokyo Workshop 2015 reported the *SFC*, thrust and resistance values for both cases with and without the ESD. These results are used as a validation reference for the following numerical studies.

Two approaches can be applied in this concern; the first is based on the body force method using an actuator disc approach, while the second stands for introducing the actual propeller in the simulation based on sliding or overset grids. In this study, only the sliding grid technique is used for propeller modeling because it simpler and easier to model.

#### 5.1.2.1 Analysis Conditions

The analysis conditions correspond to cases 1.5~1.8 in the Tokyo 2015 Workshop for ship with and without the ESD sailing in calm water similar like resistance simulation with speed of  $U=1.179$  m/s that corresponds to the Froude number  $Fr=0.142$  and Reynolds number

$Re=4.6 \times 10^6$ . Both cases are investigated and reported in the following sections for propulsion parameters and local flow analysis.

### 5.1.2.2 Domain & Boundary Conditions

A general computation domain for the self-propulsion simulation is represented in Fig. 5.8 showing the domain dimensions and boundary conditions.

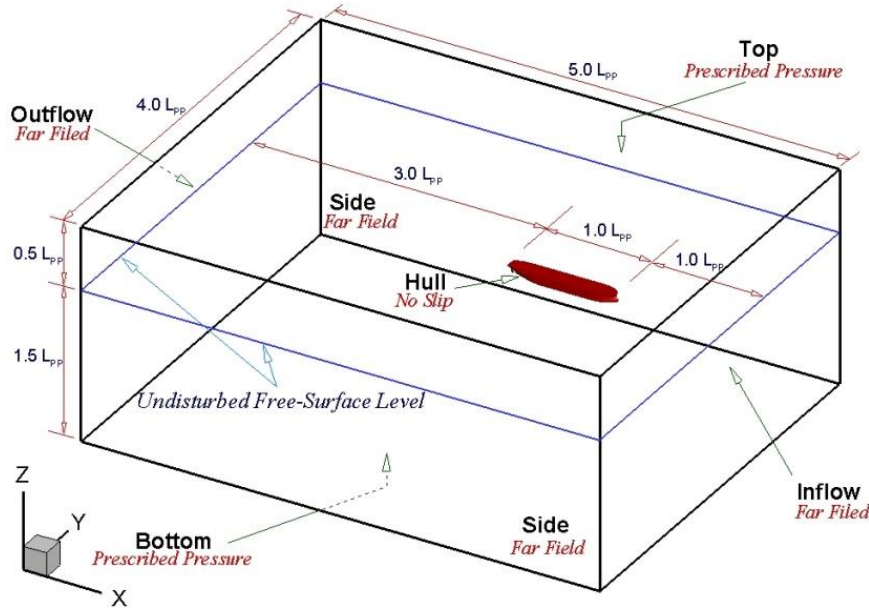


**Figure 5.8** Computational domain and boundary conditions for self-propulsion simulation

### 5.1.2.3 Computational Grids

Computational grid in this study is more complex compared to a simple resistance case. If the actuator disk method is applied, a special focus is necessary to represent properly the actuator disk refinement such that, the actuator disk refinement should be made fine enough to ensure at least 35 grid cells in the disk circumferential direction and 25 cells at the disk thickness.

The generated grids for both approaches are listed in Table 5.4 showing the total number of cells based on the grid density. Three grids are generated for every simulation to investigate the influence of the grid density on the solution accuracy, while the grid arrangement for the actuator disk and the sliding grid approach are presented in Fig. 5.10 for the ship equipped with the ESD.

**Table 5.4** Number of grid cells based on simulation conditions and grid density

Simulation	Actuator Disk Approach		Fully Discretized Propeller	
	Without ESD	With ESD	Without ESD	With ESD
Coarse (M3)	5.15	5.32	6.33	6.87
Medium (M2)	10.29	11.52	11.05	12.48
Fine (M1)	19.883	21.750	24.846	27.353

### 5.1.2.4 Simulation Strategy

For the actuator disk method, the simulation is performed on two levels; the first is identical to the resistance simulation, which is aimed at predicting of the nominal performance of the hull without the propeller including the prediction of nominal wake; the second is dedicated to the analysis of the propeller performance based on infinite-blade actuator disk approach that is used simulate the propeller performance based on the resistance results obtained in the first simulation combined with the data from open water propeller, either measured from a tank test or even computed based on the CFD method. Both simulations are similar to the resistance simulation explained in Chapter IV with a quasi-static simulation, with the same time step and solution principles.

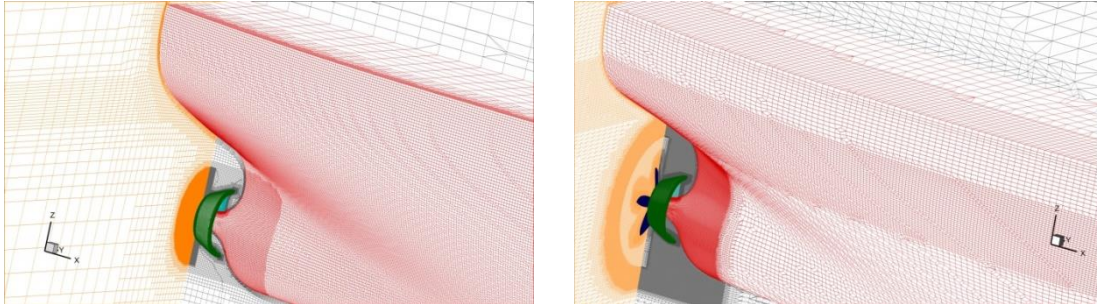


**Figure 5.10** Grid arrangement for: actuator disk(left) and sliding grid (right) approaches

For the self-propulsion prediction based on the sliding grid technique, two steps are used to perform the simulation; the first is also to estimate the nominal performance and to stabilize the resistance forces and vertical motions of the ship, while the other is used to stabilize the propeller thrust in the effective propeller performance of the propeller after connected to the hull. The first simulation corresponds perfectly with any similar resistance simulation; however, the second simulation is an unsteady simulation with a reduced time step to balance the propeller thrust and torque. The time step for the second simulation, as it is advised in the solve manual, is chosen to provide 200 time steps per propeller rotation. High performance computer is used for this simulation to ensure a quick and enough memory for the sliding grid approach, since the sliding grid technique requires a significant memory for the simulation.

### 5.1.2.5 Self-Propulsion Results

#### - Actuator Disk Method

The self-propulsion parameters computed based on the actuator disk method are listed for the three grids in Table 5.5 showing a good agreement with the EFD data. The results show a good agreement with an average error for the total resistance coefficient and propulsion parameters.

**Table 5.5** Self-propulsion results for ship with and without ESD based on actuator disk method

Coefficient	Without ESD					With ESD				
	EFD	M1	M2	M3	$ \epsilon_{av} /\%$	EFD	M2	M3	CFD	$ \epsilon_{av} /\%$
Total resistance, $C_T \times 10^3$	4.81	4.61	4.57	4.49	5.27	4.76	4.62	4.56	4.50	4.20
Thrust, $K_T$	0.217	0.2181	0.2184	0.2191	0.71	0.233	0.2332	0.2332	0.234	0.20
Torque, $10K_Q$	0.279	0.283	0.284	0.288	2.15	0.295	0.297	0.298	0.303	1.47

Advance, $J$	0.410	0.407	0.407	0.411	0.417	0.36	0.37	0.37	0.374	3.15
Thrust deduction, $(1-t)$	0.803	0.795	0.794	0.79	1.25	0.810	0.796	0.794	0.789	2.10
Wake fraction, $(1-w)$	0.552	0.524	0.517	0.511	6.28	0.471	0.461	0.457	0.459	2.55
Relative rotative, $\eta_r$	1.011	1.0	1.0	1.0	1.09	1.014	1.0	1.0	1.0	1.38
Hull efficiency, $\eta_H$	N.A	1.517	1.535	1.545	-	N.A	1.727	1.739	1.719	-

The axial velocity contours measured at the section located in the propeller reference plan is plotted in Fig. 5.11 for the ship with and without the ESD at the nominal and effective wake condition.

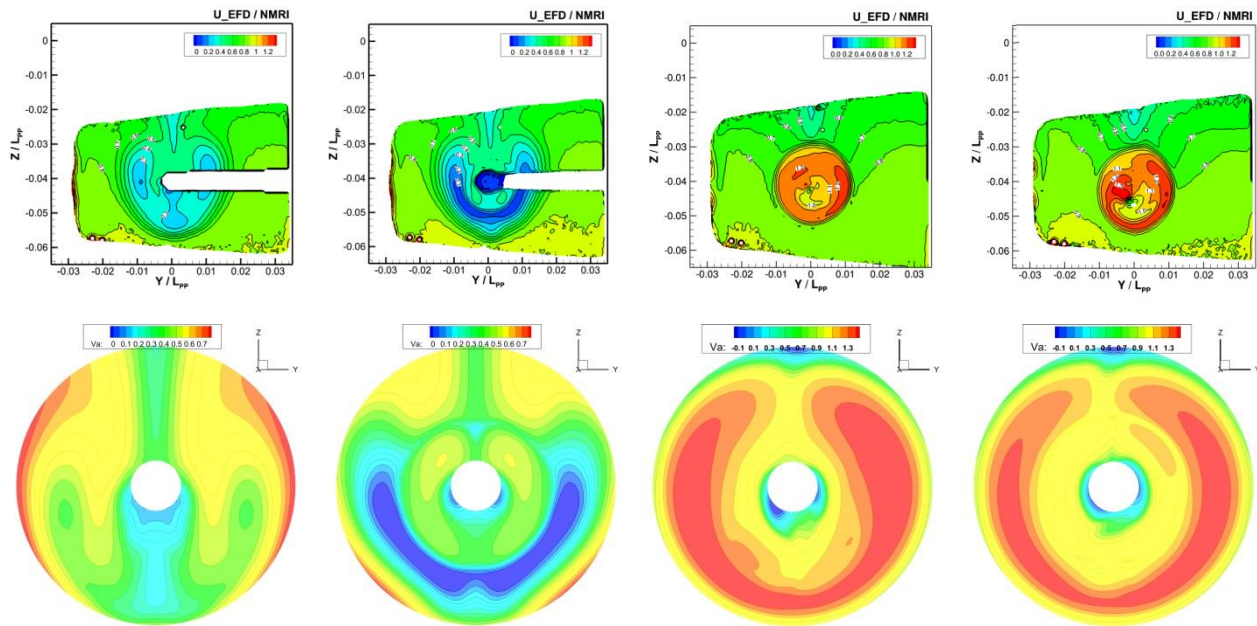


**Figure 5.11** CFD results for nominal (a and b) and effective (c and d) velocity contours computed for ship with and without ESD using actuator disk method

#### - Sliding Grid Method

The numerical results, plotted in Fig. 5.12, obtained for the propeller rotation resembles very well with the experimental data. The obtained rotation for the ship without the duct is  $n=7.7223$  rps, compared to the experimental value of  $n=7.8$  rps, with an error within 0.99%; while for the ship with the duct, the calculated propeller rotation is  $n=7.3852$  rps, compared to the experimental value of  $n=7.5$  rps, with an error 1.53%. Both values show the capability of the CFD method to predict accurately the self-propulsion point of the ship.

Similar to the results obtained in the actuator disk simulation, the resistance, thrust, torque and advance coefficients are tabulated in Table 5.6.

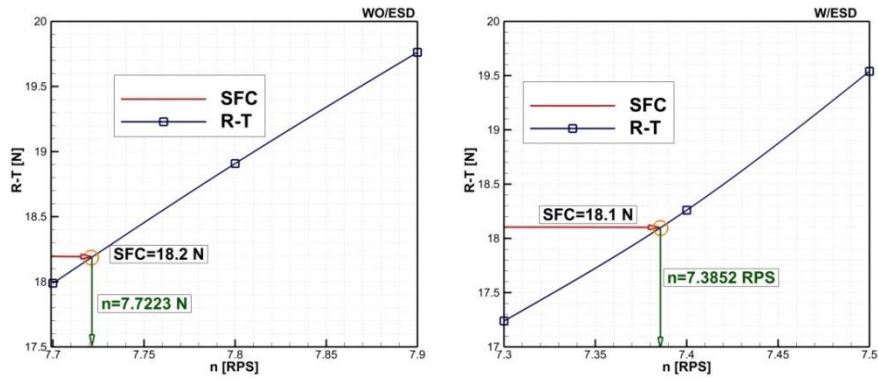


**Figure 5.12** Results interpolation to predict the propeller rotation rate

**Table 5.6** Self-propulsion coefficient for ship with and without ESD using sliding grid method

Coefficient	Without ESD			With ESD		
	EFD	CFD	$ \epsilon \%$	EFD	CFD	$ \epsilon \%$
Total resistance, $C_T \times 10^3$	4.811	4.913	2.12%	4.76	4.69	1.58%
Thrust, $K_T$	0.217	0.232	6.91%	0.233	0.243	4.16%
Torque, $10K_Q$	0.279	0.291	4.30%	0.295	0.306	3.72%
Advance ratio, $J$	0.410	0.414	0.98%	0.36	0.366	1.67%
Propeller rotation at self-propulsion point, $n$ [rps]	7.8	7.7223	0.99%	7.5	7.3852	1.53%

To have a closer look on the flow in the propeller wake, two sections are proposed to compare the flow in the stern region at stations S4 and S7. The streamwise velocity contours are compared with the EFD data and presented in Fig. 5.13, the comparison shows that the computed streamwise velocity contours are within a good correspondence with the experimental data.

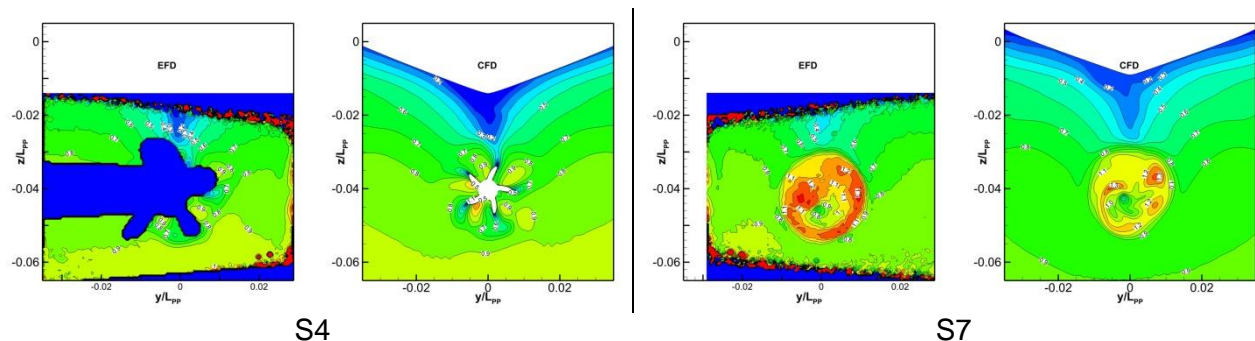


**Figure 5.13** Comparison between the streamwise velocity contours measured and ship without ESD for sections S4 and S7

More details of the velocity contours at different section for ship with and without rudder is plotted Fig 5.14 along with the second invariant iso-contours of the vortices, in order to understand the mechanism of the generated vortices. The vortices formation is similar to the open water configuration.

Finally, it is worth mentioning that the results reported in the previous sections have been partially or fully published in the conference paper by the author reported in [143, 144].

The next sections are covering the same simulation concept for open water propeller and self-propulsion simulation of the KVLCC2 ship model.

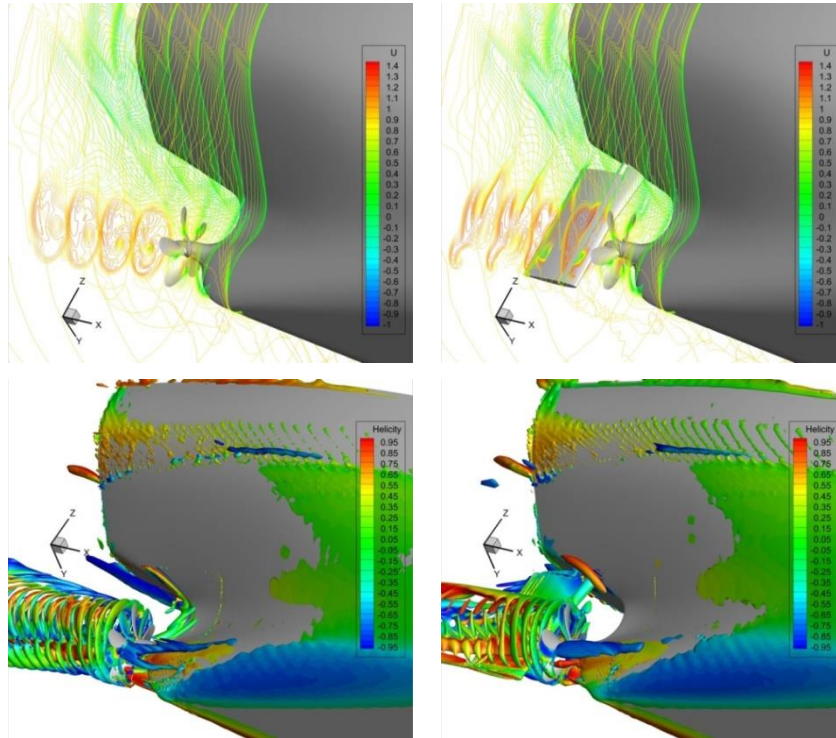


**Figure 5.14** Comparison between the streamwise velocity contours for ship without ESD and the second invariant  $Q^*=50$  for ship with and without rudder, computed using DES turbulence model



## 5.2 Propulsion Performance of the KVLCC2

Following the same principle in the previous study related to the propulsion performance of the JBC ship model, this continuous study is concerned with applying the same principles for predicting the propulsion performance of another ship type, though both hull are within the category of large block coefficient ships.

### 5.2.1 Propulsion Performance in Open Water

The propeller and rudder details are tabulated in Table 5.8, while the propeller and rudder geometry were presented in Fig. 4.12 Chapter IV.

**Table 5.8** Principal particulars of KVLCC2 E698 propeller model

Parameter	Value
Diameter, $D_p$ [m]	0.204
Boss ratio, $D_H/D_p$	0.165
Pitch ratio, $P/D_p$	0.808
Expanded area ratio, $A_E/A_0$	0.448
Number of blades, $Z$	4
Direction of rotation	clockwise

#### 5.2.1.1 Analysis Conditions

The open water simulation of the E698 propeller model corresponds to a tank test reported in the SIMMAN Workshop [146]. Similar approach like the one performed in the JBC propeller simulation is also repeated here.

#### 5.2.1.2 Domain & Boundary Conditions

The domain and boundary conditions reported in the same simulation for the JBC hull still persist in this simulation, with the same dimensions and conditions on the boundaries and surfaces.

#### 5.2.1.3 Computational Grids

Two grids were tested for simulation convergence and solution accuracy, 10.67 M and the second has 36.33 M cells, the fine grid is plotted in Fig 5.15.

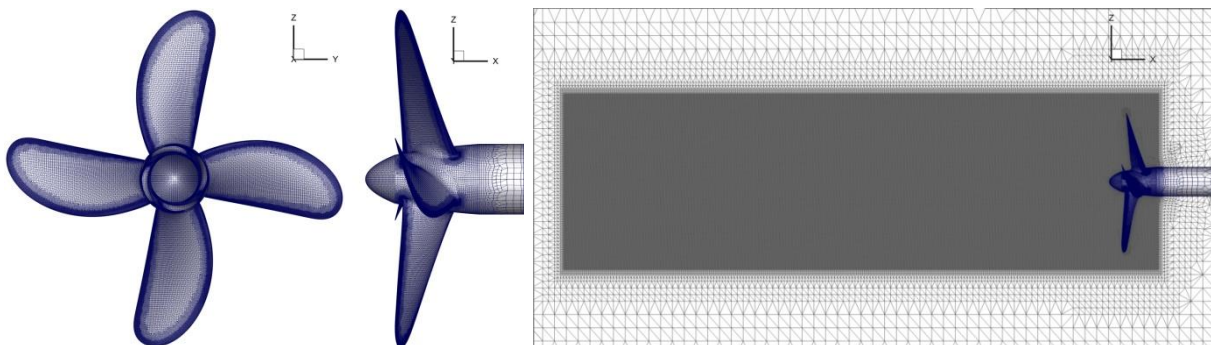


**Figure 5.15** Mesh arrangement of the fine grid

### 5.2.1.4 Simulation Strategy

The simulation strategy is similar to that for JBC ship propeller described in section 5.1.1.4.

### 5.2.1.5 Thrust and Torque Results

The numerically obtained results for the thrust coefficient  $K_T$  and torque coefficients  $K_Q$  are plotted in Fig. 5.16 compared to the available EFD data. The obtained results show a good agreement with the experimental data, especially for the light loaded propeller condition when  $J$  value increases. The average error computed for all the thrust coefficient  $K_T$  divided on the seven simulation cases is within 0.87%, while the average error for the torque coefficients  $K_Q$  is within 1.42%.

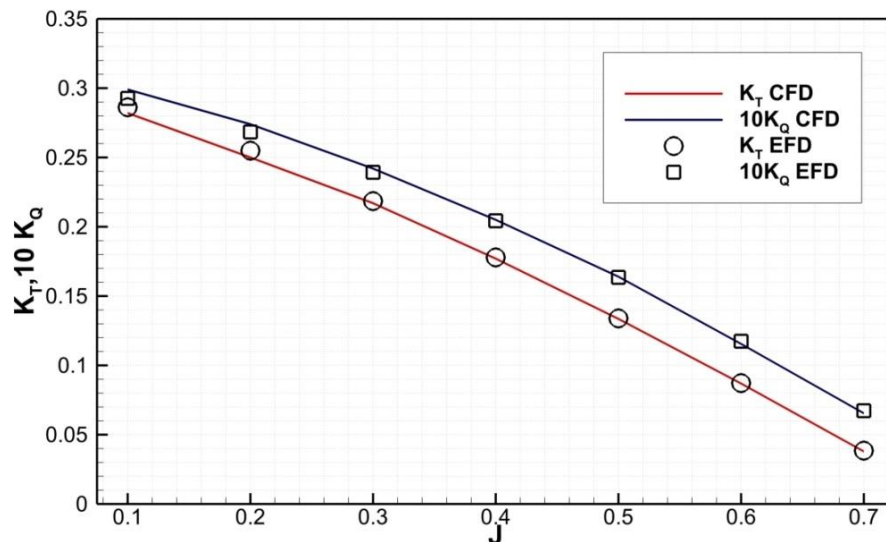


Figure 5.16 Open water propeller performance curves CFD results against EFD data

### 5.2.1.6 Local Flow Results

The local flow results are represented in Figs.5.17~5.23 for different turbulence models at various advance velocities.

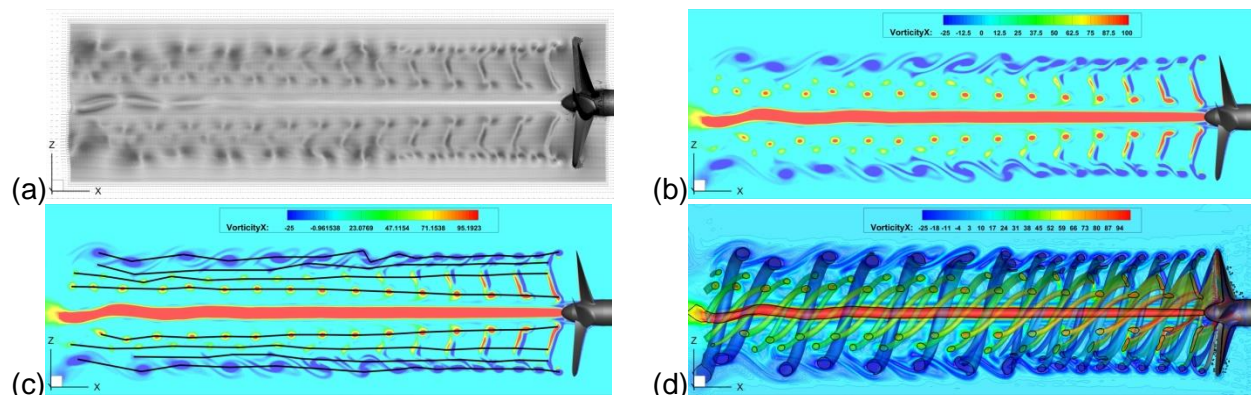
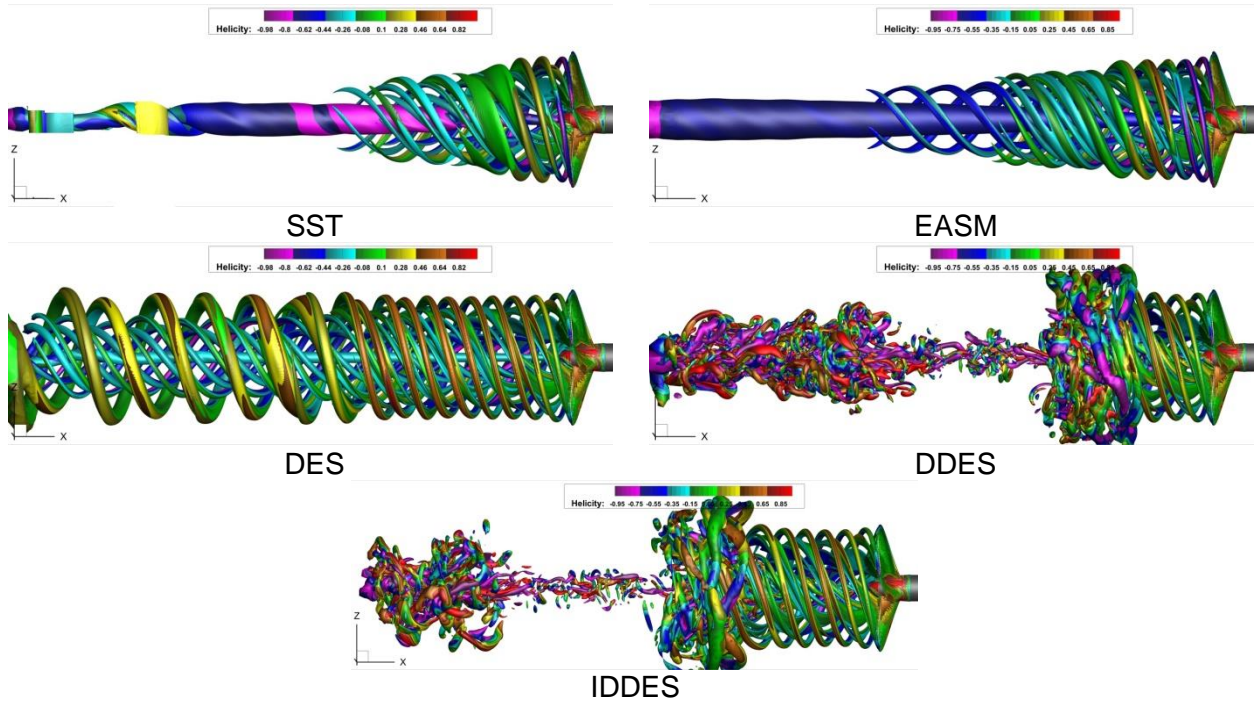
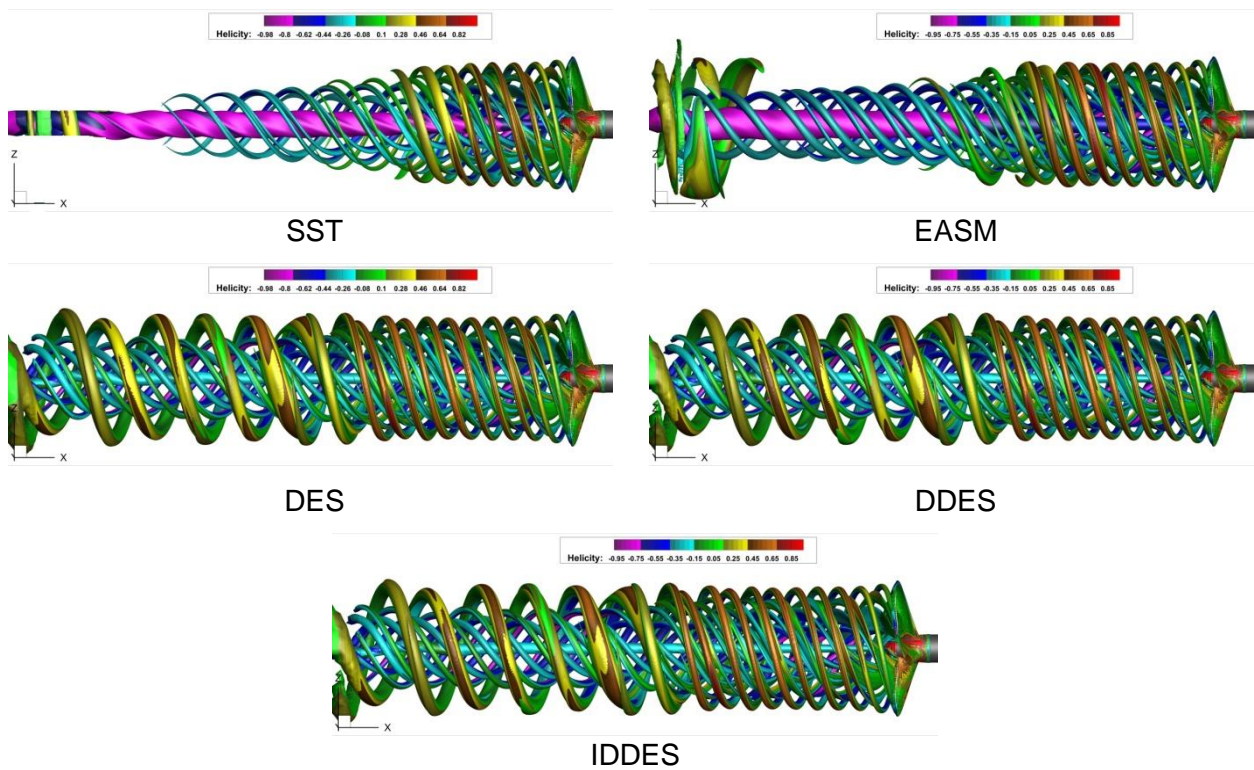


Figure 5.17 Vorticity at  $J=0.2$ : (a) vector form, (b) magnitude, (c) trajectory and (d) vortex cores



**Figure 5.18** Second invariant computed for  $J=0.2$  based on different turbulence models for iso-surface=500



**Figure 5.20** Second invariant computed for  $J=0.4$  based on different turbulence models for iso-surface=250

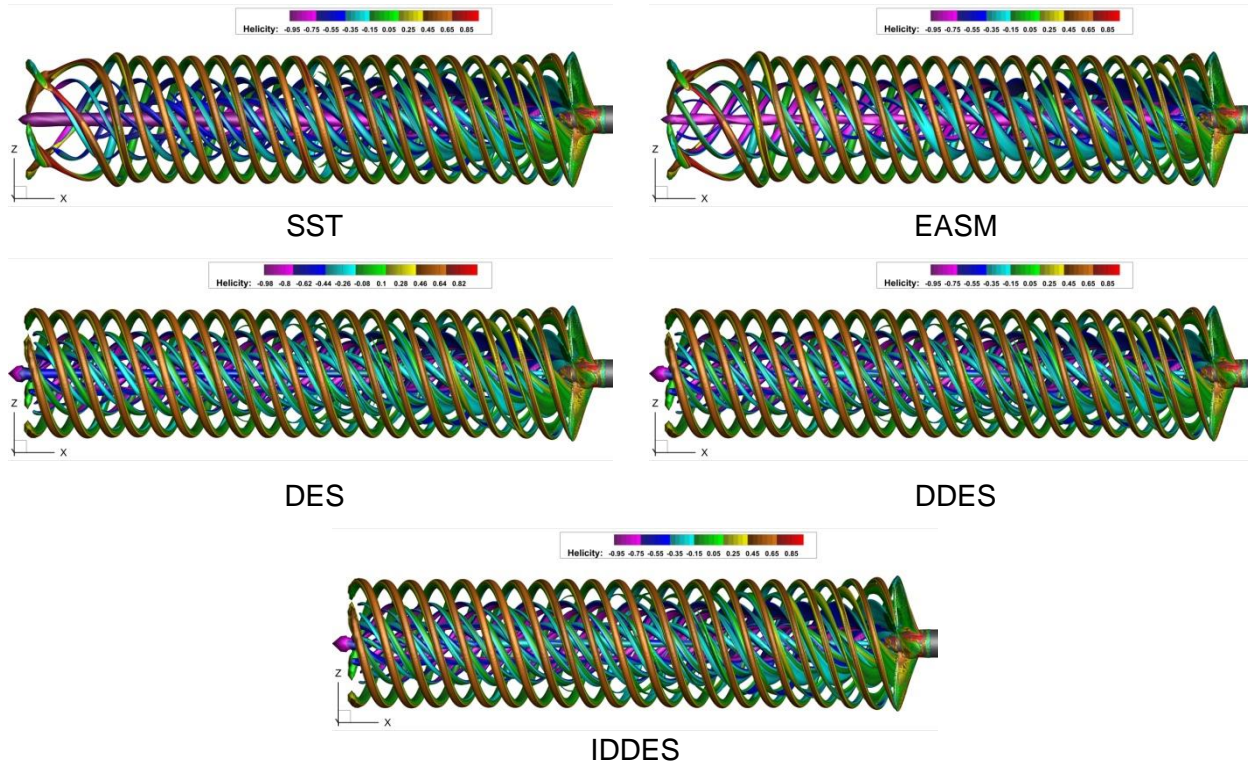


**Figure 5.22** Second invariant computed for  $J=0.6$  based on different turbulence models for iso-surface=125

Last but not the least, the results from this study were partially published in [135].

### 5.2.2 Self-Propulsion Performance

The same principle applied for the JBC ship is repeated here for the KVLCC2 ship model in order to compute the self-propulsion performance characteristics and local flow. The solution is achieved also by applying the body force method based on the actuator disk approach and the second is dedicated for the self-propulsion using a fully discretized propeller modeling based on the sliding grid technique.

The results show a good agreement with the experimental data with an error range between 1.61% and 13.27%. The maximum error is recorded for the torque coefficient of the bare hull ship. Similar significant error for the same case was reported in the study reported in [145] where the EFD data are imported from.

**Table 5.10** Thrust and torque coefficients computed using the actuator disk method compared to the EFD data extracted from [145]

Parameter	Bare hull			With simplified rudder			With actual rudder		
	EFD	CFD	$ \varepsilon \%$	EFD	CFD	$ \varepsilon \%$	EFD	CFD	$ \varepsilon \%$
Thrust coefficient, $K_T$	0.195	0.1983	1.69	0.198	0.208	5.05	0.198	0.2022	2.12
Torque coefficient, $10K_Q$	0.266	0.2307	13.27	0.228	0.2357	3.37	0.228	0.2307	1.18



## Chapter VI

# Ship Seakeeping Performance

Studying ship hydrodynamic performance in wave comes with great importance from multiple perspectives. For example, considering ship motions in waves, potential hazards can result from severe motions, which may have negative effects on the ship stability, safety, survivability and finally working operations on board, if green water phenomena occur. Handling the problem from the ship powering point of view, it is very important to estimate the added resistance in waves to provide sufficient power margin to overcome the drag resulting from sailing in waves.

### 6.1 Seakeeping Performance in Regular Head Waves

The seakeeping performance of the DTMB ship model in head waves is analyzed and presented for two cases; wave diffraction and wave radiation. All the numerical results obtained in both cases are validated compared to the experimental results reported in [87, 130].

#### 6.1.1 Seakeeping in Wave Diffraction Condition

In this simulation, the ship is sailing in regular sinusoidal head waves with no degrees of freedom, i. e. all the motions are restricted. The main scope is to analyze the forces, free-surface and flow features in the ship domain. The ship model used in this simulation is the DTMB surface combatant whose geometry and principal dimensions were presented in Chapter V.

##### 6.1.1.1 Analysis Conditions

Correlating the simulation conditions as described in case 3.5 from G2010 [47] with respect to the wave steepness  $Ak$ . Table 6.1 summarises simulation conditions and corresponding wave characteristics.

**Table 6.1** Simulation conditions and corresponding wave parameters

Wave Parameter	$Ak$ [-]	$\lambda$ [m]	$H_w$ [m]	$T$ [s]	$f_w$ [Hz]	$T_e$ [s]	$f_e$ [Hz]
Value	0.025	4.572	0.03638	1.711	0.584	1.088	0.919
	0.050		0.07276				
	0.075		0.10914				

##### 6.1.1.2 Domain & Boundary Conditions

The domain and boundary conditions are depicted in Fig. 6.1.

##### 6.1.1.3 Computational Grids

The grid configuration for fore, aft regions and a longitudinal section are presented in Fig. 6.2.

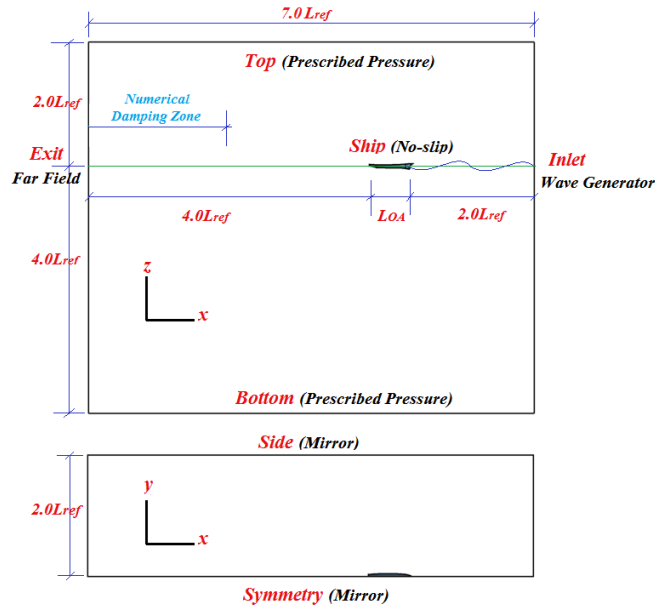


**Figure 6.1** Domain geometry, dimensions and boundary conditions

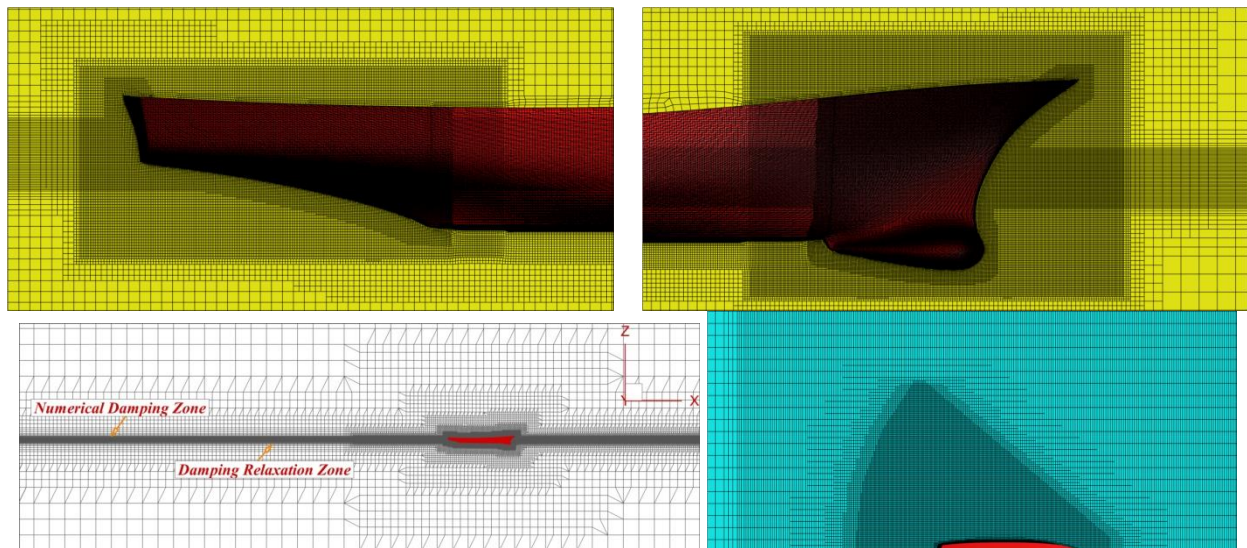


**Figure 6.2** Grid configuration showing: stern, bow, longitudinal section free-surface top view

Three grids are generated to study the effect of the grids on the accuracy of the numerical results. The numbers of grid cells are 6.21, 8.186 and 14.39 M cells.

#### 6.1.1.4 Simulation Strategy

Unsteady simulations are performed until the ship encounters 15 consecutive waves to ensure sufficient convergence, or until the numerical residuals are sufficiently reduced. The discretization in time is made to provide 150 time steps/ wave period for wave fixed ship condition, and 200~250 time steps for motion condition. Integration in time is imposed with fourth order convergence criteria, combined upwind and central schemes with 12~20 nonlinear iterations are used. All the simulations are performed on HPC concept with available resources for this simulation of 120 cores and 128 GB of RAM at 1.6 GHz. Physical simulation time is recorded within 28 and 268 hours, depending on the grid resolution and simulation time.

### 6.1.1.5 Resistance, Forces and Moments Results

Case 3.5 proposed in the G2010 Workshop was basically a speed diffraction problem with no degrees of freedom available for the ship. In this case, the results are concerned with the forces acting on the hull for resistance, heave and pitch. For this reason, the results obtained in the CFD simulation is compared with the EFD data provided from the workshop in [47] and represented in Table 6.2 and Fig. 6.3.

**Table 6.2** Computed versus measured  $C_T$ ,  $C_H$ ,  $C_M$  coefficients

Variables	Resistance ( $C_T$ )		Heave ( $C_H$ )		Pitch ( $C_M$ )	
	0 <sup>th</sup> Amplitude	1 <sup>st</sup> Amplitude	0 <sup>th</sup> Amplitude	1 <sup>st</sup> Amplitude	0 <sup>th</sup> Amplitude	1 <sup>st</sup> Amplitude
EFD [47]	0.00462	0.00608	-0.0334	0.0357	$-6.08 \times 10^{-4}$	0.0108
CFD	0.00447	0.00664	-0.0242	0.0422	$-6.84 \times 10^{-4}$	0.0119
$ \varepsilon \%$	3.25	9.21	27.55	18.21	12.50	10.19

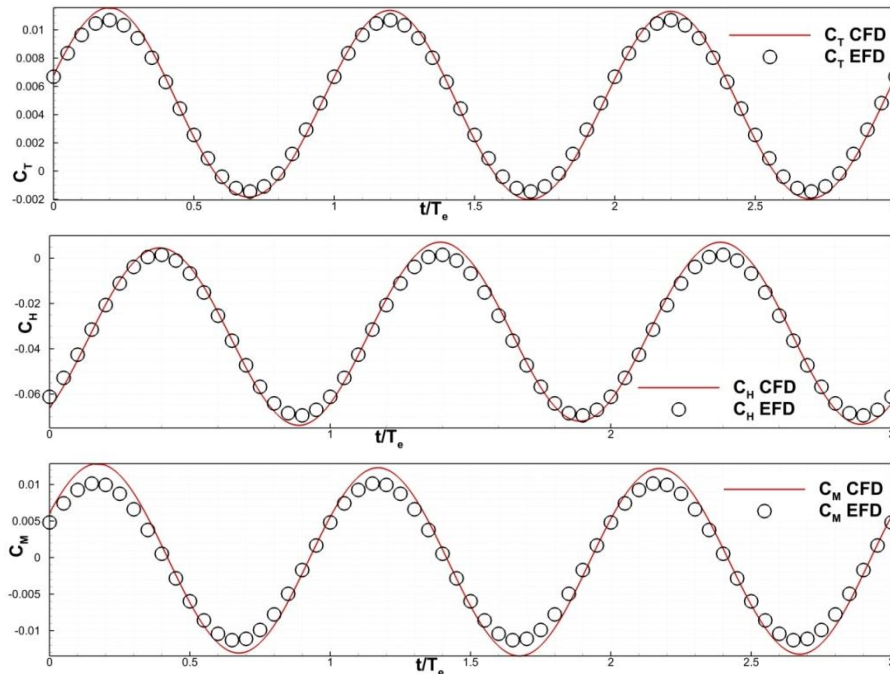


**Figure 6.3** Resistance  $C_T$ , Heave  $C_H$  and Pitch  $C_M$  coefficients compared to EFD [47]

The free-surface comparison presented in Fig. 6.7 shows that qualitatively and quantitatively, the computed free-surface is within a good agreement with the experimental results. However, it is worth mentioning that the free-surface elevation is slightly under predicted in the region away from the hull. Near to the hull region, the agreement between CFD and EFD is encouraging. This is related to the existence of the Kelvin batter refinement, which seems to be sufficient with 100 cell/wave length. Yet, for coarser grids, the free-surface was under predicted.



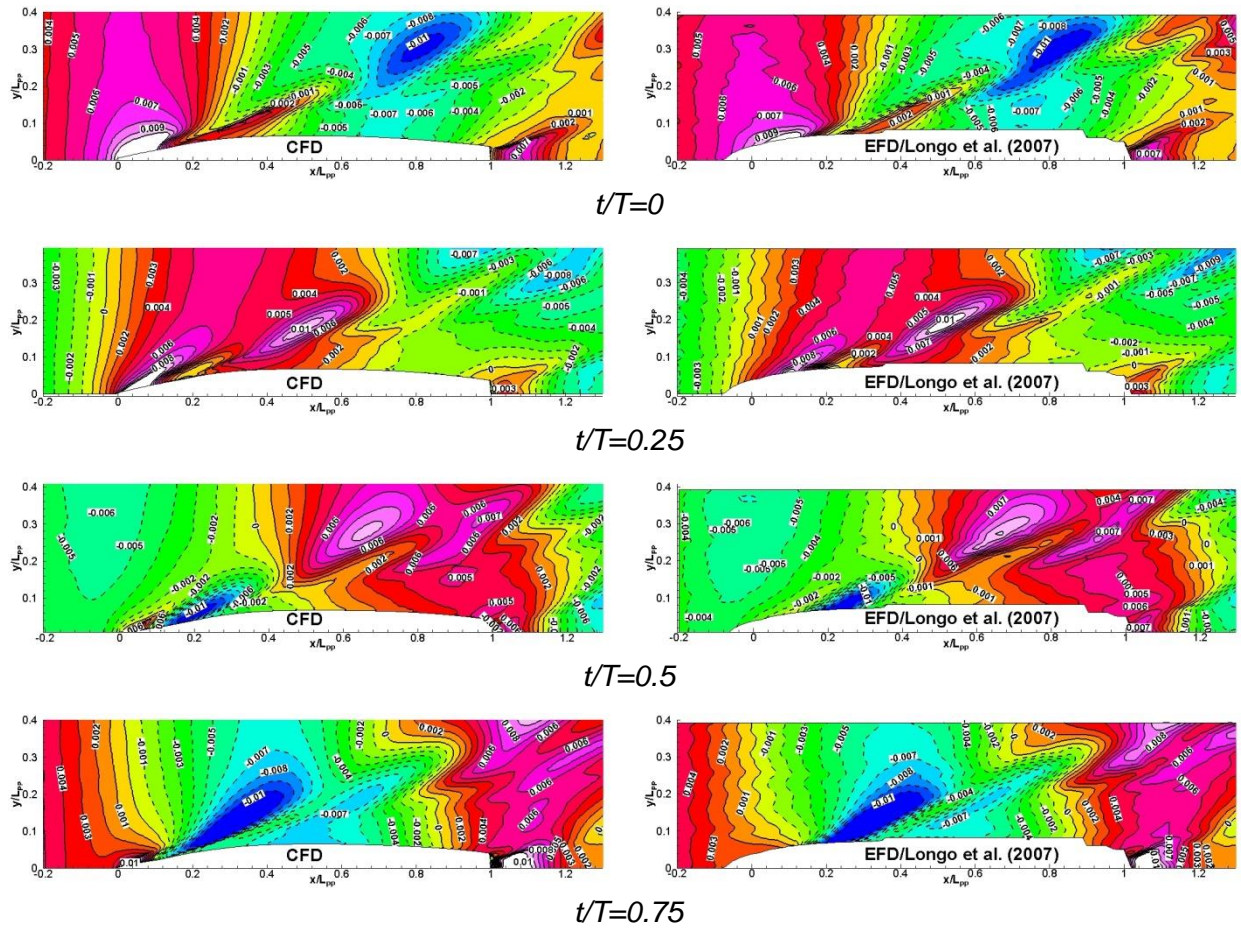


Figure 6.7 Computed free-surface at four wave quarters compared EFD [47, 87]

## 6.1.2 Seakeeping in Wave Radiation Condition

In this simulation condition, the ship is free to heave and pitch. Total resistance and ship responses are important to be taken in to consideration is this study. The target is to analyze the total resistance in wave and to attempt to correlate it to the total resistance in the calm water condition to extract the added resistance in wave. As for the ship motions, ship responses have very significant importance, because it might impose a direct or indirect impact on ship safety and operability.

### 6.1.2.1 Analysis Conditions

The simulation conditions are divided in this case into four major categories, as it is listed in Table 6.3.

**Table 6.3** Simulation cases parameters and corresponding grid density

Simulation cases	$\lambda/L_{PP}$	$Ak$	$Fr$	Grid density ( $\times 10^6$ )
a. V&V study				
C1	1.5	0.025	0.28	3.1, 4.8, 7.2, 10.3
b. Response and added resistance in waves based on $\lambda$				
C2-C8	0.50	0.025	0.28	6.5
	0.75			6.3
	1.00			2.9
	1.25			2.6
	1.50			3.1
	1.75			3.9
	2.00			2.9
c. Zero Speed				
C9-C10	1.5	0.025 & 0.050	0	2.6
d. Free-surface & Wake Flow				
C11-C12	1.50	0.025	0.28 & 0.41	14.4

### 6.1.2.2 Domain & Boundary Conditions

The domain dimensions, configuration, boundary conditions are the same like the one used for diffraction condition.

### 6.1.2.3 Computational Grids

To keep the consistency of the numerical solution at different simulation conditions, same grid generation parameters are maintained for the spatial discretization of the simulation of each case. The resulting difference in the simulation grid is influenced by the length and amplitude of the wave. The full details of the grid resolution have been represented in Table 6.3.

### 6.1.2.5 Results

Depending on the simulation case scope, the results are obtained for every case and validated with the experimental results, if exist. The following subsections will cover every case individually focusing on the obtained results and their validation outcomes.

**- Case1: Verification and Validation**

The verification and validation studies showed that the simulation is more grid dependent than time step dependent, especially when the time step is reduced within 500 time steps / wave period. Verification and validation results are represented in the main context of the thesis.

**- Case 2–8: Ship Responses and Added Resistance In Waves  $C_{aw}$  Based On Wave Length  $\lambda$**

The calculations for the added resistance coefficient in waves  $C_{AW}$  are presented in Table 6.11.

**Table 6.11** Added resistance in waves for cases C2–C8

$\lambda/L_{PP}$	Total Resistance Coefficients		Added Resistance in Waves	Ratio
	In Waves $C_{TW}$	In Calm Water $C_{TCW}$	$C_{AW}$	$C_{AW} \% C_{TCW}$
0.50	0.00459	0.00425	0.00034	8.1
0.75	0.00473		0.00048	11.2
1.00	0.00527		0.00102	24.0
1.25	0.00592		0.00167	39.2
1.50	0.00528		0.00113	24.2
1.75	0.00521		0.00096	22.6
2.00	0.00498		0.00073	17.3

Taking a closer look at the results for heave and pitch responses which are presented in Fig. 6.17, a reasonable agreement with the experimental data can be observed for the heave response with an average error for the seven points within 5.6%.

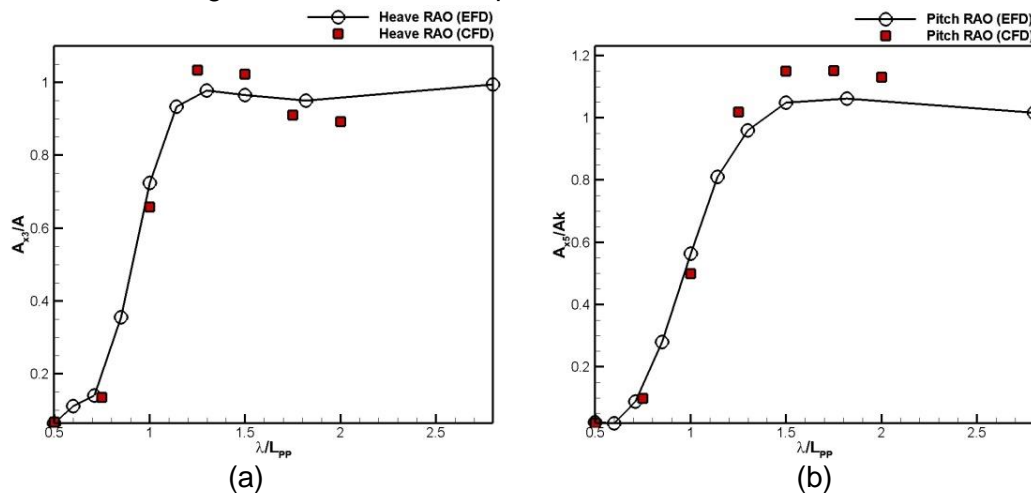


**Figure 6.17** RAO for: (a) heave and (b) pitch compared to EFD data [87] at cases2–8

**- Case 9-10: Zero Speed**

Analysing the results for zero speed case, which are summarised in table 6.12, for cases C9 and C10, the absolute average error range for heave response is within 4.1 and 4.3%, which is considered reasonable. On the other hand, the pitch response has an error that is still considerably significant at 11.4%.

**Table 6.12** Heave and pitch responses in at different  $Ak$  from C9

$Ak$	$TF$ Motion	EFD [87]	CFD	$ \epsilon /\%$
0.025	Heave	0.604	0.580	4.1
	Pitch	0.780	0.869	11.4
0.05	Heave	0.607	0.581	4.3
	Pitch	0.788	0.878	11.4

**- Case 11: Free surface**

The interaction between wave and hull is spotted and presented in Fig. 6.20 in the hull vicinity at the previously reported moments to get a closer look at the wave separation and any breaking effect during the simulation. The figures insure the aforementioned separation at the flare on one side, whereas on the other side closer to the ship stern, the rooster-tail separation and breaking effect seems to be more obvious compared to the fixed case. The same conclusion remains for the reason behind this effect, which returns to the interaction that occurs as the ship encounters the wave.

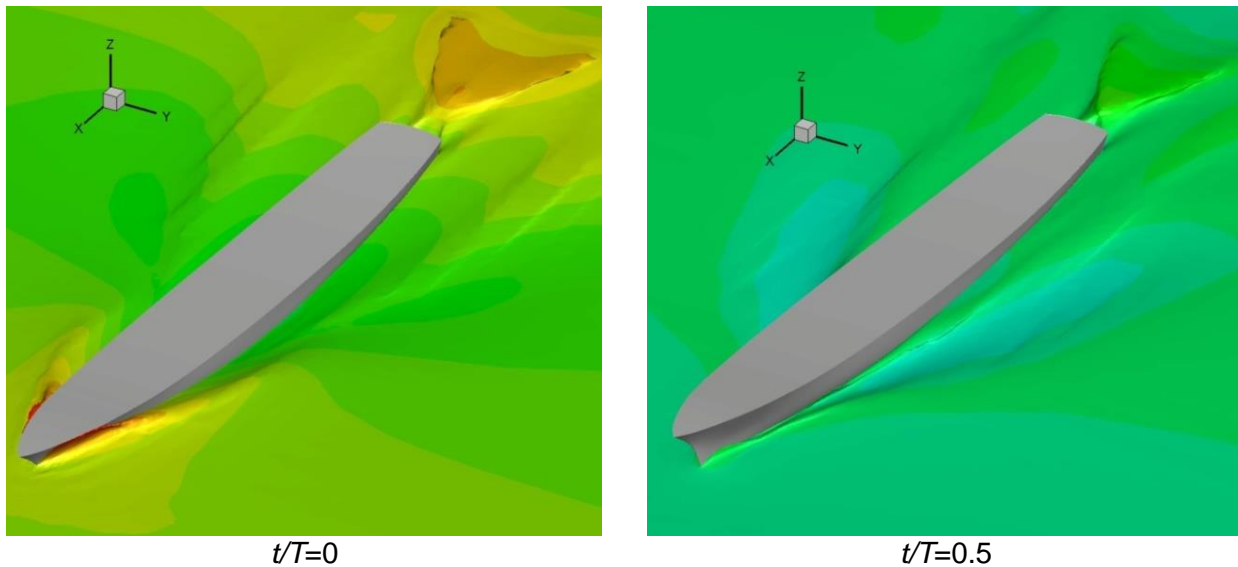


**Figure 6.20** Hull wave interaction at  $t/T=0$  and  $t/T=0.5$

**- Case 12: Wake Flow Assessment**

The development of the flow around the hull at ten different sections located at equal distance  $\Delta x/L_{pp}=0.1$  is presented for the current simulation compared to the calm water condition. The streamwise velocity contours and the second invariant iso-surface=50 are plotted in Fig. 6.22, showing the development of the axial velocity distribution along the hull and revealing the formation of the vortices.

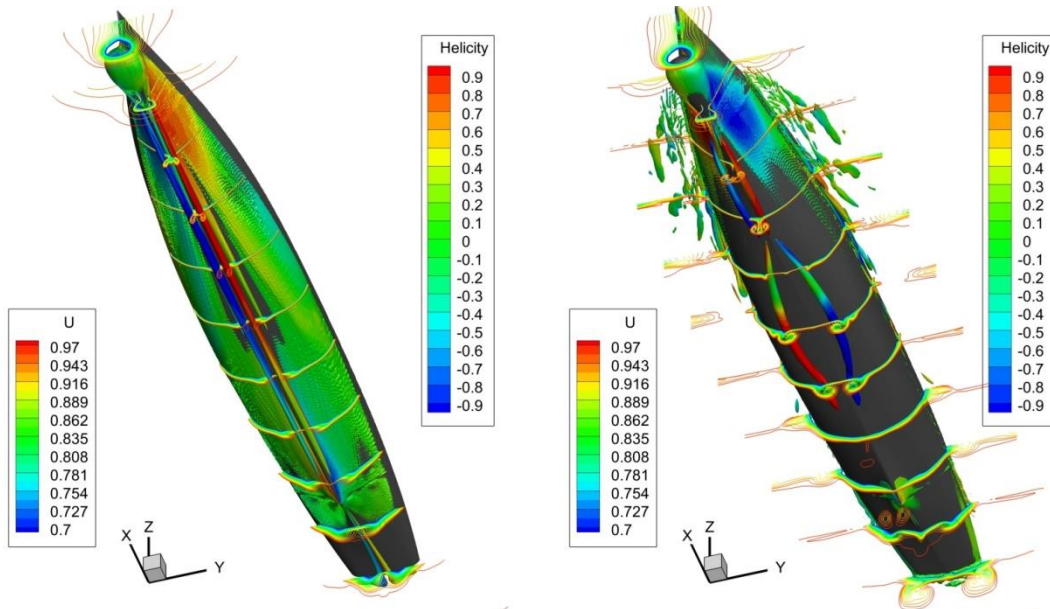


**Figure 6.22** Axial velocity contours computed at equal distances  $\Delta x=0.1L_{pp}$ , and second invariant iso-surface=50 at a random moment during simulation

## 6.2 Roll Decay Performance in Calm water

This study is concerned with the analysis of ship hydrodynamic performance in roll decay condition, so the ship is sailing in calm water and has only one degree of freedom to oscillate around its centerline axis, the motion that is known as roll. Conceptually, the ship is towed at an initial inclined angle then released to oscillate and the roll motion amplitudes are recorded. The resulting curve of oscillation is called the roll decay curve.

### 6.2.1 Simulation Conditions

The study performed in this section corresponds to the case 3.6, which was proposed for the DTMBT sip model appended with bilge keels in roll decay condition. The experimental results for this case can be found in [47, 150].

### 6.2.2 Domain & Boundary Conditions

Full ship domain is used to represent the control volume of the numerical simulation because the half domain is not applicable in this case study. Fig. 6.24 shows the simulation domain and the boundary conditions imposed on the exterior boundaries.

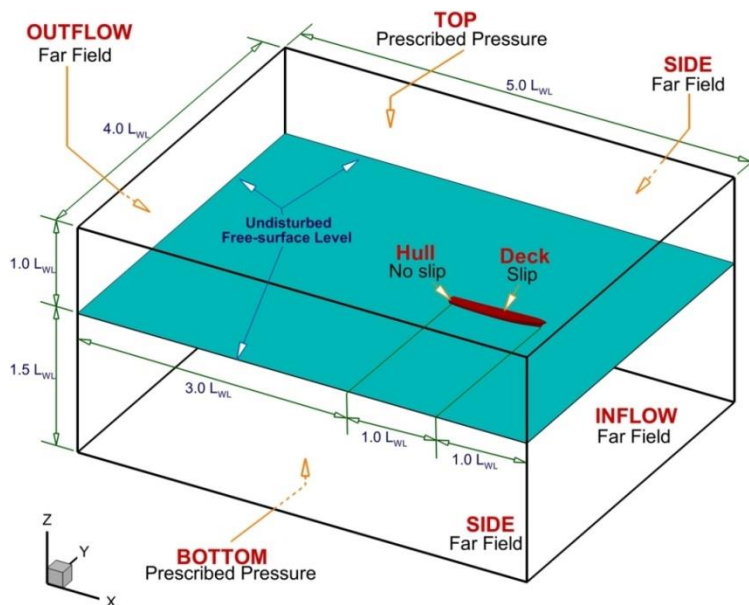
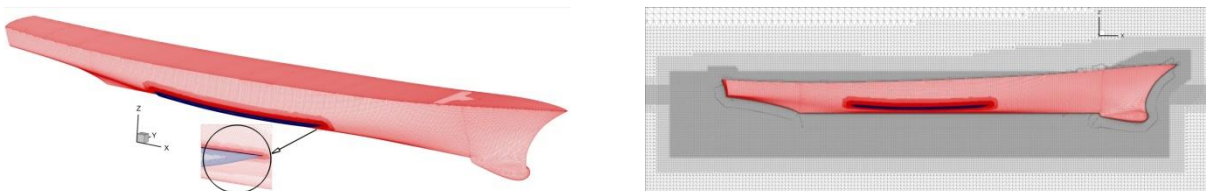
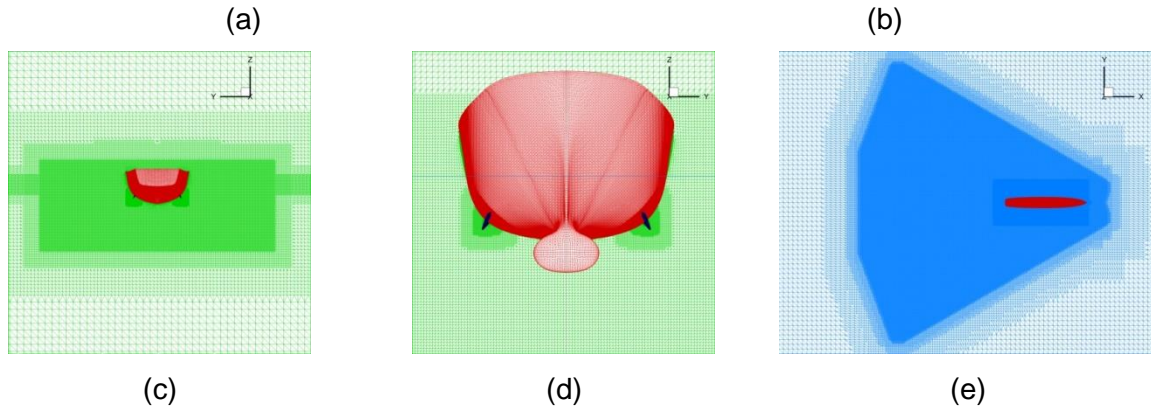


Figure 6.24 Simulation domain and boundary conditions

### 6.2.3 Computational Grids

Fig. 6.25 represents the finest grid with longitudinal, transversal and horizontal sections to show the box refinements close to the hull and bilge keels, with a top view showing the free-surface refinement.





**Figure 6.25** Finest grid discretization, spotting: (a) 3D hull; (b): longitudinal section; (c,d): lateral section depicting the refinement boxes around the hull and bilge keels; (e): free-surface refinement section top view

Table 6.13 summarizes the computational grids for the Grid convergence study, where M1 denotes the finest grid and M4 stands for the coarsest.

**Table 6.13** Grid arrangement for the grid convergence study

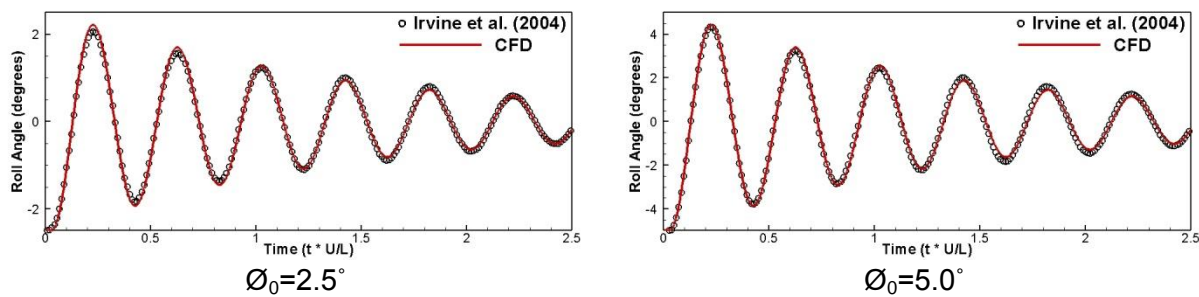
Computational Grid	M4	M3	M2	M1
Number of cells ( $\times 10^6$ )	15.15	23.43	33.59	46.71
$r_G$	1.55	1.43	1.39	

### 6.2.4 Simulation Strategy

Two simulations are performed for every initial roll angle in an unsteady mode. The ship is towed ahead with an imposed target roll angle to generate the initial roll angle before the release. The second simulation is dedicated for the roll damping calculations. The simulation is performed until it counts full six roll periods to be sufficient for results validation against EFD data.

### 6.2.5 Roll Motion Results

The results are validated based on direct comparison with the EFD data provided for the similar test case reported in [47, 150] when the ship is sailing at medium speed with  $Fr=0.138$ . Various initial roll angles were tested starting from  $\varnothing_0=2.5^\circ$  up to  $\varnothing_0=20^\circ$ , with a step  $\Delta\varnothing_0=2.5$  in every simulation. The comparison between CFD and EFD is plotted in Fig. 6.26.



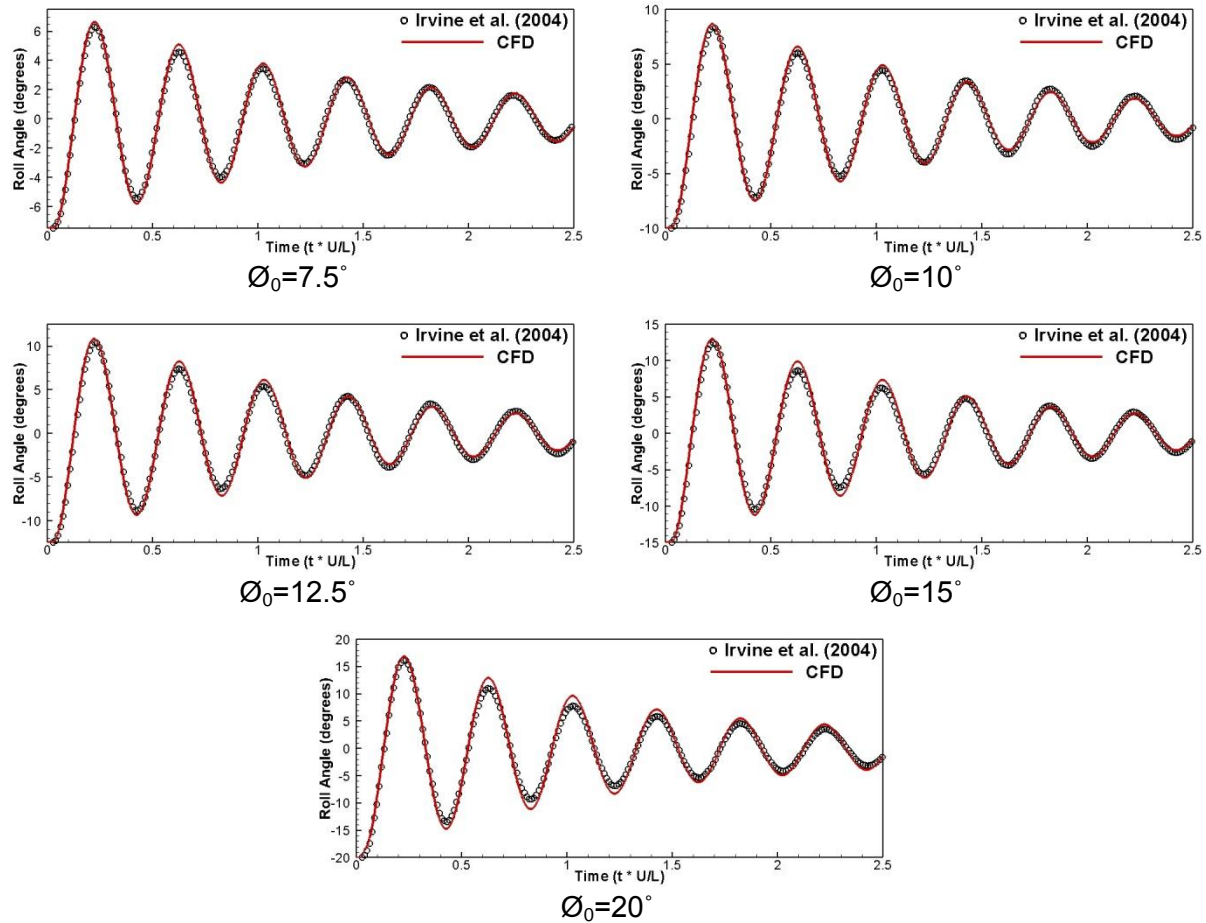


Figure 6.26 Time history for roll simulation at altered initial roll angles

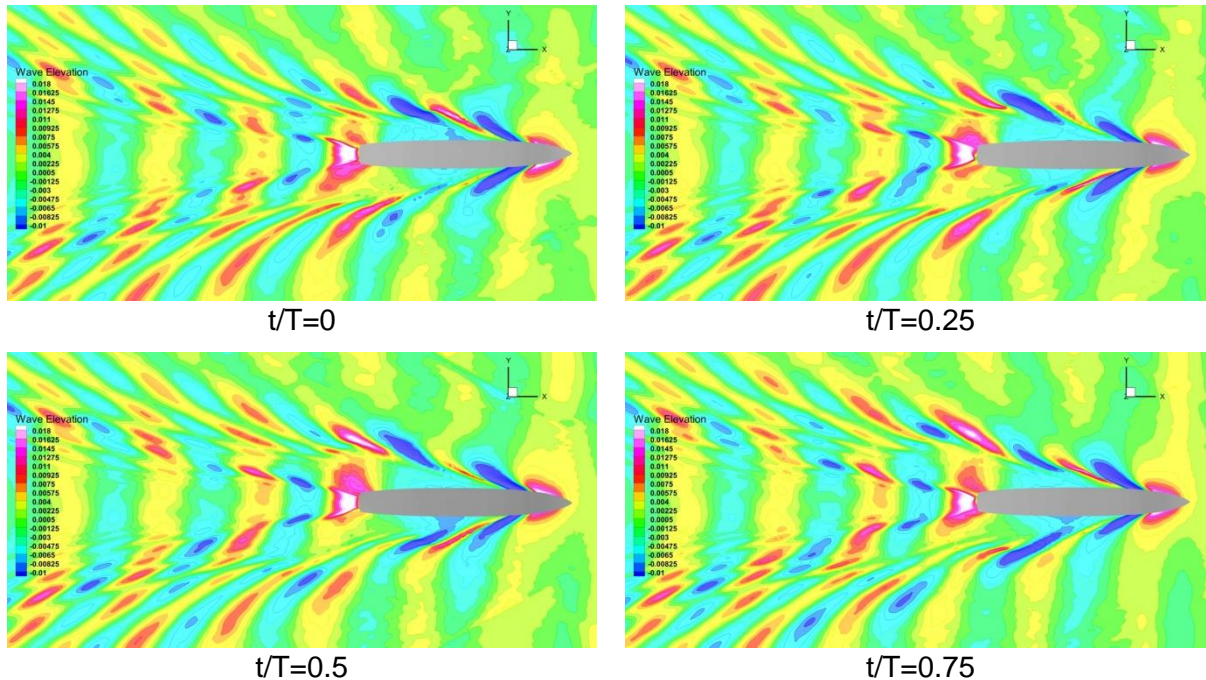
**- Verification & Validation of Numerical Errors**

The verification and validation studies showed that the simulation is more grid dependent than time step dependent, especially when the time step is reduced within 350 time steps / roll period. Verification and validation results are represented in the main context of the thesis.

**6.2.6 Free-Surface Analysis**

The free-surface configuration at these four instances are represented in Fig. 6.29, showing that the pressure and viscous effect resulting from the roll motion have a noticeable influence on the free-surface of the ship during the roll motion. Closer to the hull skin, the viscous effect imposed by the no slip condition on the hull induces a vertical velocity component that creates a trough or crest, depending on ship heeling position. This interacts with the regular Kelvin pattern generated by the hull, adding or subtracting from the generated wave height. On the other hand, the pressure effect during the roll pushes or drags the flow laterally, resulting of an upstream propagation of the generated waves. This can be observed clearly closer to the forward shoulders of the ship.

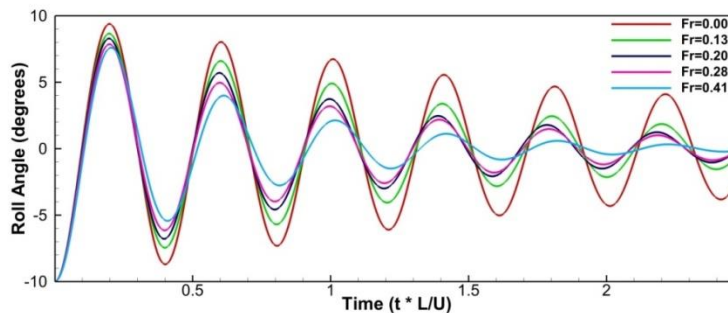




**Figure 6.29** Free-surface topology recorded in the second roll period at the four quarters in case of initial roll angle  $\varnothing_0=10$  and  $Fr=0.28$

**- Speed Effect on the Roll Damping**

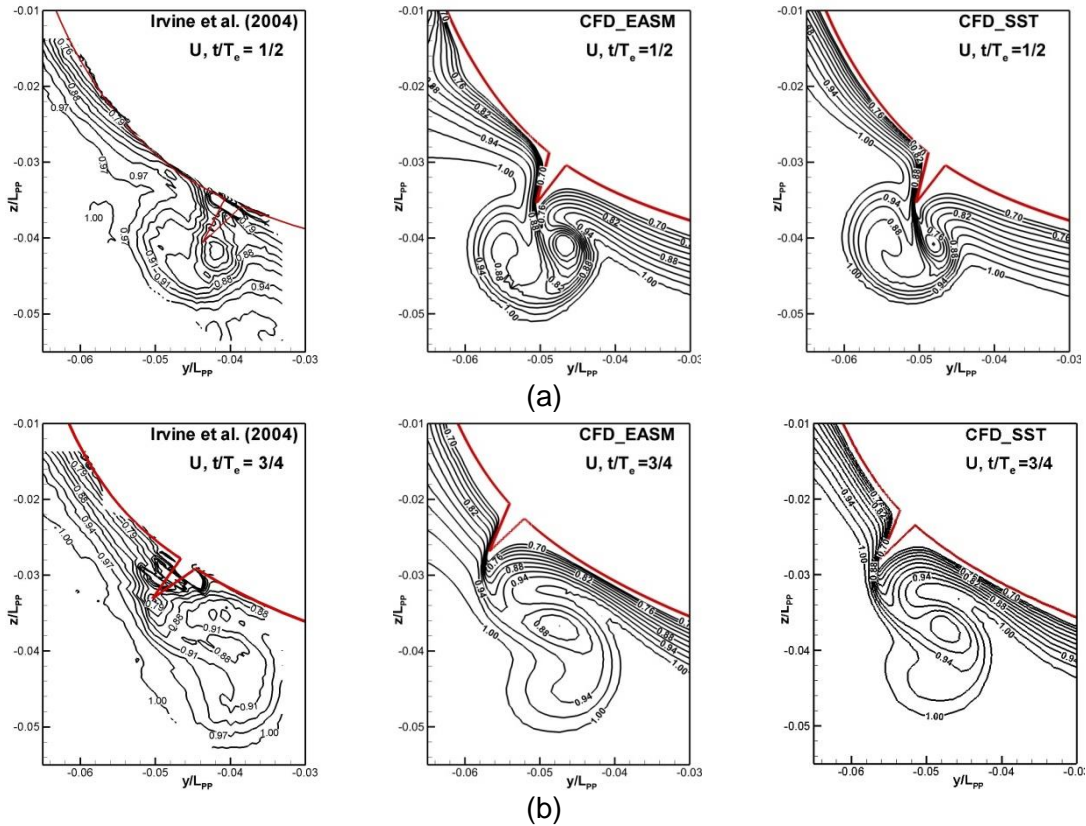
The computed results for the roll damping time history are plotted in Fig. 6.30, showing that the speed effect increases the damping effect on the hull, which diminishes the motion amplitude very fast at  $Fr=0.41$  soon after the fourth damping period. This observation complies also with the similar observation reported in the tank test in [150, 153]. It is also noticed that the speed effect has an influence on the roll damping period, which can be observed from the different in phase between the various ship velocities. Apparently, the periodicity of the roll is lost gradually as the ship speed increase.



**Figure 6.30** Time history for roll decay curves corresponding to various ship speeds

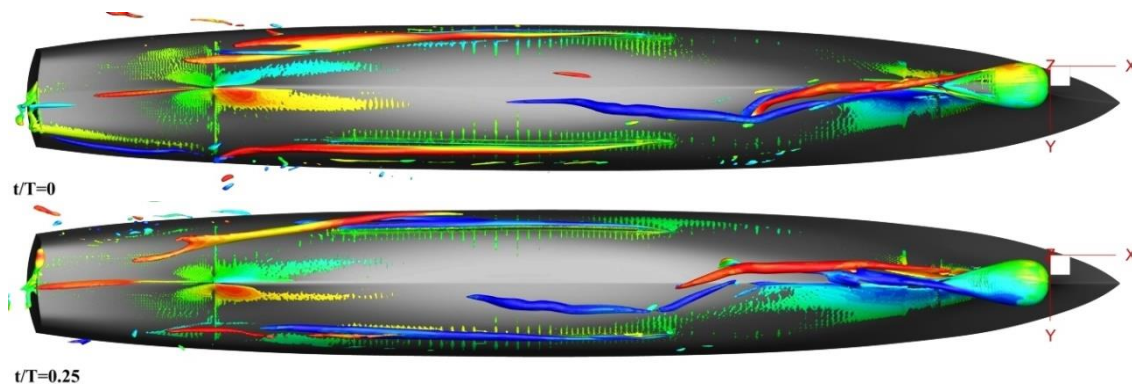
**6.2.7 Local Flow Analysis during Roll Damping**

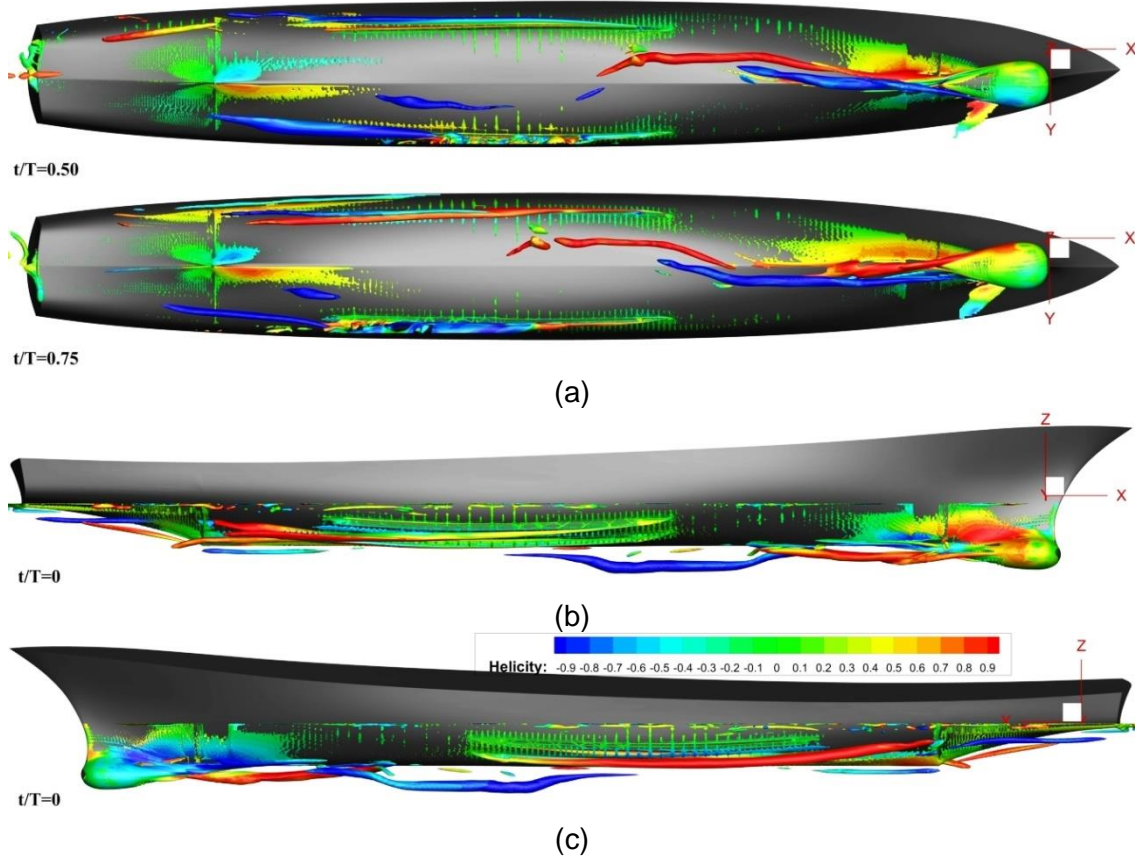
The comparison between CFD and EFD results is represented in Fig. 6.32 for ship sailing with  $Fr=0.138$  and initial roll angle  $\varnothing_0=10^\circ$ . The results are plotted for the two instances  $t/T=0.5$  and  $0.75$ , i.e. when the ship is at the trough and in the zero position while heading back to the crest, respectively.



**Figure 6.32** Computed and measured velocity contours at  $x/L_{pp}=0.675$  for the second roll period instances: (a)  $t/T=0.5$ ; (b):  $t/T=0.75$

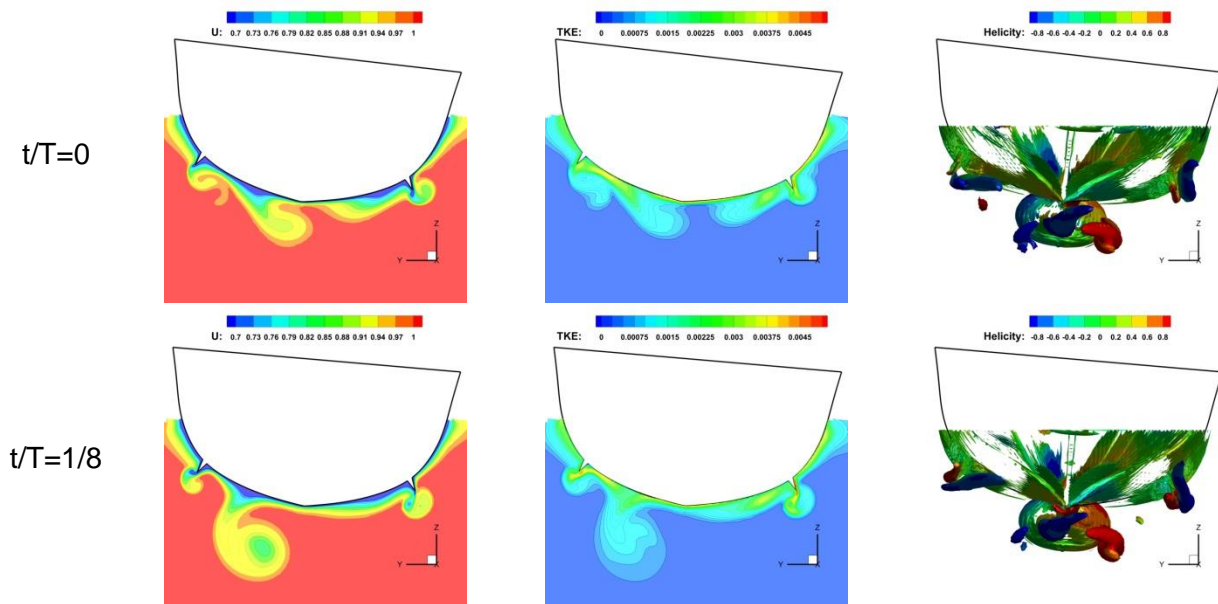
The vortices formations and their behavior can be comprehended from the four instances plotted in Fig. 6.30. The SDV and FBKV are generated as usually immediately after the flow separation at the sonar dome, yet they do not have a straight pattern like in calm water. The oscillation of the ship causes the vortices to create a sinusoidal-like pattern moving laterally along with the ship rolling. Vertically, and due to the viscous effect, the vortices tubes are also fluctuating as the ship rolls. Having a closer look to the BKV generated at the bilge keel, these vortices formation differs from the ones obtained in the classic resistance simulation, since the BKV at the bilge keel seem to have two contra rotating components; one on the suction side of the bilge keel and the other on the pressure side. The intensity of the vortices is influenced by the ship roll position, as it is emphasized in Fig. 6.31.

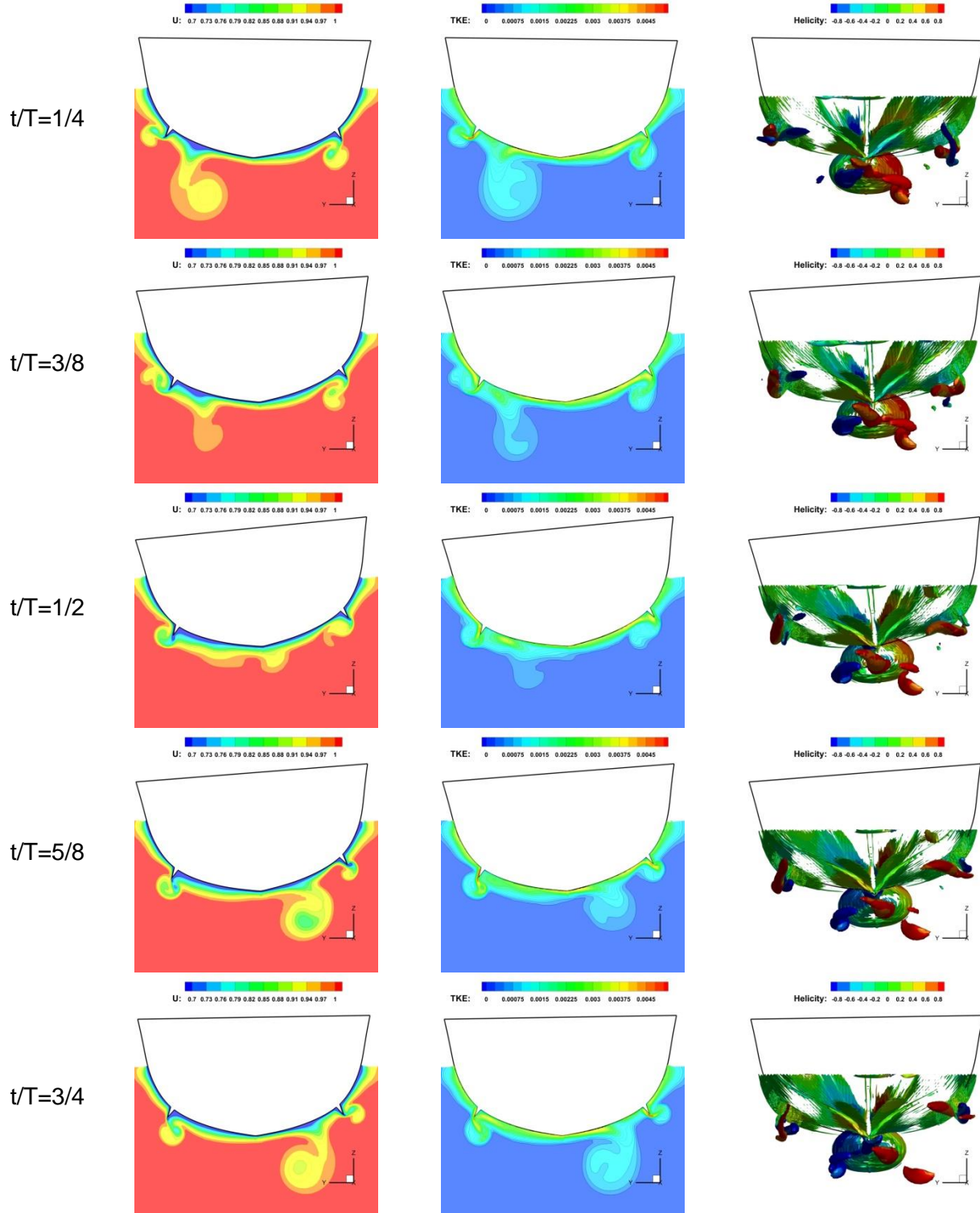




**Figure 6.33** Vortices formations during the roll period quarters showing: (a) ship bottom, (b, c) starboard port sides, respectively for  $t/T=0$

The vortical formations is combined with the axial velocity and the TKE contours to understand the flow configuration during the full period of roll, as illustrated in Fig. 6.34 at 8 different instances, i.e. the roll period is split into 8 segments this time.





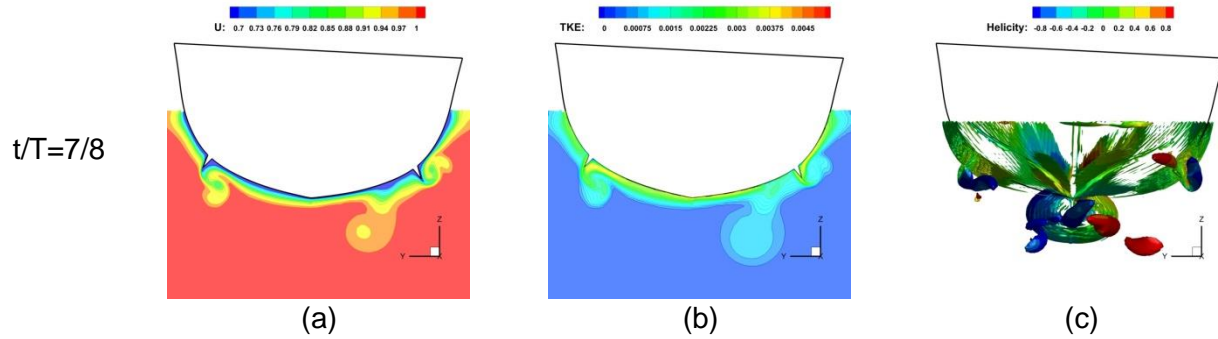


**Figure 6.34** (a): U contours, (b): TKE contours and (c):  $Q^*=25$  second invariant visualized at section  $x/L_{pp}=0.675$  at 8 segments of the roll period

Having in hand the initially expressed objectives from this study and the obtained results, it can be concluded that the CFD method can provide well representation for the roll decay performance from all the aspects of interest. Regarding the ship motions, free-surface and local flow, all were obtained successfully and the results verification and validation confirmed this. All the results for roll damping performance were published in [154].

Generally, for the seakeeping applications, CFD can ensure a suitable, flexible and very reliable tool to predict with satisfying level of accuracy the ship performance in seakeeping simulations.

## Chapter VII

# Conclusions, Contributions and Recommendations

The numerical simulation of the ship hull hydrodynamic performance was presented for multiple ship hydrodynamic aspects concerning; ship resistance applications, propulsion performance or ship powering prediction, and finally, the seakeeping performance in regular head waves and roll decay analysis. The CFD method is used to represent the ship performance based on the finite volume method, using the viscous flow solver ISIS-CFD of the FINE<sup>TM</sup>/Marine that is provided by NUMECA. Rigorous analysis were carried out for various ship types with different characteristics from geometry, dimensions, configuration, function and main purpose points of view. This selection was necessary to insure that the proposed methodology is generic and can be applicable for different types of ships with different considerations.

The global objective of the presented studies is to survey the possibilities of a unique CFD code to solve different ship hydrodynamic aspects and remark its capabilities and limits of the methodology. This investigation was also aimed at providing a suitable, flexible and reliable solution tool for the recent intricate demands in ship design. Overall, it can be concluded that the global research objective have been achieved. The results obtained in the numerical simulations performed for specially selected ship hydrodynamic problems proved to be sufficiently accurate and reliable compared to other well recognized and internationally approved method, which is the tank test experiments. In the search for creating a balance between the available resources, the current capabilities and level of accuracy required for ship applications, this point was well covered, judging the level of accuracy achieved for the different CFD simulations concerning different ship hydrodynamic problems. Nevertheless, there were some limitations regarding the physical modeling of the CFD problem, which could have been enhanced by introducing more complex turbulence models, for example the use of Hybrid RANSE/LES models in complicated analysis concerning multiphase flow simulations in resistance, seakeeping and roll decay assessment. These limitations are not related to the incompatibility of using the CFD in these applications, but to the fact that these applications required significant computational resources and very long simulation time. This also does not deny the fact that these complex models were applied in this study, when possible, in mono-fluid applications concerning propulsion performance in open water and in the self-propulsion applications, showing a recognized success in predicting the main hydrodynamic aspects of the ship flow and ship fluid interactions. The contribution in this research study could provide a proper balance between accuracy and reliability within the available resources and the objectives of each and every study individually.

As for the local objectives in the implemented studies, it was necessary to ensure that the proposed methodology should cover and predict accurately the main variables of concern in ship applications, such as local and global forces, velocity and pressure fields, ship motions, free-surface, wake flow, vortex detection, flow separation, etc. For this purpose, all the obtained results were not just introduced to show that it can be analyzed and predicted, but also validated against experimentally measured data, showing that both numerically and experimentally obtained results were within a good agreement.

## 7.1 Concluding Remarks

Having a thorough review on the main objectives and the achievement is this dissertation research; the following general points can be concluded:

### - **For resistance performance**

1. for ship resistance applications, thorough studies were performed for three ship models; the JBC, KVLCC2 and the DTMB surface combatant. The obtained results for all the ship types compared to the available experimental data were within a very good level of accuracy, where the error range for the three ships for predicted resistance forces was within 0.45% and 7.82%, with a global average value within 3.7%. This value complies very well with the required level of accuracy for marine application for resistance studies, which was proposed in G2010 and Tokyo 2015 Workshops to be less than 4% [47, 48];
2. vertical motions prediction; i.e. sinkage and trim, in ship resistance applications have been recorded for the three ships with an error range within 0.5 and 14.1%, where the maximum error was recorded for the coarsest grid in the slowest ship speed condition that consequently result in most cases in significant discrepancy between measured and computed results. The average error of 5.4%. Again this level is considered more than sufficient for design considerations;
3. free-surface prediction has shown a remarkable success in predicting wave configurations and profiles for the three ships with an error 2.52% in the computed wave elevation for JBC ship, 0.4% for the KVLCC2 and 1.1% for the DTMB ship model. The reason behind the discrepancy in the predicted wave profile returns to the fact that the ship speed is very small and this requires very significant grid resolution, which can increase dramatically the simulation cost. Still, 2.52% is more than acceptable for such applications with slow speed ships;
4. local flow analysis for the three ships were performed and validated showing good agreement with the experimental data. The vortices formations in the wake region of the ship have been predicted for the three hulls with a considerably successful comparison with other researches in the field;
5. the tank test data for the JBC ship model reported the influence of the ESD on the ship wake, which resulted in more enhanced uniform flow that enters to the propeller after the duct, which sequentially enhanced the propulsion efficiency. This effect has been numerically investigated and proven to be well reproduced with the CFD analysis in nominal and effective wake assessment for the JBC model;
6. since the simulation of ship performance can propose some assumptions to simplify the problem, ship resistance for the KVLCC2 with rudder was analyzed using the real rudder configuration and a simplified rudder model, to reduce the modeling and simulation effort. The simple model acted well for the resistance and vertical motion simulation, which means that some CFD assumptions can maintain the consistency of the simulation, despite the simplification performed. On the other hand, according to

the author's opinion, this can be applicable only for the resistance and forward speed simulations, where all the lateral forces are not within the scope of the study. Once the rudder angle changes or ship heading angle is not  $0^\circ$ , the exposed rudder area for the hydrodynamic forces will change, resulting in an over predicted rudder force. Which may affect the simulation accuracy in that condition;

7. an experimental approach was planned and performed in the towing tank facility available in the university with a special focus on the resistance and free-surface prediction of the DTMB ship model with the tank banking effect when the ship is sailing at medium-high speed condition. The data collected from the experiment was validated against other results from the INSEAN towing tank facility showing a reasonable agreement with an average error  $<5\%$ ; and also over validated with the CFD method, with a proper prediction of the influence of the banking effect on the resistance and free-surface wave reflections at the walls of the tank. The increment in resistance with tank effect was within  $2\%$ ;

**- For propulsion performance**

8. in the open water propeller, the analysis of the thrust, torque and efficiency for both propellers, JBC and KVLCC2 resulted in an accurate prediction of the propulsion parameters in open water. For the thrust coefficient  $K_T$ , the average error for the JBC propeller model ranged between 0.68 and 2.81%, while for the torque coefficient  $K_Q$ , the error was within 1.12 and 4.96% and finally for the propulsion efficiency, the error was within 1.82 and 4.87%. This can give an indication about the accuracy of the simulation because the maximum error is  $< 5\%$ . It was also concluded that the POW simulation is grid dependent and the wall modeling can influence significantly the overall errors. As for the KVLCC2 ship propeller, the results were more accurate, since the grid was enhanced to overcome the grid problems in the JBC propeller simulation. The average error for the seven simulation cases of POW, for  $K_T$ ,  $K_Q$  are 0.87 and 1.42%, respectively;
9. from the local flow prediction point of view, the local flow of the propeller in POW simulation for both propellers was recorded and highlighted for different propeller analysis speeds. The obtained results for velocity, pressure, TKE, vorticity, turbulent viscosity and vortices formation have been compared to similar analysis and experiments in the same context and showed a good similarity;
10. the simplified propeller model based on the actuator disk method was tested for the two ship models for nominal and effective wake prediction, as well as, for the self-propulsion parameters. The method was successful, straight forward and less expensive compared to 3D propeller modeling. The error of the numerically obtained self-propulsion parameters compared to experimental data for the JBC ship was within 0.2 and 6.28%; while for the KVLCC2 was 1.18 and 13.7%. This significant error 13.7% was for the torque coefficient  $K_Q$  in bare hull analysis, a value that similar to the one obtained with the same conditions in a research performed with different CFD code, giving a reasonable impression about the methodology. Probably the error may



return to error in the EFD data representation, since the values for ship with rudder had a very good match with the experiment;

11. the self-propulsion prediction based on the 3D sliding grid ship model could capture neatly accurate results regarding the self-propulsion parameters and the propeller rotation rate for both ship models. Minimum and maximum values, respectively, of 1.57 and 3.18% are the estimated errors for the propulsion characteristics computed based on the sliding grid technique. It was also concluded that, though the 3D propeller model is more realistic and accurate, it is still very expensive and more complex compared to the actuator disk model;
12. nominal and effective wake based on both models have been put in the validation test and succeeded to resemble accurately with the EFD results;

**- For Seakeeping performance**

13. the seakeeping has been conducted for only the DTMB ship model on 3 levels when ship is sailing in regular head waves with fixed, free condition to heave and pitch, and finally, the roll decay performance prediction. All the three aspects have been conducted and compared to the available experimental data for similar simulations, showing a good correspondence between the CFD and EFD results;
14. the results obtained for the fixed ship conditions regarding the forces and moments showed to have a good agreement for the resistance prediction with an error range of 3.25 and 9.21% for the average and first amplitude of the computed resistance in waves, on the other hand, the heave force showed a high value of the error within 18.21 and 27.55%, and 10.19 and 12.5% for pitch moment, respectively. Though the error range seems to be significant, the results were compared with the data from G2010 workshop and it was within a close range for some results with different codes;
15. free-surface and local flow were also predicted and compared to the EFD results resulting in a well predicted free-surface and close agreement for the local flow;
16. the free ship condition was conducted with a scope to assess the numerical errors, which was conducted successfully showing that the seakeeping simulation can be grid dependent and less time dependent, especially if the time step is small enough. 250 time steps/wave period were considered enough based on the obtained results;
17. Ship responses for heave and pitch were recorded within an average error of 2.54% and 9.83% for heave and pitch, respectively; while for the resistance, the error was within 5%. All considered acceptable, except for the pitch response which requires more investigation. Overall, results resembled well with the results obtained by other researchers;
18. the added resistance in wave was computed and compared with the calm water condition, which recorded an added resistance value that varied between 8.1 and 39.2% compared to the resistance in calm water, depending on the wave length. These value should be taken into considerations for any powering estimations;

19. the breaking effect, and hull wave interaction was analyzed and well predicted for the ship during the free condition showing that, the flare design pushes the flow outward during the hull-wave separation, which keeps the deck dry during the simulation. At the ship stern, a breaking roaster-tail effect waves were observed during the simulation, whose effect was increasing as the ship speed increases;
20. the analysis of local flow showed that the boundary layer of the ship is suffering a significant deformation during the wave encounter. This effect was well captured and concluded that it will have a significant impact on the propulsion performance;
21. the roll decay performance was computed and presented for different initial roll angles based on a simplified general grid approach to avoid the drawbacks from the sliding and overset grids that are usually applied in this study, which is more complex and expensive. The overall conclusion for the effect of the change in the initial roll angle reduces the accuracy of the computed roll damping, even for the finest grids;
22. the simulation was proven to be grid dependent and time independent for a time step over 300 time steps/roll period;
23. the influence of the roll damping on the free-surface topology and profile was highlighted concluding that the pressure and viscous effect cause distortion in the free-surface, which consequently might increase the wave making resistance component;
24. the speed effect on the roll damping and free-surface was demonstrated, showing that the damping increases as the speed increases; also the viscous and pressure influence on the free-surface is reduced as the ship speed increases;
25. the local flow of the ship during the roll period was manifested and explained based on the velocity contours, TKE and vortex formation. The results revealed the deformation in the boundary layer and the formation of eddies and significant flow separation at the bilge keel, which contributes in increasing the damping effect; and increases the ship resistance during the damping process.

In general, it can be concluded that the studies presented in this research dissertation can be considered as a numerical towing tank, which succeeded in reproducing the different tank test experiments in various ship hydrodynamic aspect in a numerical representation. The obtained results are encouraging to set the base for further researches in the field based on the consistent validation processes that were conducted during this research.

## 7.2 Personal Contributions

In the scope of analyzing the ship hydrodynamic performance, it was very important to generalize the method for multiple ship types, categories and geometries. For this purpose, three ships were chosen to achieve this goal. The first is the JBC bulk carrier ship model, while the second is the KVLCC2 ship model, and finally, the DTMB surface combatant model. To ensure that the computational simulations is not just theoretically approached, the practicality of the method were assessed based on the validation of the obtained results against experimental

data, to ensure, not just the capability of the method to predict ship hydrodynamic performance, but also the accuracy of the obtained results from the numerical simulations. Rigorous CFD analysis cases have been studied with different scopes to cover the main objectives concerned in every case. These cases are outlined in Table 7.1 showing the ship performance aspect of interest, main objectives from the study, and finally on which model the study was performed.

**Table 7.1** Ship performance contribution in the present study

Ship Performance		Objective		Ship Model		
				JBC	KVLCC2	DTMB
CFD	Resistance	Drag Forces	Bare Hull	✓	✓	✓
			With Appendages	✓	✓	✓
		Motions		✓	✓	✓
		Free-surface		✓	✓	✓
		Local Flow		✓	✓	✓
		Flow Separation and Vortex detection		✓	✓	✓
		Banking Effect		✗	✗	✓
	Propulsion	Open Water		✓	✓	✗
		Propulsion	Nominal Wake	✓	✗	✗
			Effective Wake	✓	✗	✗
			Self-propulsion Point	✓	✗	✗
		Local Flow & Vortex Prediction		✓	✓	✗
	Seakeeping	Forces		✗	✓	✓
		Motions		✗	✓	✓
		Free-surface		✗	✓	✓
		Local Flow & Vortex Prediction		✗	✗	✓
		Roll Damping		✗	✗	✓
Experiment	Resistance	Forces (Bare Hull)		✗	✗	✓
		Motions		✗	✗	✗
		Free-surface		✗	✗	✓
		Tank Walls Effect		✗	✗	✓

Within almost five years of research in the field, since the practical start of this dissertation work, with a special focus on studying the ship hydrodynamic performance, the scientific research effort resulted in an outcome of seventeen research papers, thirteen of which are indexed in the ISI proceedings, two are under press and expected to be indexed in ISI proceedings, one is indexed in SCOPUS and, finally, one paper indexed in the international data base IDB. One research paper is published in the Journal of Marine Science and Engineering, fifteen are published in conference proceedings from participations in ten international conferences, four of which were held in Romania, and six in different other European countries. Three awards were accomplished in three conferences for the best presentation, one as the first place, and two as the second.

Applying the same principles from this thesis work in practical applications, the thesis author worked as a team member in a national project to study the influence of mounting a central skeg on Danube pusher tug boat between the propellers in order to enhance the propeller performance and directional stability of the tug. The author performed the numerical

investigation of the problem and introduced the results for the tug separately and within the convoy.

### 7.3 Recommendations and Future Perspectives

The challenges in ship hydrodynamic field are endless; the new demands in the field are increasing progressively every day. The need to keep track of the continuous changes is urgent and still some problems need more analysis and thorough investigations. Though the research in this dissertation was conducted to cover most of the ship hydrodynamic aspects, there are still some sides have not been approached; other aspects were not difficult to perform; others were incompletely analyzed; and finally some other aspects have been analyzed and completed, yet not included in the final form of the thesis manuscript.

Heading from the fact that nothing is complete and there is always a window to enhance the proposed work in this thesis, the following points can be expressed as a future plan to continue in the same direction in ship hydrodynamic performance research:

1. in the ship resistance simulations, the method was applied only on model scale ship with various turbulence models. In the same scope, a study with more complex turbulence model can help understanding the interaction between the flow and the hull, showing more details in the wake field of the ship, to set a proper base for ship hull performance enhancement. Further beyond the scope, the analysis of full scale ships can provide better and more realistic representation of the hull performance in real sailing conditions. Despite the fact that this requires more complex studies, advanced resources and rigorous research effort to keep the work intact, it is still a very good base for the future research plan;
2. for the propulsion performance, in the same scope, the analysis performed in this thesis did not include the cavitation performance of the propeller. This is one of the most important aspects regarding the propeller performance prediction in both POW and behind the ship. This should be conducted in the near future. Beyond the scope, could also be the applications of ship propulsion at the full scale;
3. as for the seakeeping performance, the studies conducted in this research work were limited for regular head waves. To keep the problem closer to the reality, the ship seakeeping performance at different heading angles should be conducted with all the six degrees of freedom. This can provide better understanding of the ship behavior in waves, especially with the advance in predicting the viscous flow effect during seakeeping simulation, compared to the classic BEM-based methods. In addition, it should be carried out a study for the ship performance in a seaway, which will be more realistic and more accurate from the physical modeling point of view. Still, this problem is very complex and requires massive computational resources and significant research effort.

Finally, the results obtained within the current research in the scope of predicting the maneuvering performance of the ship can be published in recognized journal or conference proceedings.



## References

- [1] ITTC. *The Stability in Waves Committee, Final Report and Recommendations to the 28<sup>th</sup> ITTC*. Proceedings of the 28<sup>th</sup> International Towing Tank Conference, Vol. I (2017), 275–335, Wuxi, China.
- [2] Tursini, L. *Leonardo da Vinci and the problems of navigation and naval design*. Transactions of the Institute of Naval Architects, 95 (2) (1953) 97–102.
- [3] Gawn, R. W. L., *Historical Notes on Investigations at the Admiralty Experiment Works, Torquay*. Transactions of the Institute of Naval Architects, 8 (1941) 80–139.
- [4] Gawn, R. W. L. *The Admiralty experiment works, Haslar*. Transactions of the Institute of Naval Architects, 97 (1) (1955) 1–35.
- [5] Froude, W. *Experiments on surface friction*. British Association Reports (1872, 1874).
- [6] Froude, W. *On Experiments with H.M.S. Greyhound*, Transactions of the Institute of Naval Architects, 15 (1874) 36–73.
- [7] Dejhalla, R. and Prpić-Oršić J. *A Review of the state-of-the art in marine hydrodynamics*, Journal of Brodogradnja Ship Building, 57 (1) (2006) 13–22.
- [8] ITTC, *The Resistance Committee, Final Report and Recommendations to the 25<sup>th</sup> ITTC*, Proceedings of the 25<sup>th</sup> International Towing Tank Conference, Vol. I (2008), 21–81, Fukouka, Japan.
- [9] Taylor, D.W. *Speed and power of ships*. Press of Ransdell (1933), Washington. DC.
- [10] Gertler, M. *A re-analysis of the original test data for the Taylor standard series*. TMB Report 806 (1954) DTRC.
- [11] Keuning, J. A. and Sonnenberg, U. B. *Approximation of the hydrodynamic forces on sailing yacht hulls based on the Delft systematic yacht hull series*. 15<sup>th</sup> International HISWA Symposium on Yacht Design and Yacht Construction (1998) 99–152, Amsterdam, Netherlands.
- [12] Doust, D. J., and O'Brien, T. P. *Resistance and propulsion of trawlers*. North East Coast Institution of Engineers and Shipbuilders Transactions, 75 (1959).
- [13] Holtrop, J. and Mennen, G. G. J. *An approximate power prediction method*. International Shipbuilding Progress, 29 (335) (1982) 166–170.
- [14] Bertram V. *Practical Ship Hydrodynamics*. 2<sup>nd</sup> Edition, Butterworth Heinemann (2000), Oxford, ISBN 0-7506-4851-1.
- [15] Thompson, W. (Lord Kelvin). *On ship waves transactions*. IME, 3 (1887), 409–433.
- [16] Thompson, W., (Lord Kelvin). *On deep water two-dimensional waves produced by any given initiating disturbance*. Proceedings of the Royal Society of Edinburgh, 25 (1) (1904), 185–196.
- [17] Havelock, T.H., *The wave-making resistance of ships: a theoretical and practical analysis*. Proceedings of the Royal Society, A. 82 (1909), Fellow of St. John's College, Cambridge, Lecturer in Applied Mathematics, Armstrong College, New east Leon-Tyne.
- [18] Wigley, C. *Ship Wave Resistance*. North East Coast Institution of Engineers and Shipbuilders Transactions, 47 (1931).
- [19] Wigley, C. *A comparison of experiment and calculated wave profiles and wave resistance for a form having parabolic waterlines*. Proceedings of the Royal Society, 144 (851) (1934), 144–159.
- [20] Michell, J. H. *The wave resistance of a ship*. Philosophical Magazine, 5 (1898), 45.
- [21] Havelock, T.H. *Wave resistance theory and its application to ship problems*. Transactions of the Society of Naval Architects and Marine Engineers, 59 (1951) 13–24.

- [22] Hess, J.L., Smith, A.M.O. *Calculation of non-lifting potential flow about arbitrary three-dimensional bodies*. Douglas Aircraft Report, No. ES40622 (1962), Long Beach, CA: Douglas Aircraft.
- [23] Baar, J. J. M., and Price, W. G. *Developments in the calculation of the wave making resistance of ships*. Proceedings of the Royal Society of London, 416 (1988) 115–147.
- [24] Tuck, E. O. *The wave resistance formula of J.H. Michell (1898) and its significance to recent research in ship hydrodynamics*. Journal of the Australian Mathematical Society, Series B, 30 (1989), 365–377.
- [25] Dawson, C. *A practical computer method for solving ship wave problems*. 2<sup>nd</sup> International Conference on Numerical Hydrodynamics (1977) 30–38. Berkeley, CA.
- [26] Raven, H.C. *A solution method for the nonlinear ship wave resistance problem*. Ph.D. Thesis (1996), Technical University of Delft, MARIN, Holland.
- [27] Larsson, L. and Raven H.C. *Ship resistance and flow. Principles of naval architecture series*, The Society of Naval Architects and Marine Engineers, (2010), New Jersey, ISBN 978-0-939773-76-3.
- [28] Janson, C. E. *Potential flow panel methods for the calculation of free surface flows with lift*, PhD Thesis, Chalmers University of Technology, (1997).
- [29] VIRTUE, NSC Members, *Best practice guidelines for marine application in computational fluid dynamics*. VIRTUE – The Virtual Tank Utility in Europe, MARNET CFD (2008).
- [30] Larsson, L., Regnström, B., Broberg, L., Li, D.Q. and Janson, C.E. *Failures, fantasies, and feats in the theoretical/numerical prediction of ship performance*. The 22<sup>nd</sup> Symposium on Naval Hydrodynamics, (1999) 11-32, Washington, D.C.
- [31] von Kerczek, C.H. *A new generalized cross-flow momentum integral method for three-dimensional ship boundary layers*. SAI Report No. 463-82-085-LJ (1982).
- [32] von Kerczek, C.H., Christoph, G., and Stern, F. *Further developments of the momentum integral method for ship boundary layers*. SAI Report No. 8413046 (1984).
- [33] Stern, F. *Effects of waves on the boundary layer of a surface-piercing body*, Journal of Ship Research, 30 (4) (1986) 256–274.
- [34] Larsson, L. *Proceedings of the 1980 SSPA-ITTC Workshop on ship boundary layers*. SSPA Publication No. 90 (1981). Gothenburg: Swedish State Shipbuilding Experiment Tank, SSPA.
- [35] Stern, F., Yang, J., Wang, Z., Sadat-Hosseini, H., Mousaviraad, M., Shanti, B., Xing, T. *Computational ship hydrodynamics: nowadays and way forward*. International Shipbuilding Progress, 60 (1-4) (2013), 3–105.
- [36] Blazek, J. *Computational fluid dynamics: principles and applications*. 1<sup>st</sup> Edition (2001), Elsevier, Oxford, ISBN 0-08-043009-0.
- [37] Larsson, L., Patel, V. C., and Dyne, G. (Eds.). *SSPA-CTH-IIHR Workshop on ship viscous flow*. Report No. 2 (1991). Gothenburg: FLOWTECH International AB.
- [38] Wilson, R. V. *A review of computational ship hydrodynamics*. Technical report, SimCenter: National Center for Computational Engineering, The University of Tennessee at Chattanooga, College of Engineering and Computer Science, (2008).
- [39] Tahara, Y., Stern, F., and Rosen, B. *An interactive approach for calculating ship boundary layers and wakes for nonzero Froude number*. Journal of Computational Physics, 98 (1) (1992) 33–53, IIHR Reprint No. 892.
- [40] Wackers, J., Koren, B., Raven, H. C. van der Ploeg, A., Starke, A. R. Deng, G. B., Queutey, P., Visonneau, M., Hino, T. and Ohashi K. *Free-surface viscous flow solution*

- methods for ship hydrodynamics*. Archives of Computational Methods in Engineering, 18(1) (2011) 1–41.
- [41] Kodama, Y., Takeshi, H., Hinatsu, M., Hino, T., Uto, S., Hirata, N. and Murashige, S. (eds.) *Proceedings, CFD Workshop 1994*. Ship Research Institute, Tokyo, Japan.
- [42] Wilcox, D.C. *Turbulence modeling for CFD*. 2<sup>nd</sup> Edition (1998) DCW Industries, La Canada, CA. ISBN: 978-0963605153.
- [43] Larsson, L., Stern F. and Bertram V. (eds.) *Gothenburg 2000 a workshop on numerical ship hydrodynamics*. Chalmers University of Technology (2000), CHA/NAV/R-02/0073.
- [44] Larsson, L., Stern, F. and Bertram, V. *Benchmarking of computational fluid dynamics for ship flows: the Gothenburg 2000 workshop*. Journal of Ship Research, 47 (1) (2003) 63–81.
- [45] Hino, T. (editor). *CFD Workshop Tokyo 2005*, National Maritime Research Institute (2005), Tokyo, Japan.
- [46] Xing, T., Carrica, P., and Stern, F. *Computational Towing Tank Procedures for Single Run Curves of Resistance and Propulsion*. ASME Journal of Fluids Engineering. 130 (2) (2008) 1–14.
- [47] Larsson, L., Stern, F., Visonneau, M., (eds.). *Numerical ship hydrodynamics: an assessment of the Gothenburg 2010 Workshop*. Springer (2013). ISBN 978-94-007-7188-8.
- [48] NMRI, Tokyo 2015, *A Workshop on CFD in ship hydrodynamics*, National Maritime Research institute (2015), <http://www.t2015.nmri.go.jp/jbc.html>.
- [49] Larsson, L., *Resistance, sinkage, trim and wave pattern review*, National Maritime Research Institute, Tokyo 2015 Workshop, [http://www.t2015.nmri.go.jp/Presentations/Day1-AM4-JBC-Resist\\_etc-Larsson.pdf](http://www.t2015.nmri.go.jp/Presentations/Day1-AM4-JBC-Resist_etc-Larsson.pdf).
- [50] Kim, J. *Report of the results for KCS Resistance & self-propulsion*. National Maritime Research Institute, Tokyo 2015 Workshop, [http://www.t2015.nmri.go.jp/Presentations/Day2-AM2-KCS-Resistance\\_SP-Kim.pdf](http://www.t2015.nmri.go.jp/Presentations/Day2-AM2-KCS-Resistance_SP-Kim.pdf).
- [51] Larsson, L. *CFD in ship hydrodynamics*. Chalmers University of Technology Gothenburg (2008), Sweden.
- [52] Carlton, J. S. *Marine Propellers and Propulsion*. 2<sup>nd</sup> Edition, Butterworth Heinemann (2007), Oxford, UK. ISBN 9780080549231.
- [53] Rankine, W. J. M. *On the mechanical principles of the action of propellers*. Transactions of the Institution of Naval Architects, 6 (1865) 13–39.
- [54] Froude, R.E. *On the part played in propulsion by differences in fluid pressure*. Transactions of the Royal Institution of Naval Architects, 30 (1889) 390–405.
- [55] Froude, W. *On the elementary relation between pitch, slip and propulsive efficiency*. Transactions of the Institution of Naval Architects, 19 (1878) 47–65.
- [56] Betz, A. *Schraubenpropeller mit geringstem Energieverlust*. K. Ges. Wiss, Gottingen Nachr. Math.-Phys., (1919) 193–217.
- [57] Goldstein, S. *On the vortex theory of screw propellers*. Proceedings of the Royal Society, London Series A, 123 (1929) 440–465.
- [58] Burrill, L. C. *Calculation of marine propeller performance characteristics*. North East Coast Institution of Engineers and Shipbuilders Transactions, 60 (1944).
- [59] Lerbs, H. W. *Moderately loaded propellers with a finite number of blades and an arbitrary distribution of circulation*. Transactions of the Society of Naval Architects and Marine Engineers, 60 (1952) 73–123.



- [60] Molland, A. F., Turnock, S. R. and Hudson D. A. Ship resistance and propulsion, practical estimation of ship propulsive power. Cambridge University Press (2011), New York, US, ISBN 978-0-521-76052-2.
- [61] Sparenberg, J.A. *Application of lifting surface theory to ship screws*. Proceedings of the Koninklijke Nederlandse Akademie van Wetenschappen, Series B, Physical Sciences, 62 (5) (1959) 286–298.
- [62] Pien, P.C. *The calculation of marine propellers based on lifting surface theory*. Journal of Ship Research, 5 (2) (1961) 1–14.
- [63] Kerwin, J.E. *A deformed wake model for marine propellers*. Department of Ocean Engineering Rep. 76–6, MIT (1976).
- [64] Greeley, D.A. and Kerwin, J. E. *Numerical methods for propeller design and analysis in steady flow*. SNAME Transactions, 90 (1982).
- [65] Kerwin, J.E., Chang-Sup Lee. *Prediction of steady and unsteady marine propeller performance by numerical lifting-surface theory*. SNAME Transactions, Paper No. 8 (1987), Annual Meeting.
- [66] ITTC. *The Propulsion Committee, Final Report and Recommendations to the 24<sup>th</sup> ITTC*. Proceedings of the 24<sup>th</sup> International Towing Tank Conference, Vol. I (2005), 73–136, UK.
- [67] Hess, J. L. and Valarezo, W. O. *Calculation of steady flow about propellers by means of a surface panel method*. AIAA Paper No. 85-0283 (1985).
- [68] Kim, H. T. and Stern, F. *Viscous flow around a propeller-shaft configuration with infinite pitch rectangular blades*. Journal of Propulsion and Power, 6 (4) (1990) 434–444.
- [69] Uto, S. *Computation of incompressible viscous flow around a marine propeller*. Journal of Society of Naval Architects of Japan, 172 (1992) 213–224.
- [70] Stern, F., Kim, H. T., Patel, V. C. and Chen, H. C. *A Viscous flow approach to the computation of propeller-hull interaction*. Journal of Ship Research 32(4) (1988) 246–262.
- [71] Guilmineau, E., Deng, G. B., Leroyer, A., Queutey, P., Visonneau, M. and Wackers, J. *Influence of the turbulence closures for the wake prediction of a marine propeller*. Proceedings of the 4<sup>th</sup> International Symposium on Marine Propellers, smp'15 (2015), Austin, Texas, USA.
- [72] Wang, L. Z., Guo, C. Y., Su, Y. M. and Wu, T. C. *A numerical study on the correlation between the evolution of propeller trailing vortex wake and skew of propellers*. International Journal Naval Architecture & Ocean Engineering, 10 (2018) 212-224.
- [73] Stern, F., Kim, H. T., Zhang, D. H., Toda, Y., Kerwin, J. and Jessup, S. *Computation of viscous flow around propeller-body configurations: series 60 CB = 0.6 ship model*. Journal of Ship Research 38 (2) (1994) 137-157.
- [74] ITTC. *The Specialist Committee on Computational Fluid Dynamics, Final Report and Recommendations to the 26<sup>th</sup> ITTC*. Proceedings of the 26<sup>th</sup> International Towing Tank Conference, Vol. II (2011), 337–377, Rio de Janeiro, Brazil.
- [75] Zhang Z. R., *Verification and validation for RANS simulation of KCS container ship without/with propeller*. Journal of Hydrodynamics, 22 (5) (2010) 932–939.
- [76] Visonneau, M., Queutey, P., Deng, G. B., Wackers, G., Guilmineau, J., Leroyer, A. and Benoit, M. *Computation of free-surface viscous flows around self-propelled ships with the help of sliding grids*. 11<sup>th</sup> International Conference on Computer Applications and Information Technology in the Maritime Industries, COMPIT (2012), Liege, Belgium.

- [77] Shen, Z. and Korpus, R. *Numerical simulations of ship self-propulsion and maneuvering using dynamic overset grids in OpenFOAM*. Tokyo 2015 Workshop on CFD in Ship Hydrodynamics, Tokyo (2015), Japan.
- [78] Castro, A., Carrica, P. M. and Stern, F. *Full scale self-propulsion computations using discretized propeller for KRISO containership KCS*. Journal of Computer and Fluids, 51 (2011) 35–47.
- [79] Chase, N., Carrica, P. M. *Submarine propeller computations and application to self-propulsion of DARPA Suboff*. Ocean Engineering, 60 (2012) 68-80.
- [80] Mofidi, A. J. Martin, E. and Carrica, P. M. *RANS, DES and DDES simulations of self-propulsion of the Japan Bulk Carrier*. Tokyo 2015 Workshop on CFD in Ship Hydrodynamics, Tokyo (2015), Japan.
- [81] International Symposiums on Marine Propulsors (SMP), <http://www.marinepropulsors.com/proceedings.php>.
- [82] Sadat-Hossieni, H., Wu, P. C., Carrica, P. M., Kim, H., Toda, Y. and Stern, F. *CFD verification and validation of added resistance and motions of KVLCC2 with fixed and free surge in short and long head waves*. Journal of Ocean Engineering, 59 (2013) 240-273.
- [83] Kim, M., Hizir, O., Turan, O. and Incecik, A. *Numerical studies on added resistance and motions of KVLCC2 in head seas for various ship speeds*. Ocean Engineering, 140 (2017) 446–476.
- [84] Sato, Y., Miyata, H., and Sato, T., *CFD simulation of 3D motion of a ship in waves: application to an advancing ship in regular heading waves*. Journal of Marine Science and Technology 4(1999)108–116.
- [85] Stern, F., Wilson, R., Longo, J., Carrica, P. M., Xing, T., Tahara, Y., Simonsen, C., Kim, J., Shao, J., Irvine, M., Kandysamy, M., Ghosh, S. and Weymouth, G. *Paradigm for development of simulation based design for ship hydrodynamics*. The 8<sup>th</sup> International Conference on Numerical Ship Hydrodynamics (2003), Busan, Korea.
- [86] Carrica, P. M., Wilson, R. V., Noack, R. W. and Stern, F. *Ship motions using single phase level set with dynamic overset grids*. Computers and Fluids 36 (9) (2007)1415–1433.
- [87] Irvine, M., Longo, J. and Stern, F., *Pitch and heave tests and uncertainty assessment for a surface combatant in regular head waves*. Journal of Ship Research 52(2) (2008) 146–163.
- [88] Deng, G. B., Queutey, M. and Visonneau, M. *RANS prediction of the KVLCC2 tanker in head waves*. Journal of Hydrodynamics. 22 (5) (2010) 476–481.
- [89] Queutey, P., Visonneau, M., Leroyer, A., Deng, G. and Guilmineau, E. *RANSE simulations of a naval combatant in head waves*. In Proceedings of the 11<sup>th</sup> Numerical Towing Tank Symposium (2008) 11–16, Brest, France.
- [90] Shen, Z., Carrica, P. M. and Wan, D. *Ship motions of KCS in head waves with rotating propeller using overset grid method*. Paper OMAE2014-23657 (2014), San Francisco, California, USA.
- [91] Mousaviraad, M. Carrica, P.M. and Stern, F. *Development and validation of harmonic wave group single-run procedure for RAO with comparison to regular wave and transient wave group procedures using URANS*. Ocean Engineering, 37 (2010) 653–666.
- [92] ITTC. *The Specialist Committee on CFD in Marine Hydrodynamics - Final report and Recommendations to the 27<sup>th</sup> ITTC*. Proceedings of the 27<sup>th</sup> International Towing Tank Conference, Vol. II (2014) 522–567.

- [93] Wilson, R. V., Carrica, P. M. and Stern, F. *Unsteady RANS method for ship motions with application to roll for a surface combatant*. Computers and Fluids, Vol. 35 (5) (2006) 501-524.
- [94] Ircal, M. A. R., Nallayarasu, S. and Bhattacharyya, S. K. *CFD approach to roll damping of ship with bilge keel with experimental validation*. Applied Ocean Research. 55 (2016) 1–17.
- [95] Gao, Q. and Vassalos, D. Numerical study of the roll decay of intact and damaged ships. The 12<sup>th</sup> International Ship Stability Workshop (2011) 277–282, Washington, USA.
- [96] ITTC. *The Seakeeping Committee - Final report and Recommendations to the 28<sup>th</sup> ITTC*. Proceedings of the 28<sup>th</sup> International Towing Tank Conference, Vol. I (2017) 213–273.
- [97] Morgan, W. B. and Lin, W. C. *Predicting ship hydrodynamic performance in today's world*. Naval Engineers Journal (1998) 91–98.
- [98] Abkowitz, M.A., 1969. *Stability and motion control of ocean vehicles*. Ocean Engineering Series, MIT Press (1969) 348 p, ISBN: 9780262510066.
- [99] Nomoto, K. *Analysis of Kempf's standard maneuver test and proposed steering quality indices*. Proceedings of 1<sup>st</sup> Symposium on Ship Maneuverability, Department Of The Navy, Maryland, United State of America (1960) 275–304. Roseman, D. P. (Editor). *The MARAD systematic series of full form ship models*. SNAME (1987) 384 p.
- [100] Lewis, E. V., (Editor). *Principles of naval architecture, Vol. III - Motions in Waves and Controllability*. SNAME (1989), Jersey City, NJ, US.
- [101] Clarke, D., Gedling, P. and Hine, G. *The application of maneuvering criteria in hull design using linear theory*. The Naval Architect (1983) 45–68.
- [102] Stern F., Agdrup K., Kim S. Y., Hochbaum, A. C., Rhee, K. P., Quadvlieg, F., Perdon, P., Hino, T., Broglia, R. and Gorski, J. *Experience from SIMMAN 2008 – the first workshop on verification and validation of ship maneuvering simulation methods*. Journal of Ship Research 55 (2) (2011) 135–147.
- [103] Toxopeus, S. *Viscous flow calculations For KVLCC2 in deep and shallow water*. 4<sup>th</sup> Int. Conference Computational Methods in Marine Engineering (2011), Lisbon, Portugal.
- [104] Carrica, P. M. and Stern, F. *DES Simulations of KVLCC1 in turn and zigzag manoeuvres with moving propeller and rudder*. SIMMAN 2008, Copenhagen, Denmark.
- [105] Sadat-Hosseini, S., Kim, D. H., Taylor, G. L., Fu, T., Terril, E. and Stern, F. *Vortical structures and instability analysis for Athena in turning maneuver with full-scale validation*, 30<sup>th</sup> Symposium on Naval Hydrodynamics (2014) 23 p, Hobart, Australia.
- [106] Sadat-Hosseini, H., Sanada, Y. and Stern, F. *Experiments and CFD for ONRT course keeping and turning circle maneuvering in regular waves*. WMTC15 (2015), Providence, Rhode Island, USA.
- [107] Liu, Y., Zou, Z. J. and Zou, L. *RANS based numerical simulation of captive model tests in shallow water for the DTC container carrier*. MASHCON (2016) 73-82, Hamburg, Germany.
- [108] ITTC. *The Maneuvering Committee - Final report and Recommendations to the 27<sup>th</sup> ITTC*. Proceedings of the 27<sup>th</sup> International Towing Tank Conference, Vol. I (2014).
- [109] Queutey, P. and Visnonneau, M. *An interface capturing method for free-surface hydrodynamic flows*. Computers and Fluids, 36 (2007) 1481–11510.
- [110] NUMECA, FINE<sup>TM</sup>/Marine. *Theoretical manual, ISIS-CFD*. Equipe Dynamique des Systèmes Propulsifs, Marins, Laboratoire de Recherche en Hydrodynamique,

- Energétique, et Environnement Atmosphérique, Ecole Centrale de Nantes, Nantes Cedex 3, France (2016).
- [111] AIAA, *Guide for the verification and validation of computational fluid dynamics simulations*. The American Institute of Aeronautics and Astronautics, G-077-1998.
- [112] Roache P. J. *Verification and validation in computational science and engineering*. Hermosa Publishers: Albuquerque, NM, (1998). ISBN: 9780913478080.
- [113] ITTC, *Recommended procedures, Guide to the expression of uncertainty in experimental hydrodynamics*. International Towing Tank Conference, ITTC Recommended Procedures and Guidelines (7.5-02-01-01), Rev. 02 (2014) 17p.
- [114] ITTC, *Recommended procedures and guidelines, uncertainty analysis in CFD verification and validation methodology and procedures*. International Towing Tank Conference, ITTC Recommended Procedures and Guidelines (7.5-03-01-01), Rev. 02 (2008) 12p.
- [115] Stern, F., Wilson, R. and Shao, J. *Quantitative approach to V&V of CFD simulations and certification of CFD codes*. International Journal for Numerical Methods in Fluids, 50 (2006) 1335–1355.
- [116] Eça, L. and Hoekstra, M. *On the influence of the iterative error in the numerical uncertainty of ship viscous flow calculations*. Proceedings of the 26<sup>th</sup> Symposium on Naval Hydrodynamics, Rome, Italy (2006).
- [117] Wilson, R. V., Shao, J. and Stern, F., *Discussion: Criticisms of the “correction factor” verification method 1*. Journal of Fluids Engineering, 126(4) (2004), 704-706.
- [118] Roache, P. J. *Criticisms of the “correction factor” verification method*. Journal of Fluids Engineering, 125(4) (2003), 732–733.
- [119] Wilson, R. and Stern, F. *Verification and validation for RANS simulation of a naval surface combatant*. Standards for CFD in the aerospace industry, AIAA 2002-0904 Aerospace Sciences Meeting, Reno, Nevada (2002).
- [120] d’Aure, B., Mallol, B., Hirsch, C. *Resistance and seakeeping CFD simulations for the Korean container ship*, Proceedings of the Tokyo 2015: A Workshop on CFD in Ship Hydrodynamics (2015), [https://numeca.com/docs/2015-tokyo\\_workshop-resistance\\_and\\_seakeeping\\_cfd\\_simulations\\_for\\_the\\_korean\\_container\\_ship\\_0.pdf](https://numeca.com/docs/2015-tokyo_workshop-resistance_and_seakeeping_cfd_simulations_for_the_korean_container_ship_0.pdf)
- [121] del Toro Lorrens, Á. *CFD verification and validation of ship hydrodynamics*. École Central de Nantes. Master Thesis (2015).
- [122] Crepier, P. *Ship resistance prediction: verification and validation exercise on unstructured grids*. Proceedings of the 7<sup>th</sup> International Conference on Computational Methods in Marine Engineering, MARINE (2017), 365–376.
- [123] ITTC, *Recommended procedures and guidelines, Practical guidelines for ship CFD applications*. International Towing Tank Conference, ITTC Recommended Procedures and Guidelines (7.5-03-02-03), Rev. 01 (2011), 18p.
- [124] Larsson, L. *JBC, Resistance, sinkage, trim and wave pattern-review*. Power point presentation, Tokyo 2015, A Workshop on CFD in ship hydrodynamics, National Maritime Research institute (2015), [https://t2015.nmri.go.jp/Presentations/Day1-AM4-JBC-Resist\\_etc-Larsson.pdf](https://t2015.nmri.go.jp/Presentations/Day1-AM4-JBC-Resist_etc-Larsson.pdf).
- [125] Hirata, N. *JBC, Test Data in NMRI*. Power point presentation, Tokyo 2015, A Workshop on CFD in ship hydrodynamics, National Maritime Research institute (2015), <https://t2015.nmri.go.jp/Presentations/Day1-AM2-JBC-TestData1-Hirata.pdf>.
- [126] Visonneau, M. *JBC, Local Flow Analysis*. Power point presentation, Tokyo 2015, A Workshop on CFD in ship hydrodynamics. National Maritime Research institute (2015), <https://t2015.nmri.go.jp/Presentations/Day1-PM1-JBC-LocalFlow-Visonneau.pdf>.

- [127] Menter, F. R., Kuntz, M., Langtry, R., *Ten Years of Industrial Experience with the SST Turbulence Model*. Turbulence, Heat and Mass Transfer 4, ed: K. Hanjalic, Y. Nagano, and M. Tummers, Begell House, Inc., (2003), 625–632.
- [128] Kim, W. J., Van, D. H., Kim D. H., *Measurement of flows around modern commercial ship models*. Exp. Fluid 31(2001), 567–578.
- [129] Olivieri, A., Pistani, F., Avanzini A., Stern, F., *Towing Tank Experiments of Resistance and Trim, Boundary Layer, Wake, and Free-Surface Flow Around a Naval Combatant INSEAN2340 Model*. Iowa Institute of Hydraulic Research, The University of Iowa, IHR report No.421, (2001).
- [130] Longo, J., Shao, J., Irvine, M., Stern F., *Phase-averaged PIV for the nominal wake of a surface ship in regular head waves*. ASME, J. Fluids Eng. 129(5) (2007), 524–540.
- [131] ITTC, *Recommended procedures and guidelines, Resistance Test*. International Towing Tank Conference, ITTC Recommended Procedures and Guidelines (7.5-02-02-01), Rev. 03 (2011), 13p.
- [132] Bekhit, A., Lungu, A., *Numerical Simulation of the Hydrodynamic Ship Performance*. Proceedings of the 1<sup>st</sup> International Conference on the Intelligent Transport System, INTSYS 2017, 29–30 November, Hyvinkää, Finland, published in Lecture Notes of the Institute for Computer Science, Social Informatics and Telecommunication Engineering, (2018), 120–129.
- [133] Bekhit, A., Popescu, F., *Local Flow Assessment of the Japan Bulk Carrier using Different Turbulence Models*, Proceedings of the 9<sup>th</sup> International Conference on Modern Technology in Industrial Engineering, MODTECH 2021, 23–26 June, online edition, Romania, IOP Conference Series: Material Science Engineering. Under press (2021).
- [134] Bekhit, A., Lungu, A., *Numerical Study of the Resistance, Free-Surface and Self-Propulsion Prediction of the KVLCC2 Ship Model*. Proceedings of the International Conference on Traffic and Transport Engineering, ICTTE Belgrade 2018, 27–28 September, Belgrade, Serbia. (2018), 333–340.
- [135] Bekhit, A., Lungu, A., *Verification and Validation Study for the Total Ship Resistance of the DTMB 5415 Ship Model*. Annals of “Dunarea de Jos” University of Galati, **Fascicle XI – Ship Building**, (2017), 53–60.
- [136] Bekhit, A., Lungu, A., *A Viscous Flow Simulation around a Fully Appended Ship Hull by Using a Finite Volume Technique*, Proceedings of the International Conference on Traffic and Transport Engineering, ICTTE Belgrade 2018, 27–28 September, Belgrade, Serbia. (2018), 325-332.
- [137] Bekhit, A., Obreja D., *Numerical and Experimental Investigation on the Free-surface Flow and Total Resistance of the DTMB Surface Combatant*. Proceedings of the 8<sup>th</sup> International Conference on Modern Technology in Industrial Engineering, MODTECH 2020, 23–27 June, online edition, Romania, IOP Conference Series: Material Science Engineering. **916**(012008) (2020).
- [138] Guilmineau, E., Deng, G. B., Leroyer, A., Queutey, P., Visonneau, M., Wackers, J., *Numerical Simulations of the Cavitating and Non-Cavitating Flow around the Potsdam Propeller Test Case*, Proceedings of the 4<sup>th</sup> Int. Symposium on Marine Propellers, smp’15, (Austin, Texas, USA, June, 2015).
- [139] Felli, M., Guj, G, Camussi, R., *Effect of the number of blades on propeller wake evolution*, Exp. Fluids **44** (3), (2008), 409–418.
- [140] M. Felli, R. Camussi and F. Di Felice, *Mechanisms of evolution of the propeller wake in the transition and far fields*, J. Fluid Mech. 682, (2011), 5–53.

- [141] Wang, L. Z., Guo, C. Y., Su, Y. M. Wu, T. C., *A numerical study on the correlation between the evolution of propeller trailing vortex wake and skew of propellers*, Int. J. Naval Architecture and Ocean Eng. 10 (2018), 212–224.
- [142] Bekhit A., Lungu A., *Simulation of the POW Performance of the JBC Propeller*, Proceedings of the 16<sup>th</sup> International Conference on Numerical Analysis and Applied Mathematics, ICNAAM 2018, 13–18 September, Rhodes, Greece. American Institute of Physics, AIP Conference Proceedings, **2216**, 450007, (2019).
- [143] Bekhit A., 2018, *Numerical Simulation of The Ship Self-propulsion Prediction using Body Force Method and Fully Discretized Propeller Model*, Proceedings of the 6<sup>th</sup> Modern Technology in Industrial Engineering Conference, MODTECH 2018, 13–16 June, Constanța, Romania. IOP Conference Series: Materials Science and Engineering 400 (2018), 042004.
- [144] Bekhit A., Pacuraru F., Pacuraru S. 2019, *Hull-Propeller-Rudder Interaction of the JBC Ship Model*, Proceedings of the 17<sup>th</sup> International Conference on Numerical Analysis and Applied Mathematics, ICNAAM 2019, 23 – 28 September 2019, Rhodes, AIP Conference Proceedings 2293, 420091, (2020).
- [145] Win, Y. N., *Computation of the propeller-hull and propeller-hull-rudder interaction using simple body-force distribution model*, PhD thesis, Osaka University OUKA. Japan (2014).
- [146] SIMMAN, *Workshop on Verification and Validation of Ship Maneuvering Simulation Methods* (2014), <https://simman2014.dk/>.
- [147] Bekhit A., Lungu A., *URANSE Simulation for the Seakeeping of the KVLCC2 Ship Model in Short and Long Regular Head Waves*, Proceedings of the 7<sup>th</sup> Modern Technology in Industrial Engineering Conference, MODTECH 2019, 17–20 June, Iasi, Romania, IOP Conference Series: Material Science Engineering. **591(2019)** 012102.
- [148] Ozdemir, Y. H., Barlas, B. *Numerical study of ship motions and added resistance in regular incident waves of KVLCC2 model*, International Journal of Naval Engineering **9**(2017), 149-159.
- [149] Bekhit A., Lungu A., *Numerical Simulation for Predicting Ship Resistance and Vertical Motions in Regular Head Waves*, Proceedings of the ASME 2019, 38th International Conference on Ocean, Offshore and Arctic Engineering – OMAE (2019), 9–14 June, Glasgow, Scotland, UK, OMAE2019-95237.
- [150] Irvine, M., Longo, J., Stern, F. *Towing tank tests for surface combatant for free roll decay and coupled pitch and heave motions*, In Proceedings of the 25<sup>th</sup> Symposium on Naval Hydrodynamics, St Johns, Canada, 8-13 August 2004. National Academy of Sciences, the National Academies Press, (2005).
- [151] ITTC. *Recommended Procedures and Guidelines: Numerical Estimation of Roll Damping*. (7.5-02 -07-04.5), Rev. 00; (2011) 32p.
- [152] Begovic, E., Day, A.H., Incecik, A., Mancini, S., Pizzirusso, D., *Roll damping assessment of intact and damaged ship by CFD and EFD methods*. In Proceedings of the 12<sup>th</sup> international conference on the stability of ships and ocean vehicles (STAB2015), Glasgow, UK, 13–19 June (2015), 14–19.
- [153] Atsavapranee, P., Carneal, J. B.; Grant, D., Percival, A. S., *Experimental investigation of viscous roll damping on the DTMB model 5617 hull form*, In Proceedings of the ASME 26<sup>th</sup> International Conference on Offshore Mechanics and Arctic Engineering. California, USA, 10-15 June 2007. OMAE2007-29324.
- [154] Bekhit A., Popescu F., *URANSE-Based Numerical Prediction for the Free Roll Decay of the DTMB Ship Model*, Journal of Marine Science and Engineering, **9**(5), (2021), 452.

- [155] Piomelli, U. and Balaras, E. *Wall-layer models for large eddy simulations*. Annual Reviews of Fluid Mechanics, Vol. 34 (2002), 349–374.
- [156] Bhushan, S. and Wlatter, D. K. *A dynamic hybrid RANS/LES modeling framework*. Physics of Fluids, Vol. 24, 015103 (2012).
- [157] Boussinesq, J. *Theorie de L'Écoulement tourbillant. mem*, Presentes par Divers Savants Acad. Sci. Inst. Fr., Vol. 23 (1877) 46–50.
- [158] Smith, A. M. O. and Cebeci, T. *Numerical solution of the turbulent boundary layer equations*. Douglas Aircraft Division report, DAC 33735 (1967).
- [159] Baldwin, B. S. and Lomax, H. *Thin Layer Approximation and Algebraic Model for Separated Turbulent Flows*. American Institute of Aeronautics and Astronautics (1978), AIAA paper 78-257.
- [160] Spalart, P. R. and Allmaras, S. R. *A one-equation turbulence model for aerodynamic flows*. American Institute of Aeronautics and Astronautics (1992), AIAA paper 92-0439.
- [161] Baldwin, B. S. and Barth, T. J. *A one-equation turbulence transport model for high Reynolds number wall-bounded flows*. American Institute of Aeronautics and Astronautics (1991), AIAA paper 91-0610.
- [162] Ferziger, J. H. and Perić, M. *Computational methods for fluid dynamics*. 3rd Edition (2002), Springer, ISBN 3-540-42074-6.
- [163] Versteeg, H. K. and Malasekera W. *An introduction to computational fluid dynamics, the finite volume method*. 1<sup>st</sup> Edition, Longman Scientific and Technical, Harlow, England, ISBN 0-582-21884-5.
- [164] Nichols B. D. and Hirt. C. W. *Improved Free surface boundary conditions for numerical incompressible flow calculations*. Journal of Computational Physics, Vol. 8 (1971), 434–448.
- [165] Nichols B. D. and Hirt. C. W. *Calculating three-dimensional free surface flows in the vicinity of submerged and exposed structures*. Journal of Computational Physics, Vol. 12 (1973) 234–246.
- [166] Donea, S., Guilian, S. and Halleux J. P. *An arbitrary Lagrangian-Eulerian Finite Element Method for Transient Dynamic Fluid-Structure Intercations*. Computer Methods in Applied Mechanics and Engineering, Vol.33 (1982), 689–723.
- [167] Harlow, F. H. and Welch, J. E. *Numerical calculation of time-dependent viscous incompressible flow of fluid with free surface*. The Physics of Fluid, Vol. 8 (1965), 2182–2189.
- [168] Osher, S., Sethian J. A. *Fronts propagating with curvature-dependent speed: Algorithms based on Hamilton-Jacobi formulations*. Journal of Computational Physics. Vol. 79 (1988), 12–49.

# Appendix A

## Numerical Methods used in Ship Hydrodynamics Applications

The recent applications of numerical methods in ship hydrodynamics comprise mainly three important elements: physical modeling; numerical modeling and finally the computational framework. This division is very important to be taken into consideration for highlighting and understanding the CFD process and its basic levels of errors, as it will be discussed later in Chapter III. The physical modeling describes the basic problem and how it can be solved. Basic models in ship hydrodynamics include flow modeling, whether one- or two-phase flow, turbulence models, propulsion models, cavitation models, wave models, etc. On the other hand, the numerical modeling describes the techniques used to solve the physical models, such as solution algorithm, discretization methods, interface or free-surface modeling, grid generation, etc. Finally, the computational framework describes the computational capacity available for the simulation, which relies recently on the HPC allowing broader capabilities for using finer grids, more advanced turbulence models, parallel computing and significantly fast simulation turnaround time. The flow chart in Fig. 3.1 shows the main components of computational methods in ship hydrodynamics.

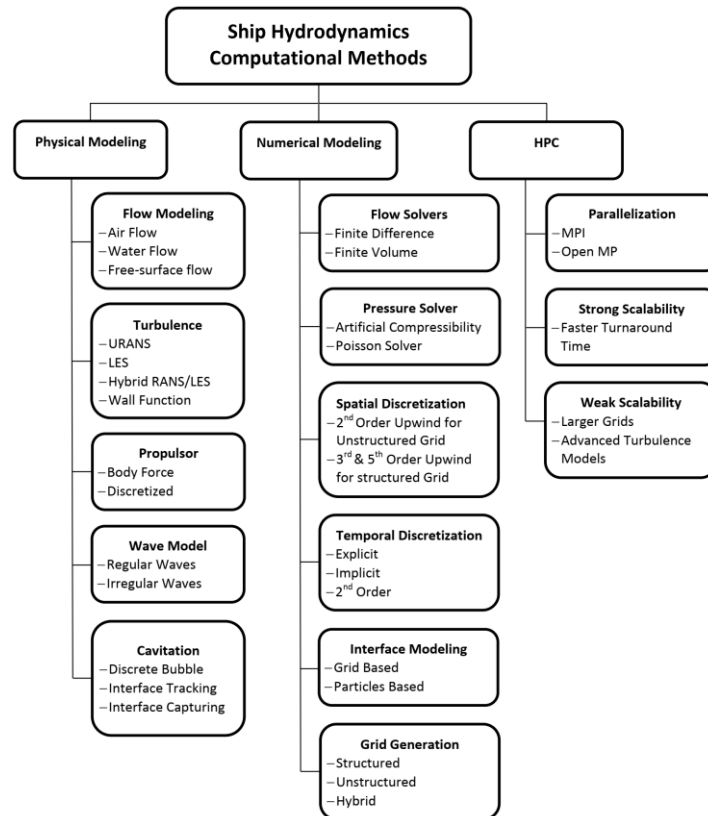


**Figure A.1** Main components of the ship hydrodynamics computational methods [35, 74]

This chapter provides in brief a general review for the basic numerical methods applied in ship hydrodynamics, summarizing the important techniques and highlights their applications and



limitations. It is worth mentioning that some of the listed models in the flow chart are not covered in the following breakdown, since they are either beyond the scope of this thesis such as the HPC or not included in the numerical simulations performed in this dissertation, such as the cavitation models. In addition, the propulsion model was basically covered in Chapter I.

# List of Publications

## ISI Web Of Science

1. **Bekhit A.**, Lungu A., 2018, “*Numerical Simulation of the Hydrodynamic Ship Performance*”, Proceedings of the 1<sup>st</sup> International Conference on the Intelligent Transport System, INTSYS 2017, 29–30 November, Hyvinkää, Finland, published in Lecture Notes of the Institute for Computer Science, Social Informatics and Telecommunication Engineering, pp. 120-129. DOI: 10.1007/978-3-319-93710-6\_14, WOS:000656446200014, [https://link.springer.com/chapter/10.1007%2F978-3-319-93710-6\\_14](https://link.springer.com/chapter/10.1007%2F978-3-319-93710-6_14)
2. **Bekhit A.**, 2018, “*Numerical Simulation of The Ship Self-propulsion Prediction using Body Force Method and Fully Discretized Propeller Model*”, Proceedings of the 6<sup>th</sup> Modern Technology in Industrial Engineering Conference, MODTECH 2018, 13–16 June, Constanta, Romania. IOP Conference Series: Materials Science and Engineering **400(2018)** 042004. DOI: 10.1088/1757-899X/400/4/042004, WOS:000461147400076, <http://iopscience.iop.org/article/10.1088/1757-899X/400/4/042004/pdf>
3. **Bekhit A.**, 2018, “*Unsteady RANSE Simulation for Ship Resistance, Heave and Pitch in Regular Head Waves*”, Proceedings of the 6th Modern Technology in Industrial Engineering Conference, MODTECH 2018, 13–16 June, Constanta, Romania. IOP Conference Series: Materials Science and Engineering **400(2018)** 082004. DOI: 10.1088/1757-899X/400/8/082004, WOS:000461147400184, <http://iopscience.iop.org/article/10.1088/1757-899X/400/8/082004/pdf>
4. **Bekhit A.**, Lungu A., 2018, “*A Viscous Flow Simulation around a Fully Appended Ship Hull by Using a Finite Volume Technique*”, Proceedings of the International Conference on Traffic and Transport Engineering, ICTTE Belgrade 2018, 27–28 September, Belgrade, Serbia. pp. 325-332, ISBN:978-86-916153-4-5, WOS:000542956800043, [http://ijtte.com/uploads/news\\_files/Proceedings%202018%20final.pdf](http://ijtte.com/uploads/news_files/Proceedings%202018%20final.pdf)
5. **Bekhit A.**, Lungu A., 2018, “*Numerical Study of the Resistance, Free-Surface and Self-Propulsion Prediction of the KVLCC2 Ship Model*”, Proceedings of the International Conference on Traffic and Transport Engineering, ICTTE Belgrade 2018, 27–28 September, Belgrade, Serbia. pp. 333-340, ISBN:978-86-916153-4-5, WOS:000542956800044, [http://ijtte.com/uploads/news\\_files/Proceedings%202018%20final.pdf](http://ijtte.com/uploads/news_files/Proceedings%202018%20final.pdf)
6. **Bekhit A.**, Lungu A., 2018, “*Simulation of the POW Performance of the JBC Propeller*”, Proceedings of the 16<sup>th</sup> International Conference on Numerical Analysis and Applied Mathematics, ICNAAM 2018, 13–18 September, Rhodes, Greece. American Institute of Physics, AIP Conference Proceedings, **2216**, 450007 (2019). DOI: 10.1063/1.5114474, WOS:000521108600455, <https://aip.scitation.org/doi/10.1063/1.5114474>
7. **Bekhit A.**, Lungu A., 2018, “*Numerical Free Roll Decay Prediction for the DTMB Hull*”, Proceedings of the 16<sup>th</sup> International Conference on Numerical Analysis and Applied Mathematics, ICNAAM 2018, 13–18 September, Rhodes, Greece. American Institute of Physics, AIP Conference Proceedings, **2216**, 450050 (2019). DOI: 10.1063/1.5114517, WOS:000521108600497, <https://aip.scitation.org/doi/abs/10.1063/1.5114517>
8. **Bekhit A.**, Lungu A., 2019, “*Numerical Simulation for Predicting Ship Resistance and Vertical Motions in Regular Head Waves*”, Proceedings of the ASME 2019, 38<sup>th</sup> International Conference on Ocean, Offshore and Arctic Engineering – OMAE 2019, 9–14 June, Glasgow, Scotland, UK, OMAE2019-95237. DOI: 10.1115/OMAE2019-95237, WOS:000513070800009, <https://asmedigitalcollection.asme.org/OMAE/proceedings-abstract/OMAE2019/58776/V002T08A009/1067538>
9. **Bekhit A.**, Lungu A., 2019, “*URANSE Simulation for the Seakeeping of the KVLCC2 Ship Model in Short and Long Regular Head Waves*”, Proceedings of the 7<sup>th</sup> Modern Technology in Industrial Engineering Conference, MODTECH 2019, 17–20 June, Iasi, Romania, IOP Conference Series: Material Science Engineering. **591(2019)** 012102. DOI: 10.1088/1757-899X/591/1/012102, WOS:000562929900102, <https://iopscience.iop.org/article/10.1088/1757-899X/591/1/012102/meta>

10. **Bekhit A.**, Păcuraru F., Păcuraru S. 2019, “*Hull-Propeller-Rudder Interaction of the JBC Ship Model*”, Proceedings of the 17<sup>th</sup> International Conference on Numerical Analysis and Applied Mathematics, ICNAAM 2019, 23 – 28 September 2019, Rhodes, AIP Conference Proceedings 2293, 420091 (2020); DOI:10.1063/5.0027325, WOS:000636709500408, <https://doi.org/10.1063/5.0027325>
11. Păcuraru F., Păcuraru S. **Bekhit A. S.** 2019, “*Numerical Analysis of Ship Motions for an Offshore Vessel*”, Proceedings of the 17<sup>th</sup> International Conference on Numerical Analysis and Applied Mathematics, ICNAAM 2019, 23 – 28 September 2019, Rhodes, AIP Conference Proceedings 2293, 420092 (2020); DOI: 10.1063/5.0027329, WOS:000636709500409, <https://doi.org/10.1063/5.0027329>.
12. **Bekhit A.**, Obreja D., 2020, “*Numerical and Experimental Investigation on the Free-surface Flow and Total Resistance of the DTMB Surface Combatant*” Proceedings of the 8<sup>th</sup> International Conference on Modern Technology in Industrial Engineering, MODTECH 2020, 23–27 June, online edition, Romania, IOP Conference Series: Material Science Engineering. 916 (2020), 012008; DOI:10.1088/1757-899X/916/1/012008, WOS:000625330000008, <https://iopscience.iop.org/article/10.1088/1757-899X/916/1/012008>.
13. **Bekhit A.**, Popescu F. 2021, “*URANSE-Based Numerical Prediction for the Free Roll Decay of the DTMB Ship Model*”. Journal of Marine Science and Engineering. 2021; **9**(5):452. DOI:10.3390/jmse9050452. WOS:000662367200001; <https://doi.org/10.3390/jmse9050452>.
14. **Bekhit A.**, Popescu F., 2020, “*Local Flow Assessment of the Japan Bulk Carrier using Different Turbulence Models*” Proceedings of the 9<sup>th</sup> International Conference on Modern Technology in Industrial Engineering, MODTECH 2021, 23–26 June, online edition, România, IOP Conference Series: Material Science Engineering. *Under press*.
15. **Bekhit A.**, Popescu F., 2020, “*Numerical Investigation of the Shallow Water Effect on the Total Resistance, Vertical Motion and Wave Profile of a Container Ship Model*” Proceedings of the 9<sup>th</sup> International Conference on Modern Technology in Industrial Engineering, MODTECH 2021, 23–26 June, online edition, România, IOP Conference Series: Material Science Engineering. *Under press*.

### **SCOPUS:**

16. Păcuraru F., Presura A., **Bekhit A.**, Păcuraru S., 2019, “*Full-Scale Self-Propulsion Simulation for an Inland Catamaran Ferry*”, Proceedings of the 19<sup>th</sup> International Multidisciplinary Scientific GeoConference Surveying Geology and Mining Ecology Management, SGEM 2019, 30 June – 6 July, Varna, Bulgaria, SGEM 19(4.1), pp. 633-641. DOI: 10.5593/sgem2019/4.1/S17.081, <https://www.sgem.org/index.php/elibrary?view=publication&task=show&id=5886>

### **IDB:**

17. **Bekhit A.**, Lungu, A., 2017, “*Verification and Validation Study for the Total Ship Resistance of the DTMB 5415 Ship Model*”. Annals of “Dunarea de Jos” University of Galati, **Fascicle XI – Ship Building**, pp. 53-60, <http://www.gup.ugal.ro/ugaljournals/index.php/fanship/article/view/1061/1276>.

PERSONAL INFORMATION

**Adham Saber Mahmoud Mohamed Aly Bekhit**



 59-61, Garii street, Galti, 800217, Romania

 (+40) 755329082

 [adham.bekhit@ugal.ro](mailto:adham.bekhit@ugal.ro)

Sex Male | Date of birth 29/11/1983 | Nationality Egyptian

DOMAIN OF COMPETITION

Marine Hydrodynamics, Computational Fluid Dynamics, Fluid-Structure Interaction, Naval Architecture

WORK EXPERIENCE

September 2020 – present

**Assistant professor**

Faculty of Naval Architecture, “Dunarea de Jos” University of Galati, Romania (<http://www.ugal.ro>),

([http://www.naoe.ugal.ro/index\\_1](http://www.naoe.ugal.ro/index_1))

- Practical and theoretical demonstrator

Faculty of Naval Architecture

February 2019 – September 2020

**Research Engineer (part-time)**

Faculty of Naval Architecture, “Dunarea de Jos” University of Galati, Romania (<http://www.ugal.ro>),

([http://www.naoe.ugal.ro/index\\_1](http://www.naoe.ugal.ro/index_1)), (<http://www.reform.ugal.ro/>)

- Performing researches in ship hydrodynamics

Naval Architecture Research Center (CCAN) – Multidisciplinary Research Platform (ReForm–UDJG)

November 2011 – November 2013

**Engineer**

Alexandria Shipyard, Egypt (<http://www.alexyard.com.eg/>)

- planning and scheduling the required man-hours and material for production
- solving outfitting production problems

Technology Management Department

August 2011 – October 2011

**Supervisor QA/QC Engineer**

Alexandria Navy Shipyard, Egypt

- supervising, planning, scheduling and monitoring of welding process and ship hull maintenance operations and plans

Hull and Welding Department

June 2010 – August 2011

**Mechanical Engineer**

Alexandria Naval Forces, Egypt

- operation, maintenance and repair of marine diesel engines and auxiliary systems
- planning, scheduling and supervising the periodical maintenance and dry docking of the ship

September 2008 – April 2009

**Demonstrator Engineer**

Faculty of Engineering, Alexandria University, Egypt (<https://eng.alexu.edu.eg/index.php/en/>)

- demonstrating ship structural analysis, risk management and machines & marine technical drawing

Naval Architecture & Marine Engineering Department

EDUCATION AND TRAINING

**Education**

- October 2015 – Present **Ph.D. student**  
 Faculty of Naval Architecture, “Dunarea de Jos” University of Galati, Romania  
[\(http://www.ugal.ro/\)](http://www.ugal.ro/)  
 [\(http://www.naoe.ugal.ro/index\\_1\)](http://www.naoe.ugal.ro/index_1)

  - Thesis title “Numerical Simulation of the Ship Hull Hydrodynamic Performance”
  
- October 2013 – July 2015 **Master Degree of Science M.Sc.**  
 Faculty of Naval Architecture, “Dunarea de Jos” University of Galati, Romania  
[\(http://www.ugal.ro/\)](http://www.ugal.ro/)  
 [\(http://www.naoe.ugal.ro/index\\_1\)](http://www.naoe.ugal.ro/index_1)

  - Thesis title “ Local Strength Assessment in Equivalent Quasi-Static Head Waves, for a Tanker Ship Structure, Based on Three Cargo Holds 3D-FEM Model ”
  
- September 2003 – May 2008 **Bachelor Degree of Science B.Sc.**  
 Faculty of Engineering, Alexandria University, Egypt (<https://eng.alexu.edu.eg/index.php/en/>)

  - Graduation project title “Safety Aspects of Offshore Structures”
  
- September 1998 – June 2003 **Advanced Technical High School Diploma in Computer Science**  
 Alexandria Advanced Technical School, Alexandria, Egypt

**Training and Internship**

- December 2012 – January 2013 **Ship Outfitting Refrigeration & HVAC Diploma**  
 China Shipbuilding Trading Company Limited, Hudong-Zhonghua Shipbuilding Group Co., Ltd, Shanghai, China ([www.cstc.com.cn/cstc\\_e](http://www.cstc.com.cn/cstc_e))

  - training course for assembly and commissioning of Refrigeration, Air-Conditioning and Ventilation
  
- August 2007 **Internship**  
 PETROJET – The Petroleum Projects and Technical Consultations Co. Alexandria, Egypt ([www.petrojet.com.eg](http://www.petrojet.com.eg))

  - training courses for: production stages of marine structures, QA/QC of welding processes, project plans and design drawings, safety systems for marine production processes
  
- July 2006 **Internship**  
 Alexandria Port Authority, Egypt ([www.apa.gov.eg](http://www.apa.gov.eg))

  - training courses for maintenance and repair of marine diesel engines and auxiliary systems

PERSONAL SKILLS

Mother tongue	Arabic				
Other language(s)	UNDERSTANDING		SPEAKING		WRITING
	Listening	Reading	Spoken interaction	Spoken production	
1) English	C1	C1	C1	C1	C1
Excellent grade by the International British Institute (IBI) in Egypt for general English levels.					
2) Romanian	B2	B2	B2	B1	B1
Department of Lifelong Learning and Technological Transfer, “Dunarea de Jos University” of Galati.					
Levels: A1/A2: Basic user - B1/B2: Independent user - C1/C2 Proficient user <a href="#">Common European Framework of Reference for Languages</a>					

## Digital skills

## SELF-ASSESSMENT

CFD	NUMECA Fine/Marine Expert user	SHIPFLOW Independent user	Tecplot Independent user		
FEM	Cosmos/M Expert user	FEMAP Independent user	EDI/SACS Basic user		
CAD & CAM	AutoCAD Independent user	Rhinoceros Expert user	Tribon Basic user	CADfix Basic user	SolidWorks Basic user

- Other**
- good command of office suite (Word, Excel, PowerPoint)
  - Basic user of Risk Assessment applications (CFAST, FDS-SMV, Pathfinder Evacuation Software)
  - Basic Knowledge of programming language (Visual Basic, C++)

**Driving licence** Category: A, B1 and B